



## Εθνικό Μετσόβιο Πολυτεχνείο

Σχολή Ηλεκτρολόγων Μηχανικών και Μηχανικών Υπολογιστών

Τομέας Σημάτων, Ελέγχου και Ρομποτικής

Εργαστήριο Όρασης Υπολογιστών, Επικοινωνίας Λόγου και Επεξεργασίας Σημάτων

Αναγνώριση και εντοπισμός ανθρώπινης  
δραστηριότητας σε βίντεο

Διπλωματική εργασία

του

Ευστάθιου Ε. Γαλανάκη

Επιβλέπων: Πέτρος Μαραγκός  
Καθηγητής Ε.Μ.Π.

Αθήνα, Νοέμβριος 2019





Εθνικό Μετσόβιο Πολυτεχνείο  
Σχολή Ηλεκτρολόγων Μηχανικών και Μηχανικών Υπολογιστών  
Τομέας Σημάτων, Ελέγχου και Ρομποτικής  
Εργαστήριο Όρασης Υπολογιστών, Επικοινωνίας Λόγου και Επεξεργασίας  
Σημάτων

## Αναγνώριση και εντοπισμός ανθρώπινης δραστηριότητας σε βίντεο

Διπλωματική εργασία

του

Ευστάθιου Ε. Γαλανάκη

Επιβλέπων: Πέτρος Μαραγκός  
Καθηγητής Ε.Μ.Π.

Εγκρίθηκε από την τριμελή εξεταστική επιτροπή την - 2019.

(Υπογραφή)

(Υπογραφή)

(Υπογραφή)

.....  
Πέτρος Μαραγκός  
Καθηγητής  
Ε.Μ.Π

Αθήνα, Νοέμβριος 2019



(Τπογραφή)

.....  
**Ευστάθιος Ε. Γαλανάκης**

Διπλωματούχος Ηλεκτρολόγος Μηχανικός και Μηχανικός Υπολογιστών Ε.Μ.Π.

Copyright © Ευστάθιος Ε. Γαλανάκης, 2019.  
Με επιφύλαξη παντός δικαιώματος. All rights reserved.

Απαγορεύεται η αντιγραφή, αποθήκευση και διανομή της παρούσας εργασίας, εξ ολοκλήρου ή τμήματος αυτής, για εμπορικό σκοπό. Επιτρέπεται η ανατύπωση, αποθήκευση και διανομή για σκοπό μη κερδοσκοπικό, εκπαιδευτικής ή ερευνητικής φύσης, υπό την προϋπόθεση να αναφέρεται η πηγή προέλευσης και να διατηρείται το παρόν μήνυμα. Ερωτήματα που αφορούν τη χρήση της εργασίας για κερδοσκοπικό σκοπό πρέπει να απευθύνονται προς τον συγγραφέα.

Οι απόψεις και τα συμπεράσματα που περιέχονται σε αυτό το έγγραφο εκφράζουν τον συγγραφέα και δεν πρέπει να ερμηνευθεί ότι αντιπροσωπεύουν τις επίσημες θέσεις του Εθνικού Μετσόβιου Πολυτεχνείου



# Ευχαριστίες



# Περίληψη

Σκοπός αυτής της διπλωματικής εργασίας είναι ο σχεδιασμός ενός δικτύου αναγνώρισης και εντοπισμού των ανθρώπινων ενεργειών σε βίντεο. Το δίκτυο μας στοχεύει να προσδιορίσει χωροχρονικά μια αναγνωρισμένη ενέργεια μέσα σε ένα βίντεο παράγωντας μια ακολουθία δισδιάστατων κουτιών, ένα για κάθε φραμε του βίντεο, που περικλείει το άτομο που εκτελεί την αναγνωρισμένη ενέργεια.

Η ανίχνευση και η αναγνώριση των ενεργειών σε βίντεο είναι μια από τις μεγαλύτερες προκλήσεις στο πεδίο της Όρασης Υπολογιστών. Οι πιο πρόσφατες προσεγγίσεις περιλαμβάνουν ένα δίκτυο ανίχνευσης αντικειμένων το οποίο προτείνει δυσδιάστατα κουτάκια ανά φραμε, έναν αλγόριθμο σύνδεσης για τη δημιουργία υποψήφιων αστιον τυβες και έναν ταξινομητή για την ταξινόμησή τους. Πάνω σάντο, οι περισσότερες από αυτές τις προσεγγίσεις εξαγάγουν τις χρονικές πληροφορίες από ένα δίκτυο το οποίο εκτιμά οπτική ροή σε επίπεδο πλαισίου. Η εισαγωγή των τρισδιάστατων συνελικτικών δικτύων μας έχει βοήθησε να μπορούμε να υπολογίσουμε τις χωροχρονικές πληροφορίες από τα βίντεο και ταυτόχρονα να εξάγουμε χωροχρονικά χαρακτηριστικά. Η προσέγγισή μας προσπαθεί να συνδυάσει τα οφέλη του να χρησιμοποιείς δίκτυα ανίχνευσης αντικειμένων και τρισδιάστατες συνελίξεις. Σχεδιάζουμε ένα δίκτυο του οποίου η δομή βασίζεται στα κλασσικά δίκτυα εντοπισμού δράσης και το ονομάζουμε ΑστιονNet. Το πρώτο στοιχείο είναι ένα τρισδιάστατο ReoNet34 το οποίο χρησιμοποιείται για τη χωροχρονική εξαγωγή χαρακτηριστικών. Επίσης, σχεδιάζουμε ένα δίκτυο για προτείνει υποψήφιες ακολουθίες από δισδιάστατα κουτιά με βάση τα χωροχρονικά χαρακτηριστικά, που το ονομάζουμε Τυβε Προποσαλ Νετωορχ. Αυτό το δίκτυο είναι μια επέκταση του Reenet Προποσαλ Νετωορχ παίρνοντας ως είσοδο τα εξαγώμενα χαρακτηριστικά και δίνοντας ως εξόδων κ προτεινόμενες ακολουθίες από δισδιάστατα κουτιά. Εξετάζουμε 2 προσεγγίσεις για τον καθορισμό των τρισδιάστατων προκαθορισμένων κουτιών, τα οποία χρησιμοποιεί το TPN. Επιπλέον, σχεδιάζουμε έναν αλγόριθμο σύνδεσης για τη σύνδεση των προτεινόμενων αστιον τυβες. Τέλος, διερευνούμε αρκετές τεχνικές ταξινόμησης, συμπεριλαμβανομένου ενός ταξινόμησή Σ'Μ, ενός Λινεαρ, ενός PNN και ενός ΜΛΠ για τα σύνολα δεδομένων ΘΗΜΔΒ και ΥΦ101.

## Λέξεις κλειδία



# Abstract

The purpose of this diploma thesis is the design of a network for recognizing and localising human actions in videos. Our network aims to spatio-temporally localize a recognized action within a video producing a sequence of 2D boxes, one per frame, which includes the actor performing the recognized action.

Detecting and Recognizing actions in videos is one of the biggest challenges in the field of Computer Vision. Most recent approaches includes an object detection network which proposes bounding boxes per frame, a linking method for creating candidate action tubes and a classifier for classifying these. On top of that, most of these approaches extract temporal information from a network which estimates optical flow in frame level. The introduction of 3D Convolutional Networks has helped us estimating spatio-temporal information from videos and simultaneously extract spatio-temporal features. Our approach tries to combine the benefits from using object detection networks and 3D Convolution.

We design a network whose structure is based on standard action localization networks and we name it ActionNet. Its first element is a 3D ResNet34 which is used for spatio-temporal feature extraction. Also, we design a network for proposing action tubes based on spatio-temporal features, called Tube Proposal Network. This network is an expansion of Region Proposal Network and it gets as input the extracted features and outputs k-proposed action tubes. We explore 2 approaches for defining 3D anchors, which TPN uses. On top of that, we design a linking algorithm for connecting proposed action tubes. Finally, we explore several classification techniques including a SVM classifier and a MLP for datasets JHMDB and UCF101.

## Keywords

Action Localization, Action Recognition, Action Tubes



# Περιεχόμενα

<b>Ευχαριστίες</b>	<b>7</b>
<b>Περίληψη</b>	<b>9</b>
<b>Abstract</b>	<b>11</b>
<b>Περιεχόμενα</b>	<b>13</b>
<b>Κατάλογος Πινάκων</b>	<b>15</b>
<b>Κατάλογος Σχημάτων</b>	<b>18</b>
<b>1 Introduction</b>	<b>21</b>
1.1 Problem statement . . . . .	21
1.1.1 Human Action Recognition . . . . .	21
1.1.2 Human Action Localization . . . . .	21
1.2 Applications . . . . .	21
1.3 Challenges and Datasets . . . . .	22
1.3.1 JHMDB Dataset . . . . .	23
1.3.2 UCF-101 Dataset . . . . .	23
1.4 Motivation and Contributions . . . . .	23
1.5 Thesis structure . . . . .	24
<b>2 Background</b>	<b>27</b>
2.1 Machine Learning . . . . .	27
2.1.1 Introduction . . . . .	27
2.1.2 Neural Networks . . . . .	29
2.1.3 A single Neuron . . . . .	29
2.1.4 2D Convolutional Neural Network . . . . .	32
2.1.5 3D Convolutional Neural Network . . . . .	34
2.2 Object Detection . . . . .	35
2.2.1 Region Proposal Network . . . . .	35
2.2.2 Roi Align . . . . .	37
2.2.3 Non-maximum suppression (NMS) algorithm . . . . .	38
2.3 Losses and Metrics . . . . .	39
2.3.1 Losses . . . . .	39
2.3.2 Metrics . . . . .	40

2.4	Related work . . . . .	46
2.4.1	Action Recognition . . . . .	47
2.4.2	Action Localization . . . . .	49
<b>3</b>	<b>Tube Proposal Network</b>	<b>53</b>
3.1	Our implementation's architecture . . . . .	53
3.2	Introduction to TPN . . . . .	53
3.3	Preparation before TPN . . . . .	54
3.3.1	Preparing data . . . . .	54
3.3.2	3D ResNet . . . . .	55
3.4	3D anchors as 6-dim vector . . . . .	56
3.4.1	First Description . . . . .	56
3.4.2	Training . . . . .	56
3.4.3	Validation . . . . .	58
3.4.4	Modified Intersection over Union(mIoU) . . . . .	58
3.4.5	Improving TPN score . . . . .	59
3.4.6	Adding regressor . . . . .	60
3.4.7	Changing Regressor - from 3D to 2d . . . . .	63
3.5	3D anchors as 4k-dim vector . . . . .	63
3.5.1	Training . . . . .	65
3.5.2	Adding regressor . . . . .	66
3.5.3	From 3D to 2D . . . . .	67
3.5.4	Changing sample duration . . . . .	68
3.6	General comments . . . . .	69
<b>4</b>	<b>Connecting Tubes</b>	<b>73</b>
4.1	Introduction . . . . .	73
4.2	First approach: combine overlap and actionness . . . . .	73
4.2.1	JHMDB Dataset . . . . .	75
4.2.2	UCF dataset . . . . .	78
4.3	Second approach: use progression and progress rate . . . . .	83
4.4	Third approach : use naive algorithm - only for JHMDB . . . . .	84
4.5	General comments . . . . .	85
<b>5</b>	<b>Classification stage</b>	<b>87</b>
5.1	Introduction . . . . .	87
5.2	Preparing data and first classification results . . . . .	88
5.3	Support Vector Machine (SVM) . . . . .	90
5.3.1	Modifying 3D Roi Align . . . . .	92
5.3.2	Temporal pooling . . . . .	92
5.4	Increasing sample duration to 16 frames . . . . .	93
5.5	Adding more groundtruth tubes . . . . .	93
5.5.1	Increasing again sample duration (only for RNN and Linear) . . . . .	96
5.6	MultiLayer Perceptron (MLP) . . . . .	97
5.6.1	Regular training . . . . .	98
5.6.2	Extract features . . . . .	98
5.7	Adding nms algorithm . . . . .	99
5.7.1	General comments . . . . .	102
5.8	Classifying dataset UCF . . . . .	102

5.8.1	Introduction . . . . .	102
5.8.2	Only temporal classification . . . . .	102
<b>6</b>	<b>Conclusion - Future work</b>	<b>107</b>
6.1	Conclusion . . . . .	107
6.2	Future work . . . . .	107
	<b>Bibliography</b>	<b>109</b>



# Κατάλογος Πινάκων

2.1	Ordered by confidence predictions and their precision and recall values . . . . .	44
3.1	Recall results for both datasets using IoU and mIoU metrics . . . . .	59
3.2	Recall results after adding fixed time duration anchors . . . . .	61
3.3	Recall results after converting cuboids into sequences of frames . . . . .	63
3.4	Recall performance using 3 different feature maps as Regressor's input and 2 pooling methods . . . . .	64
3.5	Recall results using 2nd approach for anchors . . . . .	65
3.6	Recall performance when using a 3D Convolutional Layer in Regressor's architecture	67
3.7	Recall performance when using a 2D Convolutional Layer instead of 3D in Regressor's model . . . . .	68
3.8	Recall results when reducing sample duration to 4 and 8 frames per video segment	68
3.9	Recall results when a regressor and sample duration equal with 4 or 8 frames per video segment . . . . .	69
4.1	Recall results for step = 8 . . . . .	76
4.2	Recall results for step = 12 . . . . .	76
4.3	Recall results for steps = 14, 15 and 16 . . . . .	77
4.4	Recall results for step = 4 . . . . .	77
4.5	Recall results for steps = 6, 7 and 8 . . . . .	78
4.6	Recall results for UCF dataset . . . . .	79
4.7	Temporal Recall results for UCF dataset . . . . .	79
4.8	Spatio-temporal Recall results for UCF dataset . . . . .	80
4.9	Temporal Recall results for UCF dataset . . . . .	81
4.10	Spatio-temporal Recall results for UCF dataset . . . . .	81
4.11	Temporal Recall results for UCF dataset . . . . .	82
4.12	Spatio-temporal Recall results for UCF dataset using Soft-NMS . . . . .	82
4.13	Temporal Recall results for UCF dataset using SoftNMS . . . . .	82
4.14	Recall results for second approach with step = 8, 16 and their corresponding steps	84
4.15	Recall results for second approach with . . . . .	85
5.1	First classification results using Linear and RNN classifiers . . . . .	90
5.2	Our architecture's performance using 5 different policies and 2 different feature maps while pooling in tubes' dimension. With bold is the best scoring case . . .	91
5.3	Our architecture's performance using 2 different policies and 2 different pooling methods using modified Roi Align. . . . .	92
5.4	mAP results using temporal pooling for both RoiAlign approaches . . . . .	93

5.5	mAP results for policies 1,4 for sample duration = 16 . . . . .	93
5.6	RNN results . . . . .	94
5.7	Linear results . . . . .	95
5.8	SVM results . . . . .	95
5.9	RNN results for sample duration equal with 16 . . . . .	96
5.10	Linear results for sample duration equal with 16 . . . . .	97
5.11	MLP'smAP performance for regular training procedure . . . . .	98
5.12	mAP results for MLP trained using extracted features . . . . .	99
5.13	mAP results for SVM classifier after adding NMS algorithm . . . . .	99
5.14	mAP results for RNN classifier after adding NMS algorithm . . . . .	101
5.15	mAP results for Linear classifier after adding NMS algorithm . . . . .	101
5.16	mAP results for MLP classifier after adding NMS algorithm . . . . .	101
5.17	UCF's temporal localization mAP performance . . . . .	103
5.18	UCF's temporal localization recall and MABO performances . . . . .	104
5.19	Comparing TP and FP for both approaches . . . . .	104
5.20	UCF's temporal localization mAP performance . . . . .	105
5.21	UCF's temporal localization mAP performance for even smaller NMS threshold .	105

# Κατάλογος Σχημάτων

1.1 Examples of “Open” action . . . . .	23
2.1 Example of supervised Learning . . . . .	28
2.2 Example of unsupervised Learning . . . . .	28
2.3 Example of Reinforcement Learning . . . . .	29
2.4 An example of a single Neuron . . . . .	30
2.5 Plots of Activation functions . . . . .	31
2.6 An example of a Feedforward Neural Network . . . . .	32
2.7 Typical structure of a ConvNet . . . . .	33
2.8 Convolution with kernel of 3, stride of 2 and padding of 1 . . . . .	34
2.9 Example of Max pooling operation with a 2x2 filter and stride of 2 . . . . .	34
2.10 3D Convolution operation . . . . .	35
2.11 Region Proposal Network’s structure . . . . .	36
2.12 Anchors for pixel (320,320) of an image (600,800) . . . . .	36
2.13 Roi Pooling and Roi Align examples . . . . .	37
2.14 Example of bi-linear interpolation for calculation Roi Align’s final feature map .	38
2.15 Example of a situation where NMS algorithm will remove good proposals . . . . .	39
2.16 (a) and (b) show the behavior of cross-entropy loss and smooth-L1 respectively. .	41
2.17 Example of IoU scoring policy . . . . .	41
2.18 Precision/Recall curve . . . . .	44
2.19 Both P-R curves. Interpolated P-R curve has red col-our. . . . .	45
2.20 Recall versus MABO example . . . . .	46
3.1 Structure of the whole network . . . . .	54
3.2 At (a), (b) frame is its original size and at (c), (d) same frame after preprocessing part . . . . .	55
3.3 An example of the anchor $(x_1, y_1, t_1, x_2, y_2, t_2)$ . . . . .	56
3.4 Structure of TPN . . . . .	57
3.5 Groundtruth tube is coloured with blue and groundtruth rois with colour green .	57
3.6 TPN structure after adding 2 new layers, where k = 5n. . . . .	60
3.7 Structure of Regressor . . . . .	62
3.8 Structure of Regressor . . . . .	64
3.9 An example of the anchor $(x_1, y_1, x'_1, y'_1, x_2, y_2, \dots)$ . . . . .	65
3.10 The structure of TPN according to new approach . . . . .	66
3.11 3 Different candidate action tubes . . . . .	70
3.12 3 Different candidate action tubes . . . . .	71

4.1	An example of calculating connection score for 3 random TOIs taken from Hou, Chen, and Shah 2017 . . . . .	74
4.2	Example of connected tubes . . . . .	86
5.1	Structure of the whole network . . . . .	88
5.2	Types of RNN . . . . .	89
5.3	Structure of the MLP classifier . . . . .	97
5.4	Structure of the network with NMS . . . . .	100

# Chapter 1

## Introduction

Nowadays, the enormous increase of computing power help us deal with a lot of difficult situations appeared in our daily life. A lot of areas of science have managed to tackle with problems, which were considered non trivial 20 years ago. One of these areas is Computer Vision and an important problem is human action recognition and localization.

### 1.1 Problem statement

The area of human action recognition and localization has 2 main goals:

1. Automatically detect and classify any human activity, which appears in a video.
2. Automatically locate in the video, where the previous action is performed.

#### 1.1.1 Human Action Recognition

Considering human action recognition, a video may be consisted of only by 1 person doing something. However, this is an ideal situation. In most cases, videos contain multiple people, who perform multiple actions or may not act at all in some segments. So, our goal is not only to classify an action, but to determine the temporal boundaries of each action.

#### 1.1.2 Human Action Localization

Alongside with Human Action Recognition, another problem is to present spatial boundaries of each action. Usually, this means presenting a 2D bounding box for each video frame, which contains the actor. Of course, this bounding box moves alongside with the actor.

## 1.2 Applications

The field of Human Action Recognition and Localization has a lot of applications which include content based video analysis, automated video segmentation, security and surveillance systems, human-computer interaction.

The huge availability of data (especially of videos) creates the necessity to find ways to take advantage of them. About 2.5 billion images are uploaded at Facebook database every month, more than 34K hours of video in YouTube and about 5K images every minute. On top of that,

there are about 30 million surveillance cameras in US, which means about 700K video hours per day. All those data need to be separated in categories according to their content in order to search them more easily. This process takes place by hand, by a user who attaches keywords or tags to each video. However, most users avoid doing that, so many videos end up without any tagging information. This situation creates the need to create algorithms for automated indexing based on the content of the video.

Another application is video summary. This area takes place usually in movies or sports events. In movies, video analysis algorithms can create a small video containing all the important moments of the movie. This can be achieved by choosing video segments where an important action takes place such as killing the villain of the movie. In sports events, video summary applications include creating highlight videos automatically, like a video containing all achieved goals in football match.

On top of that, human action recognition can replace human operators in surveillance systems. Until now, security systems include a system of multiple cameras handled by a human operator, who judges if a person is acting normally or not. Automatic action classification systems can act like human, and immediately judge if there is any human behavioral anomaly.

Last but not least, another field of application is related with human-computer interaction. Robotic applications help elderly people deal with their daily needs. Also, gaming applications using Kinect create new kinds of gaming experience without the need of a physical game controller.

### 1.3 Challenges and Datasets

There are various types of human activities. Depending on their complexity, we conceptually categorize human activities into four different levels: gestures, actions, interactions, and group activities. Gestures are elementary movements of a person's body part, and are the atomic components describing the meaningful motion of a person. "Stretching an arm" and "raising a leg" are good examples of gestures. Actions are single person activities that may be composed of multiple gestures organized temporally, such as "walking", "waving", and "punching". Interactions are human activities that involve two or more persons and/or objects. For example, "two persons fighting" is an interaction between two humans and "a person stealing a suitcase from another" is a human-object interaction involving two humans and one object. Finally, group activities are the activities performed by conceptual groups composed of multiple persons and/or objects. "A group of persons marching", "a group having a meeting", and "two groups fighting" are typical examples of them. The wide variety of human activities and applications creates a lot of challenges which involve action recognition systems. The most important challenges include large variations in appearance of the actors, camera view-point changes, occlusions, non-rigid camera motions etc. On top of that, a big problem is that there are too many action classes which means that manual collection of training sample is prohibitive. Also, some times, action vocabulary is not well defined. As figure 1.1 shows, "Open" action can include a lot of kinds of actions, so we must carefully choose which granularity of the action we will consider.

In order to deal with those challenges, several standard action datasets have been created in order to develop robust human action recognition systems and detection algorithms. The first datasets included 1 actor performing using a static camera over homogeneous backgrounds. Even though, those datasets helped us design the first action recognition algorithms, they were not able to deal with the above challenges. This led us to design datasets containing more ambiguous videos, such as Joint-annotated Human Motion Database(JHMDB) (Kuehne et al. 2011) and UCF-101 (Soomro, Zamir, and Shah 2012). These datasets contain only human actions, the



Figure 1.1: Examples of “Open” action

second category presented above.

### 1.3.1 JHMDB Dataset

The JHMDB dataset (Jhuang et al. 2013) is a fully annotated dataset for human actions and human poses. It is consisted of 21 action categories and 928 clips extracted from Human Motion Database (HMDB51) Kuehne et al. 2011. This dataset contains trimmed videos with duration between 15 to 40 frames. Each clip is annotated for each frame using a 2D pose and contains only 1 action. In order to train our model for action localization, we modify 2D poses into 2D boxes containing the whole pose in each frame. There are available 3 different splits for training data, proposed by the authors. We chose the first split which contains 660 videos for training set and 268 for validation .

### 1.3.2 UCF-101 Dataset

The UCF-101 dataset (Soomro, Zamir, and Shah 2012) contains 13320 videos from 101 action categories. From those, for 24 classes and 3194 video spatio-temporal annotations are included. This means that there is a 2D bounding box surrounding the actor for each frame in which an action is taking place. We separate dataset’s videos into 2284 videos for training set and 910 for validation test according to the first proposed training split. For training data, there are videos up to 641 frames, while in validation data max number of frames is 900. Each video, both training and validation, is untrimmed, including sometimes more than 1 actions taking place simultaneously. We took annotations from Singh et al. 2017 because those proposed by the authors contain some mistakes.

## 1.4 Motivation and Contributions

The current achievements in Object Recognition Networks and in 3D Convolution Networks for Action Recognition have triggered us to try to combine them in order to achieve state-of-the-art results for action localization. We introduce a new network structure inspired by Hou, Chen, and Shah 2017, Girdhar et al. 2017, Ren et al. 2015 and for implementation by Yang et al. 2017.

Our contributions are the following:

1. We create a new framework for action localization extending the code taken from faster RCNN implementation. Based on the structure proposed by Hou, Chen, and Shah 2017, we modified it, using a 3D Resnet34 instead of C3D, which previous approach used.

2. Furthermore, we proposed our own TPN Network, a Network for proposing candidate action tubes give a small video segment. Following the approach Hou, Chen, and Shah 2017 proposed, we firstly implement an architecture which uses cuboids as anchors, which then using a regressor it becomes a sequence of bounding boxes, likely to contain an action. We experiment with two candidate regressor's architecture and proposed and implement a 3D RoiAlign which uses trilinear interpolation for extracting each proposed action tube's activation maps. Inspired by Girdhar et al. 2017, we proposed and implement a TPN which uses predefined sequences of bounding boxes as 3D anchors. We proposed anchors that last equal with and less than video segment's duration in order our architecture to be able to perform temporal localization. we explore two different regressors' architectures for better spatial precision using activation maps extracted from 2D RoiAlign, treating each frame seperately.
3. Inspired by liniking algorithm proposed by Hou, Chen, and Shah 2017, we introduce our own linking algorithm, which uses a combination of actioness and overlap scores in order to decide if 2 proposed action tubes would connect or not and some updatable lists. Our approach includes gathering all candidate action tubes whose score is bigger than a threshold, and use them as active action tubes for new possible connections. When the number of gathered active action tube is bigger than a threshold, we keep the k-best scoring action tubes and remove the rest. We implement this algorithm using, also, CUDA code in order to calculate connection score faster. We proposed 3 versions of this algorith:
  - (a) An approach which uses an updatable scoring threshold, in order not to calculate unnecessary connection scores
  - (b) An approach which doesn't use an updatable scoring threshold, but it just updateds "active" action tube more frequently.
  - (c) An approach which, also, uses NMS or softmax-NMS algorithms for getting wider action tube proposals.
- Also, we implement, from scratch, another connection algorithm proposed by Hu et al. 2019 and extending it in order to work for ToIs instead of frames, which they proposed. We modified our TPN structure in order to calculate progression and progress rate scores in order to calculate connection scores and generate candidate action tubes.
4. We experiment using several classifier in order to find the most suitable. We considered 2 feature maps extracted using 3D RoiAlign and proposed action tubes, without any other modification. Also, we explore the different ratios and number of groundtruth foreground tubes that should be used during training stage. Finally, we tried to perform only temporal localization using temporal information generated from proposed action tubes.

## 1.5 Thesis structure

The rest of Thesis is organized as follows. Chapter 2 provides an general introduction to Machine Learning techniques currently used. After that, we present the basic elements of object recognition systems and alongside with loss functions and evaluation metrics that we used. Also, Chapter 2 presents an brief overview of literature on human action recognition and localization. Chapter 3 introduces the first basic element of our network, Tube Proposal Network (TPN), a network which proposes Tubes of Interest (ToIs), which are sequences of bounding boxes, with are likely to contain a performed action. Furthermore, it contains all the proposed architectures

for achieving this. Chapter 4 proposes algorithms for linking the proposed TOIs from every video segment and proposal performance is presented. In Chapter 5, we present all the classification approaches we used for designing our architecture and some classification results. Chapter 6 is used for conclusions, summary of our contribution alongside with possible future work.



# Chapter 2

## Background

### 2.1 Machine Learning

#### 2.1.1 Introduction

Machine Learning (ML) is a field which is raised out of Artificial Intelligence (AI). Applying AI, we wanted to build better and intelligent machines. But except for mere tasks such as finding the shortest path between point A and B, we were unable to program more complex and constantly evolving challenges. There was a realization that the only way to be able to achieve this task was to let machines learn from themselves. This sounds similar to a child learning from its self. So machine learning was developed as a new capability for computers. And now machine learning is present in so many segments of technology, that we don't even realize it while using it.

Finding patterns in data on planet earth is possible only for human brains. Data being very massive and time taken to compute them made Machine Learning take action, in order to help people exploit them in minimum time.

There are three kinds of Machine Learning Algorithms :

1. Supervised Learning
2. Unsupervised Learning
3. Reinforcement Learning

#### Supervised Learning

A majority of practical machine learning uses supervised learning. In supervised learning, the system tries to learn from the previous examples that are given. Speaking mathematically, supervised learning is where you have both input variables ( $x$ ) and output variables ( $Y$ ) and can use an algorithm to derive the mapping function from the input to the output. The mapping function is expressed as  $Y = f(x)$ .

As shown in Figure 2.1, we have initially taken some data and marked them as ‘Spam’ or ‘Not Spam’. This labeled data is used by the training supervised model, in order to train the model. Once it is trained, we can test our model by testing it with some new mails and checking if the model is able to predict the right output.

Supervised learning problems can be further divided into two parts, namely **classification**, and **regression**.

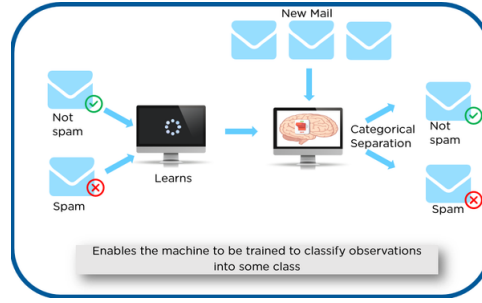


Figure 2.1: Example of supervised Learning

**Classification** : A classification problem is when the output variable is a category or a group, such as “black” or “white” or “spam” and “no spam”.

**Regression** : A regression problem is when the output variable is a real value, such as “Rupees” or “height.”

Some Supervised learning algorithms include:

- Decision trees
- Support-vector machine
- Naive Bayes classifier
- k-nearest neighbors
- linear regression

### Unsupervised Learning

In unsupervised learning, the algorithms are left to themselves to discover interesting structures in the data. Mathematically, unsupervised learning is when you only have input data ( $X$ ) and no corresponding output variables. This is called unsupervised learning because unlike supervised learning above, there are no given correct answers and the machine itself finds the answers. In Figure 2.2, we have given some characters to our model which are ‘Ducks’

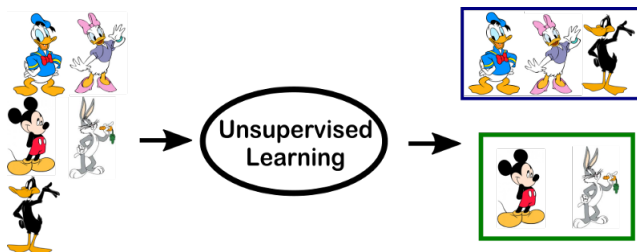


Figure 2.2: Example of unsupervised Learning

and ‘Not Ducks’. In our training data, we don’t provide any label to the corresponding data. The unsupervised model is able to separate both the characters by looking at the type of data and models the underlying structure or distribution in the data in order to learn more about

it. Unsupervised learning problems can be further divided into **association** and **clustering** problems.

**Association** : An association rule learning problem is where you want to discover rules that describe large portions of your data, such as “people that buy X also tend to buy Y”.

**Clustering** : A clustering problem is where you want to discover the inherent groupings in the data, such as grouping customers by purchasing behavior.

### Reinforcement Learning

A computer program will interact with a dynamic environment in which it must perform a particular goal (such as playing a game with an opponent or driving a car). The program is provided feedback in terms of rewards and punishments as it navigates its problem space. Using this algorithm, the machine is trained to make specific decisions. It works this way: the machine is exposed to an environment where it continuously trains itself using trial and error method. In

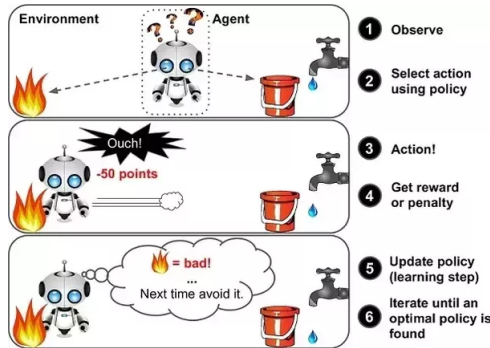


Figure 2.3: Example of Reinforcement Learning

Figure 2.3, we can see that the agent is given 2 options i.e. a path with water or a path with fire. A reinforcement algorithm works on reward a system i.e. if the agent uses the fire path then the rewards are subtracted and agent tries to learn that it should avoid the fire path. If it had chosen the water path or the safe path then some points would have been added to the reward points, the agent then would try to learn what path is safe and what path isn't

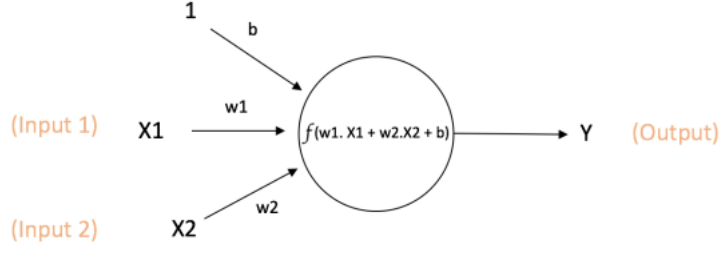
#### 2.1.2 Neural Networks

Neural Networks are a class of models within the general machine learning literature. Neural networks are a specific set of algorithms that have revolutionized the field of machine learning. They are inspired by biological neural networks and the current so called deep neural networks have proven to work quite very well. Neural Networks are themselves general function approximations, that is why they can be applied to literally almost any machine learning problem where the problem is about learning a complex mapping from the input to the output space.

#### 2.1.3 A single Neuron

The basic unit of computation in a neural network is the neuron, often called a **node** or **unit**. It receives input from some other nodes, or from an external source and computes an output. In purely mathematical terms, a neuron in the machine learning world is a placeholder for a

mathematical function, and its only job is to provide an output by applying the function on the inputs provided. Each input has an associated weight ( $w$ ), which is assigned on the basis of its relative importance to other inputs. The node applies a function  $f$  (*defined below*) to the weighted sum of its inputs as shown in Figure 2.4. The network takes numerical inputs  $X_1$  and  $X_2$  and



$$\text{Output of neuron} = Y = f(w_1 \cdot X_1 + w_2 \cdot X_2 + b)$$

Figure 2.4: An example of a single Neuron

has weights  $w_1$  and  $w_2$  associated with those inputs. Additionally, there is another *input 1* with weight  $b$  (called *Bias*) associated with it. The main function of Bias is to provide every node with a trainable constant value (in addition to the normal inputs that the node receives). The output  $Y$  from the neuron is computed as shown in the Figure 2.4. The function  $f$  is non-linear and is called **Activation Function**. The purpose of the activation function is to introduce non-linearity into the output of a neuron. This is important because most real world data are non linear and we want neurons to learn these non-linear representations.

### Activation Functions

Every activation function (or non-linearity) takes a single number and performs a certain fixed mathematical operation on it. There are several activation functions:

**Sigmoid** : takes a real-valued input and squashes it to range between 0 and 1. Its formula is:

$$\sigma(x) = \frac{1}{1 + e^{-x}}$$

It is easy to understand and apply but it has major reasons which have made it fall out of popularity:

- Vanishing gradient problem
- Its output isn't zero centered. It makes the gradient updates go too far in different directions.
- Sigmoids saturate and kill gradients.
- Sigmoids have slow convergence.

**Tanh** : takes a real-valued input and squashes it to the range  $[-1, 1]$ . Its formula is:

$$\tanh(x) = 2\sigma(2x) - 1$$

Now it's output is zero centered because its range in between -1 to 1. Hence optimization is easier in this method and in practice it is always preferred over Sigmoid function . But still it suffers from Vanishing gradient problem.

**Re-LU** : Re-LU stands for *Rectified Linear Unit*. It takes a real-valued input and thresholds it at zero (replaces negative values with zero). So its formula is:

$$f(x) = \max(0, x)$$

It has become very popular in the past couple of years. It was recently proved that it had 6 times improvement in convergence from Tanh function. Seeing the mathematical form of this function we can see that it is very simple and efficient . A lot of times in Machine learning and computer science we notice that most simple and consistent techniques and methods are only preferred and are best. Hence it avoids and rectifies vanishing gradient problem . Almost all deep learning Models use ReLU nowadays.

Figure 2.5 show each of the above activation functions.

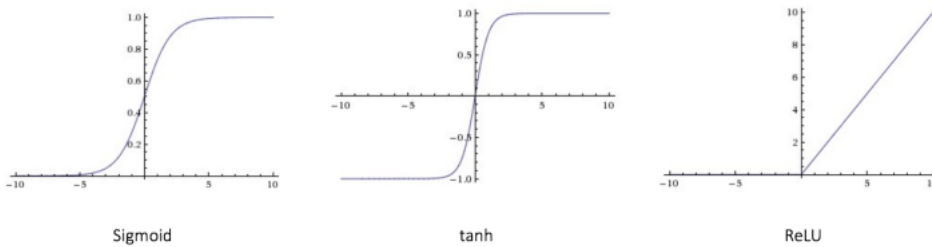


Figure 2.5: Plots of Activation functions

### Feed-forward Neural Network

Till now we have covered neuron and activation functions which together for the basic building blocks of any neural network. The feedforward neural network was the first and simplest type of artificial neural network devised. It contains multiple neurons (nodes) arranged in layers. A layer is nothing but a collection of neurons which take in an input and provide an output. Inputs to each of these neurons are processed through the activation functions assigned to the neurons. Nodes from adjacent layers have connections or edges between them. All these connections have weights associated with them. An example of a feedforward neural network is shown in Figure 2.6. A feedforward neural network can consist of three types of nodes:

**Input Nodes** The Input nodes provide information from the outside world to the network and are together referred to as the “Input Layer”. No computation is performed in any of the Input nodes – they just pass on the information to the hidden nodes.

**Hidden Nodes** The Hidden nodes have no direct connection with the outside world (hence the name “hidden”). They perform computations and transfer information from the input nodes to the output nodes. A collection of hidden nodes forms a “Hidden Layer”. While a feedforward network will only have a single input layer and a single output layer, it can have zero or multiple Hidden Layers.

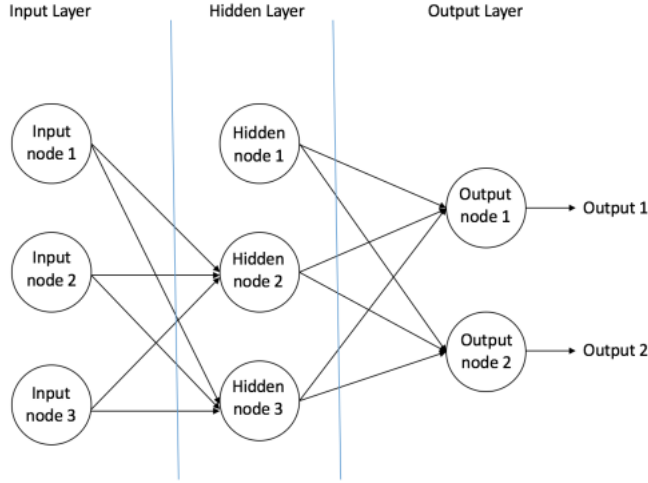


Figure 2.6: An example of a Feedforward Neural Network

**Output Nodes** The Output nodes are collectively referred to as the “Output Layer” and are responsible for computations and transferring information from the network to the outside world.

In a feedforward network, the information moves in only one direction – forward – from the input nodes, through the hidden nodes (if any) and to the output nodes. There are no cycles or loops in the network (this property of feed forward networks is different from Recurrent Neural Networks in which the connections between the nodes form a cycle). Another important point to note here is that each of the hidden layers can have a different activation function, for instance, hidden layer1 may use a sigmoid function and hidden layer2 may use a ReLU, followed by a Tanh in hidden layer3 all in the same neural network. Choice of the activation function to be used again depends on the problem in question and the type of data being used.

#### 2.1.4 2D Convolutional Neural Network

A Convolutional Neural Network (ConvNet/CNN) is one of the variants of neural networks used heavily in the field of Computer Vision. It derives its name from the type of hidden layers it consists of. The hidden layers of a CNN typically consist of convolutional layers, pooling layers, fully connected layers, and normalization layers. Here it simply means that instead of using the normal activation functions defined above, convolution and pooling functions are used as activation functions. It can take in an input image, assigning importance (learning weights and biases) to various aspects/objects in the image and be able to differentiate one from the other. The pre-processing required in a ConvNet is much lower as compared to the other classification algorithms. While in primitive method filters are hand-engineered, with enough training, ConvNets have the ability to learn these filters/characteristics.

The architecture of a ConvNet is analogous to that of the connectivity pattern of Neurons in the Human Brain and was inspired by the structure of the Visual Cortex. However, most ConvNets consist mainly in 2 parts:

- **Feature extractor :**

This part of the network takes as input the image and extract features that are meaningful

for its classification. It amplifies aspects of the input that are important for discrimination and suppresses irrelevant variations. Usually, the feature extractor consists of several layers. For instance, an image which could be seen as an array of pixel values. The first layer often learns representation that represent the presence or absence of edges at particular orientations and locations in the image. The second layer typically detects motifs by spotting particular arrangements of edges, regardless of small variations in the edge positions. Finally, the third may assemble motifs into larger combinations that correspond to paths of familiar objects, and subsequent layers would detect objects as combinations of these parts.

- **Classifier :**

This part of the network takes as input the previously computed features and use them to predict the correct label.

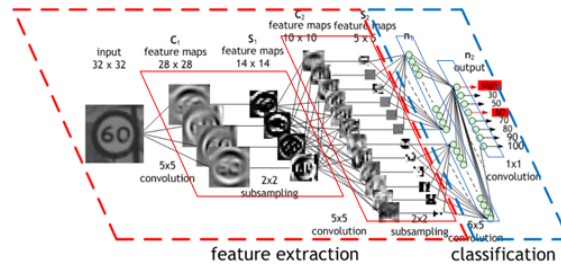


Figure 2.7: Typical structure of a ConvNet

**Convolutional Layers** In order to extract such features, ConvNets use 2D convolution operations. These operations take place in convolutional layers. Convolutional layers consist of a set of learnable filters. Every filter is small spatially (along width and height), but extends through the full depth of input. During forward pass, we slide (more precisely, convolve) each filter across the width and height of the input volume and compute dot products between the entries of the filter and the input at any position (as Figure 2.8 shows). The objective of the Convolution Operation is to extract the high-level features such as edges, from the input image. ConvNets need not be limited to only one Convolutional Layer. Conventionally, the first ConvLayer is responsible for capturing the Low-Level features such as edges, color, gradient orientation, etc. With added layers, the architecture adapts to the High-Level features as well, giving us a network which has the wholesome understanding of images in the dataset, similar to how we would.

**Pooling Layers** Pooling Layers are also referred as downsampling layers and are used to reduce the spatial dimensions, but not depth, on a convolution neural network. The intuitive reasoning behind this layer is that once we know that a specific feature is in the original input volume (there will be a high activation value), its exact location is not as important as its relative location to the other features. The main advantages of pooling layer are:

- We gain computation performance since the amount of parameters is reduced.
- Less parameters also means we deal with overfitting situations.



Figure 2.8: Convolution with kernel of 3, stride of 2 and padding of 1

The pooling operation is specified, rather than learned. Two common functions used in the pooling operation are:

**Average Pooling** Calculate the average value for each patch on the feature map.

**Maximum Pooling (or Max Pooling)** Calculate the maximum value for each patch of the feature map.

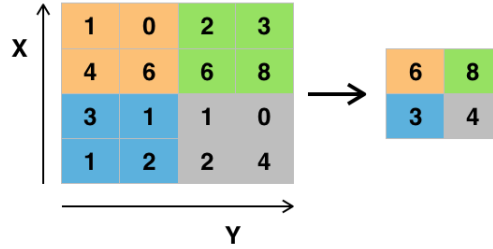


Figure 2.9: Example of Max pooling operation with a 2x2 filter and stride of 2

### 2.1.5 3D Convolutional Neural Network

Traditionally, ConvNets are targeting RGB images (3 channels). The goal of 3D CNN is to take as input a video and extract features from it. When ConvNets extract the graphical characteristics of a single image and put them in a vector (a low-level representation), 3D ConvNets extract the graphical characteristics of a set of images. 3D CNNs takes in to account a temporal dimension (the order of the images in the video). From a set of images, 3D CNNs find a low-level representation of a set of images, and this representation is useful to find the right label of the video (a given action is performed). In order to extract such features, 3D ConvNets use 3D convolution operations, whose kernel shape for a 3D Convolution is specified along 3 dimensions. When thinking about the convolution operation in terms of a kernel sliding across a multidimensional input array, for a 3D Convolution, the kernel slides in 3 directions. Their output shape is a 3 dimensional volume space such as cube or cuboid.

Also, such 3D relationship is important for some applications, such as in 3D segmentations / reconstructions of biomedical imagining, e.g. CT and MRI where objects such as blood vessels meander around in the 3D space.

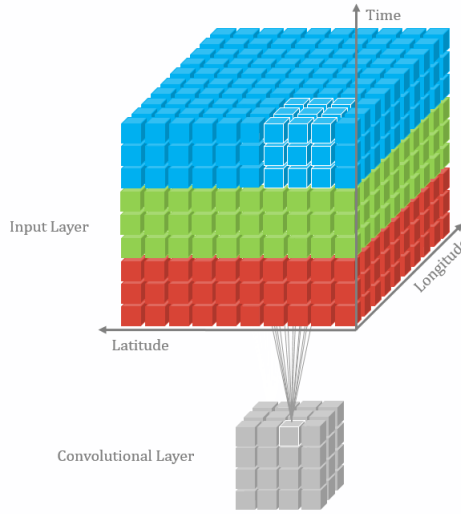


Figure 2.10: 3D Convolution operation

## 2.2 Object Detection

Within the field of Deep Learning, the sub-discipline called “Object Detection” involves processes such as identifying the objects through a picture, video or a webcam feed. The challenge of detecting all objects existing in image in counterpart of action localization in videos and a lot of object detection techniques are used in action localization architectures, so it is worth presenting it. Object Detection methods are used almost everywhere these days. The use cases are endless such as Tracking objects, Video surveillance, Pedestrian detection etc. An object detection model is trained to detect the presence and location of multiple classes of objects. For example, a model might be trained with images that contain various pieces of fruit, along with a label that specifies the class of fruit they represent (e.g. an apple, a banana, or a strawberry), and data specifying where each object appears in the image.

The main process followed by most of CNN for Object Detection is:

1. Firstly, we do feature extraction using as backbone network, the first Convolutional Layers of a known pre-trained CNN such as AlexNet, VGG, ResNet etc.
2. Then, we propose regions of interest (ROI) in the image. These regions contain possibly an object, which we are looking for.
3. Finally, we classify each proposed ROI.

### 2.2.1 Region Proposal Network

From the 3 above steps, the 2nd step is considered to be very important. That is because, in this step, we should choose regions of the image, which will be classified. Poor choice of ROIs means that the CNN will pass by some object that are located in the image, because, they were not be proposed to be classified.

The first Object-Detection CNNs use several algorithms for proposing ROIs. For example, R-CNN(Girshick et al. 2013), and Fast R-CNN(Girshick 2015) used Selective Search Algorithm for

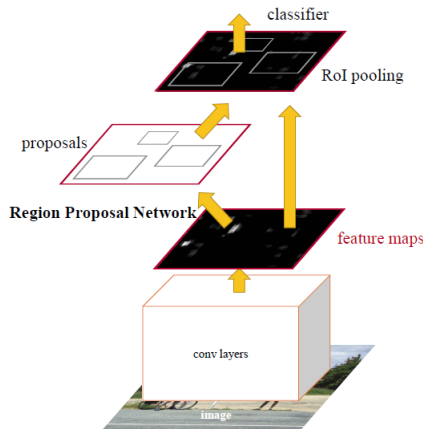


Figure 2.11: Region Proposal Network's structure

extracting ROIs. One of novelties introduced by the Faster R-CNN(Ren et al. 2015) is **Region Proposal Network** (RPN). Its function is to propose ROIs and its structure can be shown in 2.11. As we can see, RPN is consisted of:

- 1 2D Convolutional Layer
- 1 score layer
- 1 regression layer

Before describing RPN's function, we introduce another basic element of RPN which is its **anchors**. Anchors are predefined boxes used for extracting ROIs. In figure 2.12 is depicted an example of some anchors

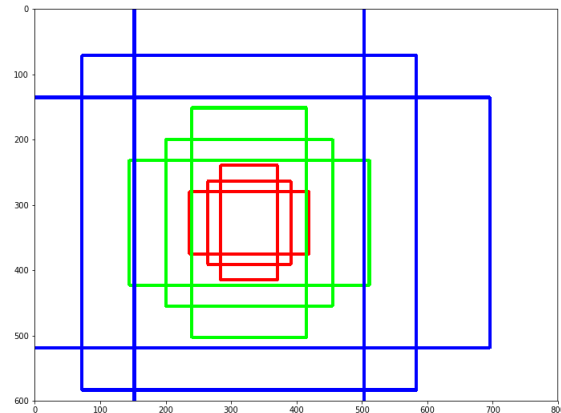


Figure 2.12: Anchors for pixel (320,320) of an image (600,800)

For each feature map's pixel corresponds  $k$  ( $k=9$ ) anchors (3 different scales and 3 different ratios 1:1, 1:2, 2:1).

So, RPN's procedure is:

1. RPN gets as input feature maps extracted from the backbone CNN.
2. Then it performs 2D convolution over this input and passes the output to its scoring layer and regression layer.
3. Scoring layer produces confidence score of existing an object in each anchor's area. On the other hand, regression layer outputs 4k displacements, 4 for each anchor. Finally, we keep as output only the *n-best scoring* anchors.

### 2.2.2 Roi Align

The biggest problem facing Object Detection Networks is the need for fixed input size. Classification networks require a fixed input size, which is easy for image classification because it is handled by resizing the input image. However, in object recognition architectures, each proposal has a different size and shape. This creates the need for converting all proposals to a fixed shape. At Fast-RCNN(Girshick 2015) and Faster-RCNN(Ren et al. 2015) methods, this operation happens by applying Roi Pooling. However, this wrapping is digitalized because the cell boundaries of the target feature map are forced to realign with the boundary of the input feature maps as shown in Figure 2.13a (the top left diagram). As a result, each target cells may not be in the same size (Figure 2.13c).

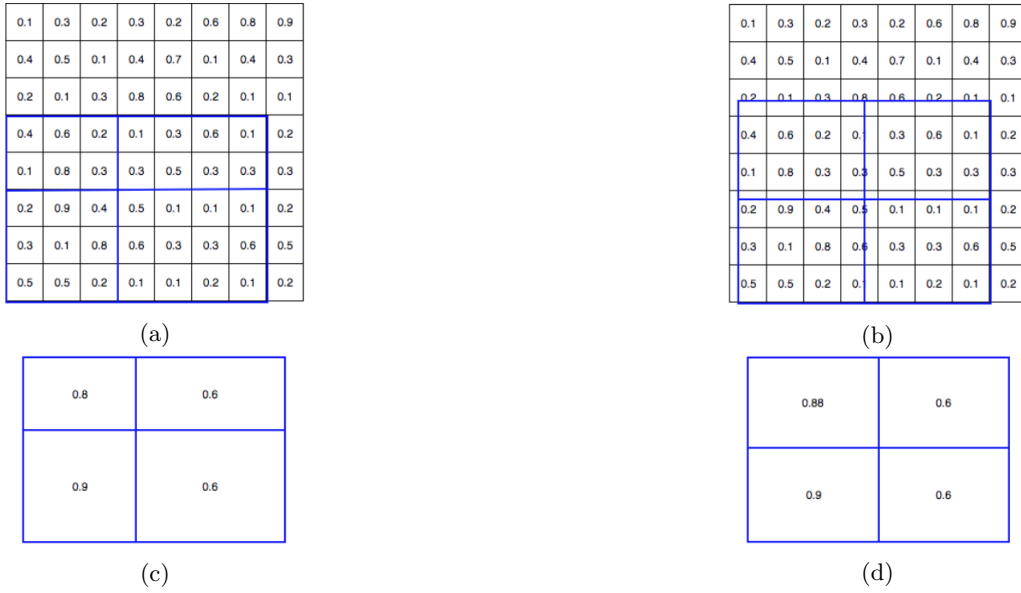


Figure 2.13: Roi Pooling and Roi Align examples

On the other hand, Mask-RCNN (He et al. 2017b) introduced Roi Align operation. Roi Align avoids digitalizing the boundary of the cells as shown in Figure 2.13b, and achieves to make every target cell to have the same size according to Figure 2.13d. In order to calculate feature maps values, Roi Align uses bi-linear interpolation as shown in Figure 2.14. This means that we calculate the value of the desired bins according to their neighbors'.

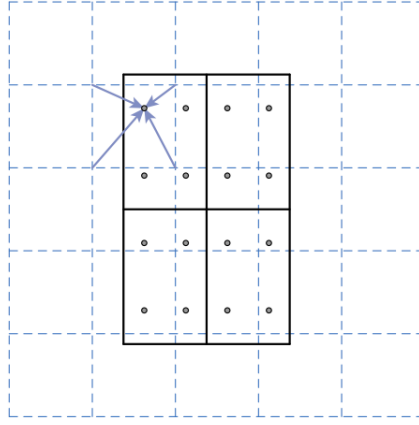


Figure 2.14: Example of bi-linear interpolation for calculation Roi Align’s final feature map

### 2.2.3 Non-maximum suppression (NMS) algorithm

Another problem that object detection networks face is that neighbor bounding boxes have similar scores to some extent. Most object detection systems employ a sliding window or a Region Proposal Network for proposing areas in the image that is likely to contain an object. These techniques, which return several areas in the images, achieve high recall performance. However, in these approaches, more than 1 proposal may be related with only one ground-truth object coordinates. This situation creates the need for choosing the best proposals, because, alternatively, hundreds of unnecessary proposals will be classified. For that reason, Non-Maximum Suppression (NMS) algorithm was proposed for filtering these proposals base on some criteria. NMS gets as input a list of proposal bounding boxes  $B$ , their corresponding confidence score  $S$  and an overlap threshold  $N$  and return as output a list of the final filtered proposals  $D$ . NMS algorithm’s steps are:

1. Initialize an empty list  $D$ . Select the proposal with the highest confidence score, remove it from  $B$  and add it to  $D$ .
2. Calculate the overlap score between this proposal and all the other proposals. For all the proposals that their overlap score is bigger than  $N$ , remove from  $B$ .
3. From the remaining proposals, picked again the one with the highest score and remove it from  $B$ .
4. Repeat steps 2 and 3 until no more proposals are left in list  $B$ .

The aforementioned algorithm shows that the whole process depends mostly on a single threshold value. So that makes the selection of threshold a crucial factor for the performance of the model. In some situations, bad choice of the threshold may make the network to remove bounding boxes with good confidence score, if there are side by side. Figure 2.15 shows a situation like this, where red and blue boxes will be removed because of the presence of the black box.

#### Soft NMS

A simple and efficient way to deal the aforementioned situation is to use Soft-NMS algorithm, which is presented in Bodla et al. 2017. Soft-NMS algorithm is based on the idea of reducing

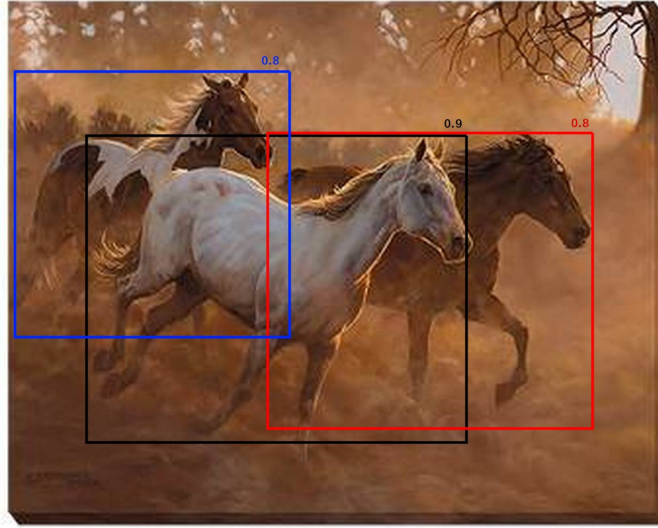


Figure 2.15: Example of a situation where NMS algorithm will remove good proposals

confidence score of the proposals proportional to their overlap score, instead of completely removing them. The score calculation follows the formula

$$s_i = \begin{cases} s_i, & \text{overlapscore}(M, b_i) < N_t \\ s_i(1 - \text{overlapscore}(M, b_i)), & \text{overlapscore}(M, b_i) \geq N_t \end{cases}$$

where  $s_i$  is the score of proposal  $i$ ,  $b_i$  is the box coordinates of proposal  $i$ ,  $M$  is the coordinates of the box with the maximum confidence and  $N_t$  is the overlap threshold. Let's, again, consider as input a list of proposal bounding-boxes  $B$ , their corresponding confidence score  $S$  and as output a list of proposals  $D$ . Soft-NMS algorithm includes the following steps:

1. Select the proposal with the highest confidence score, remove it from  $B$  and add it to  $D$ .
2. Calculate the overlap score between this proposal and all the other proposals. For all the proposals that their overlap score is bigger than  $N$ , recalculate their confidence score according to previous formula.
3. From the remaining proposals, picked again the one with the highest score and remove it from  $B$ .
4. Repeat steps 2 and 3 until no more proposals are left in list  $B$ .

## 2.3 Losses and Metrics

In order to train our model and check its performance, we use some known Loss functions and Metrics used in Object Detection systems.

### 2.3.1 Losses

For training our network, we use **Cross Entropy Loss** for classification layers and **smooth L1-loss** for bounding box regression in each frame and their diagram is show at Figure 2.16.

### Cross Entropy Loss

Cross-entropy loss, or log loss, measures the performance of a classification model whose output is a probability value between 0 and 1.

Entropy is the measure of uncertainty associated with a given distribution  $q(y)$  and its formula is:

$$H = - \sum_{i=1}^n p_i \cdot \log p_i$$

Intuitively, entropy tells us how “surprised” we are when some event E happened. When we are sure about an event E to happen ( $p_E = 1$ ) we have 0 entropy (we are not surprised) and vice versa.

On top of that, let’s assume that we have 2 distributions, one known (our network’s distribution)  $p(y)$  and one unknown (the actual data’s distribution)  $q(y)$ . Cross-entropy tells us how accurate is our known distribution in predicting the unknown distribution’s results. Respectively, Cross-entropy measures how accurate is our model in predicting the test data. Its formula is:

$$H_p(q) = - \sum_{c=1}^C q(y_c) \cdot \log(p(y_c))$$

### Smooth L1-loss

Smooth L1-loss can be interpreted as a combination of L1-loss and L2-loss. It behaves as L1-loss when the absolute value of the argument is high, and it behaves like L2-loss when the absolute value of the argument is close to zero. It is usually used for doing box regression on some object detection systems like Fast-RCNN(Girshick 2015), Faster-RCNN(Ren et al. 2015) and it is less sensitive to outliers according to Girshick 2015. As shown in Girshick 2015, its formula is:

$$\text{smooth}_{L1}(x) = \begin{cases} 0.5x^2 & \text{if } x < 1 \\ |x| - 0.5 & \text{otherwise} \end{cases}$$

It is similar to Huber loss whose formula is:

$$L_\delta(x) = \begin{cases} \frac{1}{2}a^2 & \text{for } |a| \leq \delta \\ \delta(|a| - \frac{1}{2}\delta), & \text{otherwise} \end{cases}$$

if we set  $\delta$  parameter equal 1.

Smooth L1-loss combines the advantages of L1-loss (steady gradients for large values of  $x$ ) and L2-loss (less oscillations during updates when  $x$  is small). Figure 2.16b shows a comparison between L1-norm, L2-norm and smooth-L1 .

### 2.3.2 Metrics

Evaluating our machine learning algorithm is an essential part of any project. The way we choose our metrics influences how the performance of machine learning algorithms is measured and compared. They influence how to weight the importance of different characteristics in the results and finally, the ultimate choice of classification algorithm. Most of the times we use classification accuracy to measure the performance of our model, however it is not enough to truly judge our model.

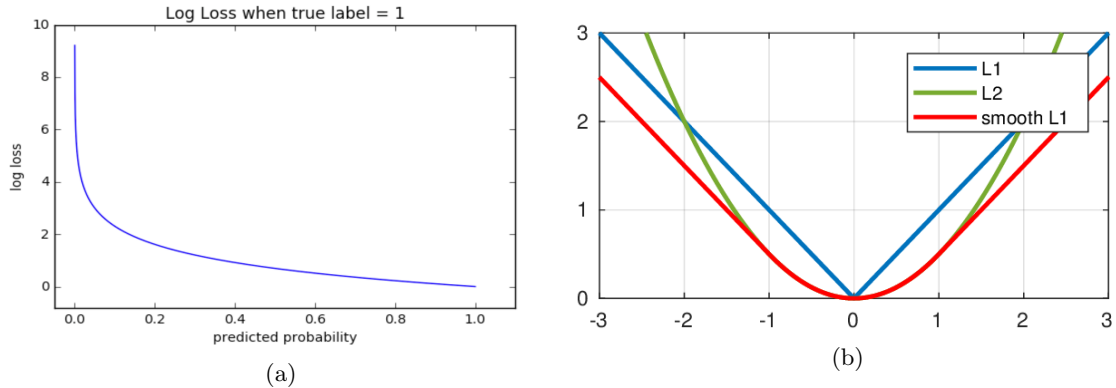


Figure 2.16: (a) and (b) show the behavior of cross-entropy loss and smooth-L1 respectively.

At first, we introduce some basic evaluation metrics in order, then, to present those we use for our assessment.

### Intersection over Union

The first and most important metric that we use is Intersection over Union (IoU). IoU measures the overlap between 2 boundaries. It is usually used in Object Recognition Networks in order to define how good overlap a predicted bounding box with the actual bounding box as shown in Figure 2.17. We predefine an IoU threshold (say 0.5) in classifying whether the prediction is a true positive or a false positive.



Figure 2.17: Example of IoU scoring policy

Intersection over Union is defined as:

$$IoU = \frac{\text{area of overlap}}{\text{area of union}}$$

In Figure 2.17, spatial IoU between 2 bounding boxes,  $(x_1, y_1, x_2, y_2)$  and  $(x_3, y_3, x_4, y_4)$ , is presented, which means IoU metric is implemented for x-y dimensions. Area of overlap and area of union can be defined as:

$$\text{Area of overlap} = \|(min(x_2, x_4) - max(x_1, x_3), min(y_2, y_4) - max(y_1, y_3))\|$$

$$\text{Area of union} = \|(max(x_2, x_4) - min(x_1, x_3), max(y_2, y_4) - min(y_1, y_3))\|$$

On top of that, we can implement IoU for 1 dimension and for 3 dimensions.

**1D IoU** We can name 1D IoU as temporal overlap. Let's consider 2 temporal segments  $(t_1, t_2)$  and  $(t_3, t_4)$ , between which we want to estimate their overlap score. Their IoU can be described as:

$$\text{Length of overlap} = \|(min(t_2, t_4) - max(t_1, t_3))\|$$

$$\text{Length of union} = \|(max(t_2, t_4) - min(t_1, t_3))\|$$

**3D IoU** 3-dimensional Intersection over Union which can, also, be named as spatiotemporal IoU, can be defined by 2 ways:

**3D boxes are cuboids** In this case, 3D boxes can be written as  $(x, y, z, x', y', z')$ . So, the IoU overlap between 2 boxes,  $(x_1, y_1, z_1, x_2, y_2, z_2)$  and  $(x_3, y_3, z_3, x_4, y_4, z_4)$ , is defined as:

$$\text{Volume of overlap} = \|(min(x_2, x_4) - max(x_1, x_3), min(y_2, y_4) - max(y_1, y_3), min(z_2, z_4) - max(z_1, z_3))\|$$

$$\text{Volume of union} = \|(max(x_2, x_4) - min(x_1, x_3), max(y_2, y_4) - min(y_1, y_3), max(z_2, z_4) - min(z_1, z_3))\|$$

**x-y are continuous and z discrete** In this case 3D boxes is defined as a sequence of 2D boxes  $(x, y, x', y')$ . For this definition, z-dimension is discrete, and IoU can be defined with 2 ways, which both result in the same overlapping score. Let's consider 2 sequences of boxes, with temporal limits  $(t_1, t_2)$  and  $(t_3, t_4)$ . We calculate their IoU following one of the following methods:

1. IoU is the product between temporal-IoU and the average spatial-IoU between 2D boxes in the overlapping temporal area and it is described as:

$$IoU = IoU((t_1, t_2), (t_3, t_4)) \cdot \frac{1}{K_2 - K_1} \sum_{i=K_1}^{K_2} IoU(X_1^i, X_2^i)$$

where

- $K_1 = min(t_2, t_4)$
- $K_2 = max(t_1, t_3)$
- $X_1^i = (x_1^i, y_1^i, x_2^i, y_2^i)$  and  $X_2^i = (x_3^i, y_3^i, x_4^i, y_4^i)$

2. IoU is the average spatial-IoU if we consider 2D boxes as  $(0, 0, 0, 0)$  if  $t \notin [t_{start}, t_{finish}]$  and it is written as:

$$IoU = \frac{1}{K} \sum_{i=min(t_1, t_3)}^{max(t_2, t_4)} IoU(X_1^i, X_2^i)$$

- $K = max(t_2, t_4) - min(t_1, t_3)$
- $X_1 = (x_1, y_1, x_2, y_2)$  if  $i \in [t_1, t_2]$  or  $(0, 0, 0, 0)$  if  $i \notin [t_1, t_2]$
- $X_2 = (x_3, y_3, x_4, y_4)$  if  $i \in [t_3, t_4]$  or  $(0, 0, 0, 0)$  if  $i \notin [t_3, t_4]$

From above implementations, we are involve mostly with temporal and spatiotemporal IoU.

### Precision & Recall

In order to describe **precision** and **recall** metrics, we will use an example. Let's consider a group of people in which, some of them are sick and the others are not. We use a network which, given some data as input, is able to predict if a person is sick or not.

**Precision** measures how accurate are our model's predictions, i.e. the percentage of predictions that are correct. In our case, how accurate is our model when it predicts that a person is sick.

**Recall** measures how well we found all the sick people. In our case, how many of the actual sick people we managed to find.

Their definitions are:

$$\text{Precision} = \frac{TP}{TP + FP}$$

$$\text{Recall} = \frac{TP}{TP + FN}$$

where

- TP = True positive, which means that we predict a person to be sick and he is actually sick.
- TN = True negative, we predict that a person isn't sick and he isn't.
- FP = False positive, we predict a person to be sick but he isn't actually.
- FN = False negative, we predict a person not to be sick but he actually is.

From these 2 metrics we use recall metric in order to evaluate our networks performance, and more specifically, its performance on finding good action tube proposals. We consider a groundtruth action as true positive when there is at least 1 proposed action tube that its IoU overlap score is bigger than a predefined threshold. If there is no such action tube, then we consider this groundtruth action tube as false negative.

### mAP

Precision and recall are single-value metrics based on the whole list of predictions. By looking their formulas, we can see that there is a trade-off between precision and recall performance. This trade-off can be adjusted by the softmax threshold, used in model's final layer. In order to have high precision performance, we need to decrease the number of FP. But this will lead to decrease recall performance and vice-versa.

As a result, these metrics fail to determine if a model is performing well in object detection tasks as well as action detection tasks. For that reason, we use mean Average Precision (mAP) metric, which for videos is named video-AP as introduced by Gkioxari and Malik 2014.

**AP (Average precision)** Before defining mAP metric, we will define Average Precision metric (AP). AP is a popular metric in measuring the accuracy of object detectors like Faster R-CNN, SSD, etc. Average precision computes the average precision value for recall value over 0 to 1. As mentioned before, during classification stage, our prediction results in True positive(TP), False positive(FP), True Negative(TN) or False Negative(FN). For object recognition and action localization networks, we don't care about TN. We consider a prediction as True positive when

our prediction (an bounding box for object detection network or a sequence of bounding boxes in action localization networks) overlaps with the groundtruth bounding box/action tube over a predefined threshold, and our predicted class is the same as groundtruth's. In addition, we consider a False Negative when either no detection overlaps with the groundtruth bounding box/action tube or our prediction's class label was incorrect. We consider a prediction as False positive, when more than one predictions overlap with the groundtruth. In this situation, we consider the prediction with the biggest confidence score as TP and the rest as FP.

For a class, we need to calculate, first, its precision and recall scores in order to calculate its AP score. We sort our predictions according to their confidence score and for each new prediction we calculate precision and recall values. An example, for a class containing 4 TP and 8 predictions is shown at Table 2.1. Precision and recall are calculated according to the number of elements that are above in the order. So, for rank #3, Precision is calculated as the proportion of TP = 2/3 = 0.67 and Recall as the proportion of TP out of all the possible TP = 2/4 = 0.5.

Rank	Prediction	Precision	Recall
1	Correct	1.0	0.25
2	Correct	1.0	0.5
3	False	0.67	0.5
4	False	0.5	0.5
5	False	0.4	0.5
6	Correct	0.5	0.75
7	False	0.42	0.75
8	Correct	0.5	1

Table 2.1: Ordered by confidence predictions and their precision and recall values

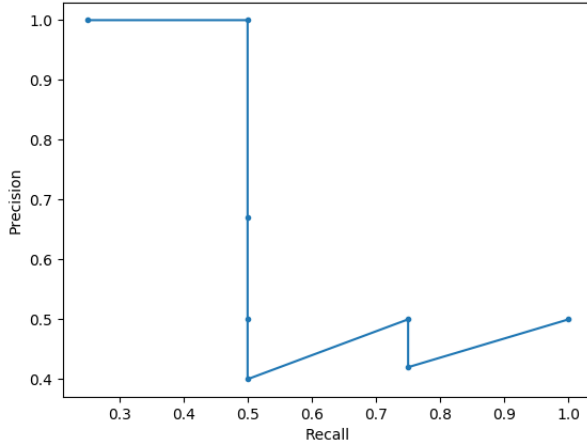


Figure 2.18: Precision/Recall curve

We plot Precision against Recall and their curve is shown in Figure 2.18. The general definition for Average Precision(AP) is finding the area under the precision-recall curve and its formula is:

$$AP = \int_0^1 p(r)dr$$

Precision and Recall values  $\in [0, 1]$ , so AP  $\in [0, 1]$ , too. This integral can be replaced with a finite, as we have a finite number of predictions. So its formula is:

$$AP = \sum_{k=1}^n P(k) \Delta r(k)$$

where  $P(k)$  is the precision until prediction  $k$  and  $\Delta r$  is the change in recall from  $k - 1$  to  $k$ .

**Interpolated Precision** As we can see at Figure 2.18, P-R curve has a zigzag pattern as it goes down with false predictions, and goes up with correct. So, before calculation AP, we need to smooth out this zigzag pattern using Interpolated precision, as introduced in Everingham et al. 2010. Interpolated precision is calculated at each recall level  $r$  by taking the maximum precision measured for that  $r$  and it is defined as:

$$p_{interp}(r) = \max_{\tilde{r}: \tilde{r} \geq r} p(\tilde{r})$$

where  $p(\tilde{r})$  is the measured precision at recall  $\tilde{r}$ . Graphically, at each recall level, we replace each precision value with the maximum precision value to the right of that recall level. At Figure 2.19 are shown both P-R curves. The previous P-R curve has blue color and the interpolated has red color.

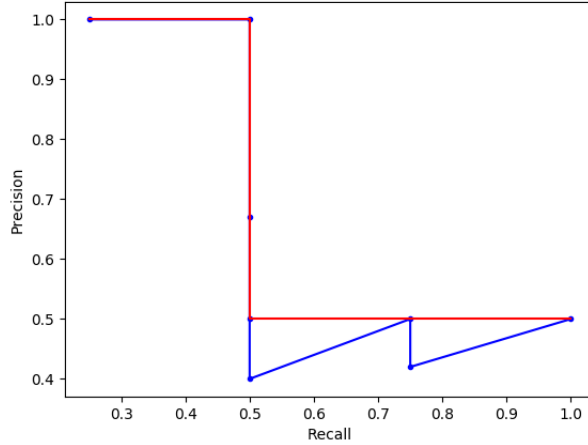


Figure 2.19: Both P-R curves. Interpolated P-R curve has red colour.

In order to calculate AP, we sample the curve at all unique recalls values, whenever the maximum precision drops. On top of that, we define mean Average Precision (mAP) the mean of the AP for each class. So, AP and mAP are defined as

$$AP = \sum (rn + 1 - r_n) p_{interp}(r_{n+1})$$

$$p_{interp}(r_{n+1}) = \max_{\tilde{r} \geq r_{n+1}} p(\tilde{r})$$

$$mAP = \frac{1}{N} \sum_{i=1}^N AP_i$$

### Mean Average Best Overlap - MABO

In order to evaluate the quality of our proposals, both during TPN and connecting tube stages, recall metric isn't enough. That's because recall metric tells us only for how many actual objects/action tubes, there was at least 1 proposal that satisfied the detection criterion. However, it doesn't tell us how close these proposals are to the actual objects/action tubes. In order to quantify this performance, Mean Average Best Overlap (MABO) was introduced by Winschel, Lienhart, and Eggert 2016. The importance of MABO can be clarified we consider figure 2.20.

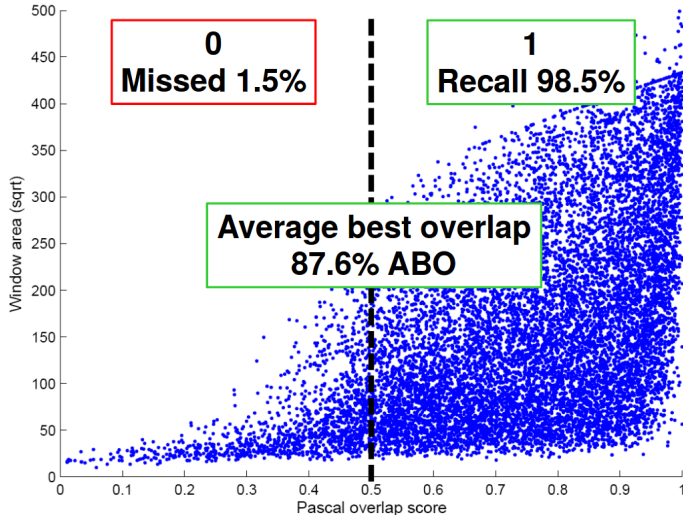


Figure 2.20: Recall versus MABO example

As we can see, recall performance is almost perfect, but, MABO performance, which tells us where most proposal overlap scores are gathered, is just fine and not perfect.

In order to define MABO, we need first to define Average Best Overlap. Let  $c \in C$  denote a class  $c$  from the set of all classes  $C$  and  $G^c$  the set of ground truth annotations of this class in all images; let  $L$  be the set of all generated object proposals for all images. Average Best Overlap is defined as the average value of the maximum overlap score, (in our situation, we use intersection over union) of  $L$  with each groundtruth annotation  $g \in G^c$ . The Mean Average Best Overlap (MABO) is defined as the average value of all class ABO values :

$$MABO = \frac{1}{|C|} \sum_{c \in C} \left[ \frac{1}{|G^c|} \sum_{g \in G^c} \max_{l \in L} IoU(g, l) \right]$$

In our situation, which we care only for the quality of our proposals, we consider only 1 class, foreground class. As a result, MABO's performance identifies with ABO's.

## 2.4 Related work

In this section, we present some of the most relevant methods to our work and others studied for designing this approach. These methods are divided into two sections: *action recognition* and *action localization*. The first part refers to classic action classification methods introduced until recently and the second part, respectively, to recent action localization methods.

### 2.4.1 Action Recognition

First approaches for action classification consisted of two steps a) compute complex handcrafted features from raw video frames such as SIFT, HOG, ORB features and b) train a classifier based on those features. These features can be separated into 3 categories: 1) space-time volume approaches, 2) trajectories and 3) space-time features. For space-time volume methods the approach is as follows: based on the training videos, the system constructs a 3D space-time model, by concatenating 2D images (x-y dimension) along time (t or z dimension), in order to represent each action. When system is given an unlabeled video, it constructs a 3D space-time volume corresponding to this video. This new 3D volume, then, is compared with each activity model to measure the similarity in shape and appearance between these two volumes. The system extracts the class label of the unknown video by corresponding to the action with the highest similarity. Furthermore, there are several variations of space-time representations. Instead of volume representation, the system may represent the action as trajectories in space-time dimensions or even more, the action can be represented as a set of features extracted from the volume or the trajectories. Pure space-time volume representations include methods of comparing foreground regions of a person (i.e. silhouettes) like Bobick and Davis 2001 did, comparing volumes in terms of their patches like Shechtman and Irani 2005. Ke, Sukthankar, and Hebert 2007 method uses oversegmented volumes, automatically calculating a set of 3-D XYT volume segments that corresponds to a moving human. Rodriguez, Ahmed, and Shah 2008 proposed filters for capturing volume's characteristics, in order to match them more reliably and efficiently. From the other hand, trajectory-based approaches include representing an action as a set of 13 joint trajectories (Sheikh, Sheikh, and Shah 2005) or using a set of XYZT-dimensions joint trajectories obtained from moving cameras (Yilmaz and Shah 2005). Finally, several methods use local features extracted from 3-dimensional space-time volumes, like extracting local features at every frame and concatenate them temporally (Chomat and Crowley 1999; Zelnik-Manor and Irani 2001; Blank et al. 2005, extracting sparse spatiotemporal local interest points from 3D volumes (Laptev and Lindeberg 2003; Dollar et al. 2005; Niebles, Wang, and Li 2006; Alper Yilmaz and Mubarak Shah 2005; Ryoo and Aggarwal 2006) These approaches made the choice of features a significant factor for network's performance. That's because different action classes may appear dramatically different in terms of their appearance and motion patterns. Another problem was that most of those approaches make assumptions about the circumstances under which the video was taken due to problems such as cluttered background, camera viewpoint variations etc. A review of the techniques, used until 2011, is presented in Aggarwal and Ryoo 2011.

Recent results in deep architectures and especially in image classification motivated researchers to train CNN networks for the task of action recognition. The first significant attempt was made by Karpathy et al. 2014. They designed their architecture based on the best-scoring CNN in the ImageNet competition. They explored several methods for fusion of spatiotemporal features using 2D operations mostly and 3D convolution only in slow fusion. Simonyan and Zisserman 2014 used a 2 CNNs, one for spatial information and one for optical flow and combined them using late fusion. They show that extracting spatial context from videos and motion context from optical flow can improve significantly action recognition accuracy. Feichtenhofer, Pinz, and Zisserman 2016 extend this approach by using early fusion at the end of convolutional layers, instead of late fusion which takes places at the last layer of the network. On top that, they used a second network for temporal context which they fuse with the other network using late fusion. Furthermore, Wang et al. 2016 based their method on Simonyan and Zisserman 2014, too. They deal with the problem of capturing long-range temporal context and training their network given limited training samples. Their approach, which they named Temporal Segment

Network (TSN), separates the input video in K segments and a short snippet from each segment is chosen for analysis. Then they fuse the extracted spatiotemporal context, making, eventually, their prediction. Most recently, Zhang et al. 2016 and Zhu et al. 2017 used two-stream approach, too. Zhang et al. 2016 replace optical flow with motion vector which can be obtained directly from compressed videos without extra calculation and feeding it to . Zhu et al. 2017 trained a CNN for calculating optical flow, calling it MotionNet and use a temporal stream cnn for project motion information to action labels. Finally, they use late fusion through the weighted averaging of the prediction scores of the temporal and spatial streams. On the other hand, a novel approach was introduced by Girdhar and Ramanan 2017 incorporating attention maps to give significant improvement in action recognition performance

Some other methods included a RNN or LSTM network for classification like Donahue et al. 2014, Ng et al. 2015 and Ma et al. 2017. Donahue et al. 2014 address the challenge of variable lengths of input and output sequences, exploiting convolutional layers and long-range temporal recursions. They propose a Long-term Recurrent Convolutional Network (LRCN) which is capable of dealing with the tasks of action Recognition, image caption and video description. In order to classify a given sequence of frames, LRCN firstly gets as input a frame, and in particular its RGB channels and optical flow and predicts a class label. After that, it extracts video class by averaging label probabilities, choosing the most probable class. Ng et al. 2015 firstly explore several approaches for temporal feature pooling. These techniques include handling video frames individually by 2 CNN architectures: either AlexNet or GoogleNet, and consisted of early fusion, late fusion of a combination between them. Furthermore, they propose a recurrent neural Network architecture in order to consider video clips as a sequences of CNN activations. Proposed LSTM takes an input the output of the final CNN layer at each consecutive video frame and after five stacked LSTM layers using a Softmax classifier, it proposes a class label. For video classification, they return a label after last time step, max-pool the predictions over time, sum predictions over time and return the max or linearly weight the predictions over time by a factor g, sum them and return the max. They showed that all approaches are 1% different with a bias for using weighting predictions for supporting the idea that LSTM becomes progressively more informed. Last but not least, Ma et al. 2017 use a two-stream ConvNet for feature extraction and either a LSTM or convolutional layers over temporally-constructed feature matrices, for fusing spatial and temporal information. They use a ResNet-101 for extracting feature maps for both spatial and temporal streams. They divide video frames in several segments like Wang et al. 2016 did, and use a temporal pooling layer to extract distinguished features. Taken these features, LSTM extracts embedded features from all segments.

Additionally, Tran et al. 2014 explored 3D Convolutional Networks (Ji, Yang, and Yu 2013) and introduced C3D network which has 3D convolutional layers with kernels  $3 \times 3 \times 3$ . This network is able to model appearance and motion context simultaneously using 3D convolutions and it can be used as a feature extractor, too. Combining Two-stream architecture and 3D Convolutions, Carreira and Zisserman 2017 proposed I3D network. On top of that, the authors emphasize in the advantages of transfer learning for the task of action recognition by repeating 2D pre-trained weights in the 3rd dimension. Hara, Kataoka, and Satoh 2017 proposed a 3D ResNet Network for action recognition based on Residual Networks (ResNet) (He et al. 2015) and explore the effectiveness of ResNet with 3D Convolutional kernels. On the other hand, Diba et al. 2017 based their approach on DenseNets(Huang, Liu, and Weinberger 2016) and extend DenseNet architecture by using 3D filters and pooling kernels instead of 2D, naming this approach as DenseNet3D. Futhermore, they introduce Temporal Transition Layer (TTL), which concatenates temporal feature-maps extracted at different temporal depth ranges and replaces DenseNet's transition layer. On top of that Diba et al. 2018 introduced a new temporal layer that models variable temporal Convolution kernel depths. Last but not least, Tran et al.

2017 experiment with several residual network architectures using combinations of 2D and 3D convolutional layer. Their purpose is to show that a 2D spatial convolution followed by a 1D temporal convolution achieves state of the art classification performance, naming this type of convolution layer as R(2+1)D. Recently Guo et al. 2018 proposed a framework which can learn to recognize a previous unseen 3D action class with only a few examples by exploiting the inherent structure of 3D data through a graphical representation. A more detailed presentation for Action Recognition techniques used until 2018 is included in Kong and Fu 2018.

#### 2.4.2 Action Localization

As mentioned before, Action Localization can be seen as an extention of the object detection problem. Instead of outputing 2D bounding boxes in a single image, the goal of action localization systems is to output action tubes which are sequences of bounding boxes that contain an performed action. So, there are several approaches including an object-detector network for single frame action proposal and a classifier.

First object detection approaches included extending a object proposal algorithm into 3-dimensions. Tian, Sukthankar, and Shah 2013 extended deformable part models (Felzenszwalb et al. 2010) by treating actions as spatiotemporal patterns and generate a deformable part for each action. Jain et al. 2014 introduced the concept of tubelets, aka sequences of bounding boxes and based their method on selective search algorithm (Uijlings et al. 2013), extending super-pixels to super-voxels for producing spatiotemporal shapes. On the other hand, Oneata et al. 2014 extend a randomized superpixel merging procedure which was used for object proposals as presented by Manen, Guillaumin, and Gool 2013. Yu and Yuan 2015 first propose bounding boxes for each frame using a human and motion detector and then by picking the best-scoring bounding boxes, they proposed a greedy linking algorithm by formulating likng task as a maximum set coverage problem. Gemert et al. 2015 generate spatiotemporal proposals directly from dense trajectories, which also used for classification. Chen and Corso 2015 create a spatiotemporal trajectory graph and select action proposals based only on intentional movement extracted from the graph. Soomro, Idrees, and Shah 2015 seperate the video segments into supervoxels and use their context as a spatial relation between supervoxels relative to foreground action. They create a graph for each video, where supervoxels form thenodes and directed edges capture the spatial relations between them.During testing, they perform a context walk where each step is guided by the context relations learned during training, resulting in a probability distribution of an action over all the supervoxels. Mettes, Gemert, and Snoek 2016, instead of annotating boxes in all frames, annotate points on a sparse subset of video frames, and use proposals obtained by an overlap measure between action proposals and points. Behl et al. 2017 deal with online action detection and localization by getting per-frame action proposal and proposing a linking algorithm which is able to construct and update action tubes at each frame.

The introduction of R-CNN (Girshick et al. 2013) achieve significant improvement in the performance of Object Detection Networks. This architecture, firstly, proposes regions in the image which are likely to contain an object and then it classifies them using a SVM classifier. Inspired by this architecture, Gkioxari and Malik 2014 design a 2-stream RCNN network in order to generate action proposals for each frame, one stream for frame level and one for optical flow. Then they connect them using the viterbi connection algorithm. Weinzaepfel, Harchaoui, and Schmid 2015 extend this approach, by performing frame-level proposals and using a tracker for connecting those proposals using both spatial and optical flow features. Also their method performs temporal localization using a sliding window over the tracked tubes. Most recently, Soomro and Shah 2017 tried to deal with the problem of unsupervised action detection and localization. Their approach included extracting supervoxel segmentation and then assigning a

weight to each supervoxel. Using extracted supervoxels, they create a graph and then using a discriminative clustering approach a classifier is trained.

The introduction of Faster RCNN (Ren et al. 2015) contribute a lot to the improvement of the performance of Action Localization Networks Peng and Schmid 2016, Saha et al. 2016 and use Faster R-CNN instead of RCNN for frame-level proposals, using RPN for both RGB and optical flow images. After getting spatial and motion proposals, Peng and Schmid 2016 fuse them exploring and from each proposed ROI, generate 4 ROIs in order to focus in specific body parts of the actor. After that, they connect the proposal using Viterbi algorithm for each class and perform temporal localization by using a sliding window, with multiple temporal scales and stride using a maximum subarray method. From the other hand, Saha et al. 2016 perform, too, frame-level classification. After that, their method performs fusion based on a combination between the actionness scores of the appearance and motion based proposals and their overlap score. Finally, temporal localization takes place using dynamic programming. On the other hand, Weinzaepfel, Martin, and Schmid 2016 use Faster RCNN for extracting human tubes from videos focusing on weakly-supervised action localization problem. Then using dense trajectories and a multi-fold Multiple Instance Learning approach (Cinbis, Verbeek, and Schmid 2016) train a classifier. Mettes and Snoek 2017 introduced a method for zero-shot action localization. Their approach includes scoring proposed action tubes according to the interactions between actors and local objects. They used Faster-RCNN, in the first step, for detecting both actors and objects and then using spatial relations between them they link the proposed boxes over time based on zero-shot likelihood from the presence of actors, relevant objects around the actors and the expected spatial relations between objects and actors. Furthermore, He et al. 2017a proposed the Tube Proposal Network (TPN) for generating generic class-independent tubelet proposals, which uses Faster-RCNN for getting 2D region proposals and a linking algorithm for linking tubelets with these region proposals. Most recently, Girdhar et al. 2018 proposed a method for action Localization on the AVA dataset (Gu et al. 2017) combining I3D (Carreira and Zisserman 2017) and Faster-RCNN architectures. They use I3D blocks for getting video representation and Fast-RCNN's RPN for generation “person” proposals for the center frame.

On top of that, Singh et al. 2017 and Kalogeiton et al. 2017 design their networks based on the Single Shot Multibox Detector Liu et al. 2015). Singh et al. 2017 created an online real-time spatiotemporal network. In order their network to execute real-time, Singh et al. 2017 propose a novel and efficient algorithm by adding boxes in tubes in every frame if they overlap more than a threshold, or alternatively, terminate the action tube if for k-frames no box was added. Kalogeiton et al. 2017 designed a two-stream network, which they called ACT-detector, and introduced anchor cuboids. For K frames, for both networks, Kalogeiton et al. 2017 extract spatial features in frame-level, then they stack these features. Finally, using cuboid anchors, the network extracts tubelets, that is a sequence of boxes, with their corresponding classification scores and regression targets. For linking the tubelets, Kalogeiton et al. 2017 follow about the same steps as Singh et al. 2017 did. For temporal localization, they use a temporal smoothing approach.

Most recently, YOLO Network (Redmon et al. 2015) became the inspiration for Hu et al. 2019 and El-Nouby and Taylor 2018. In Hu et al. 2019, concepts of progression and progress rate were introduced. Except from proposing bounding boxes in frame level, they use YOLO together with a RNN classifier for extracting temporal information for the proposals. Based on this information, they create action tubes, separated into classes. Some other approaches include pose estimation like Luvizon, Picard, and Tabia 2018 do. They proposed a method for calculating 2D and 3D poses and then they performed action classification. They use the differentiable Soft-argmax function for estimating 2D and 3D joints, because argmax function is not differentiable. Then, for T adjacent poses, they create an image representation with time and  $N_j$  joints as  $x - y$  dimensions

and having 2 channels for 2D poses and 3 channels for 3D poses. They use Convolutional Layers in order to produce action heats and then using max plus min pooling and a Softmax activation they perform action classification. Zolfaghari et al. 2017 proposed a three-stream architecture which includes 2D pose, optical flow and RGB information. These streams are integrated sequentially via a Markov chain model. In addition, Zhu, Vial, and Lu 2017 proposed an architecture using a temporal convolutional regression network, for capturing the long-term dependency and contexts among adjacent frames, and a spatial regression network, getting per-frame proposals. They use tracking methods and dynamic programming for generating action proposals.

Most of aforementioned networks use per-frame spatial proposals and extract their temporal information by calculating optical flow. On the other hand, Saha, Singh, and Cuzzolin 2017 and Hou, Chen, and Shah 2017 design an architecture which includes proposal in video segment level, handling more than 1 frame simultaneously. Saha, Singh, and Cuzzolin 2017 proposed a 3D-RPN which is able to generate and classify 3D region proposals consisted of two successive frames. Also, they proposed a linking algorithm, modifying the one proposed by Saha et al. 2016. On top of that, Hou, Chen, and Shah 2017 design an architecture for generating action proposals for more than 2 frames, which they called Tube CNN (T-CNN). In their approach, video segment level means that the whole video is separated into equal length video clips, and using a C3D for extracting features, it returns spatiotemporal proposals. After getting proposals, Hou, Chen, and Shah 2017 link the tube proposals by an algorithm based on tubes' actionness score and overlap. Finally, classification operation is performed for the linked video proposals.



# Chapter 3

## Tube Proposal Network

### 3.1 Our implementation's architecture

In this chapter, we get involved with Tube Proposal Network(TPN), one of the basic elements of ActionNet. Before describing it, we present the whole structure of our model. We propose a network similar to Hou, Chen, and Shah 2017. Our architecture is consisted by the following basic elements:

- One 3D Convolutional Network, which is used for feature extraction. In our implementaion we use a 3D Resnet network which is taken from Hara, Kataoka, and Satoh 2018 and it is based on ResNet CNNs for Image Classification (He et al. 2015).
- Tube Proposal Network for proposing ToIs (based on the idea presented in Hou, Chen, and Shah 2017).
- A classifier for classifying proposed action video tubes.

The basic procedure ActionNet follows is:

1. Given a video, we seperate it into video segments. These video segments in some cases overlap temporally and in some others don't.
2. For each video segment, after performing spatiotemporal resizing, we feed its frames into ResNet34 in order to perform feature extraction. These activation maps are, next, fed into TPN for proposing sequences of bounding boxes. We name them Tubes of Interest (ToIs), like Hou, Chen, and Shah 2017, and are likely to contain a person performing an action.
3. After getting proposed ToIs for each video segment, using a linking algorithm, ActionNet finds final cancidate action tubes. These action tubes are given as input to a classifier in order to get their action class.

A diagram of ActionNet is shown at Figure 3.1.

### 3.2 Introduction to TPN

The main purpose of Tube Proposal Network (TPN) is to propose **Tube of Interest**(TOIs). These tubes are likely to contain an known action and are consisted of some 2D boxes (1 for

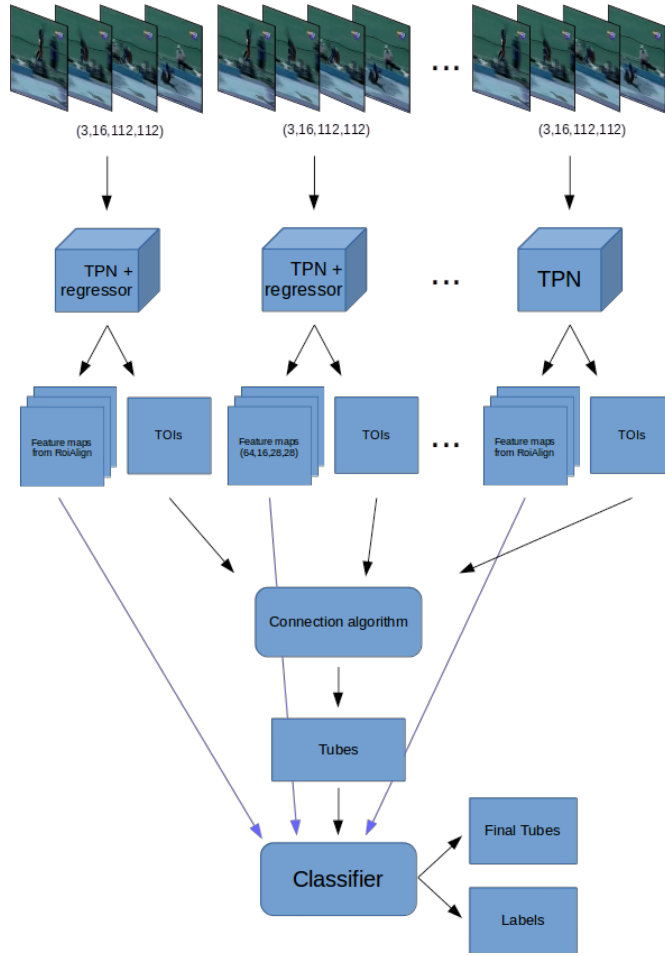


Figure 3.1: Structure of the whole network

each frame). TPN is inspired from RPN introduced by FasterRCNN (Ren et al. 2015), but instead of images, TPN is used in videos as performed by Hou, Chen, and Shah 2017. In full correspondence with RPN, the structure of TPN is similar to RPN. The only difference, is that TPN uses 3D Convolutional Layers and 3D anchors instead of 2D.

We designed 2 main structures for TPN. Each approach has a different definition of the used 3D anchors. The rest structure of the TPN is mainly the same with some little differences in the regression layer.

### 3.3 Preparation before TPN

#### 3.3.1 Preparing data

Before getting a video as input to extract its features and ToIs, this video has to be preprocessed. Preprocess procedure is the same for both approaches of TPN. Our architecture gets as input a sequence of frames which has a fixed width, height and duration. However, each video has different resolution. That's creates the need to resize each frame before feeding it to

the architecture. As mentioned in previous chapter, the first element of our network is a 3D RenNet taken from Hara, Kataoka, and Satoh 2018. This network is designed to get images with dimensions (112,112). As a result, we resize each frame from datasets' videos into (112,112) frames. In order to keep aspect ratio, we pad each frame either left and right, either above and bellow depending which dimension is bigger. In figure 3.2 we can see the original frame and the resize and padded one. In full correspondance, we resize the groundtruth bounding boxes for each frame (figure 3.2b and 3.2d show that).

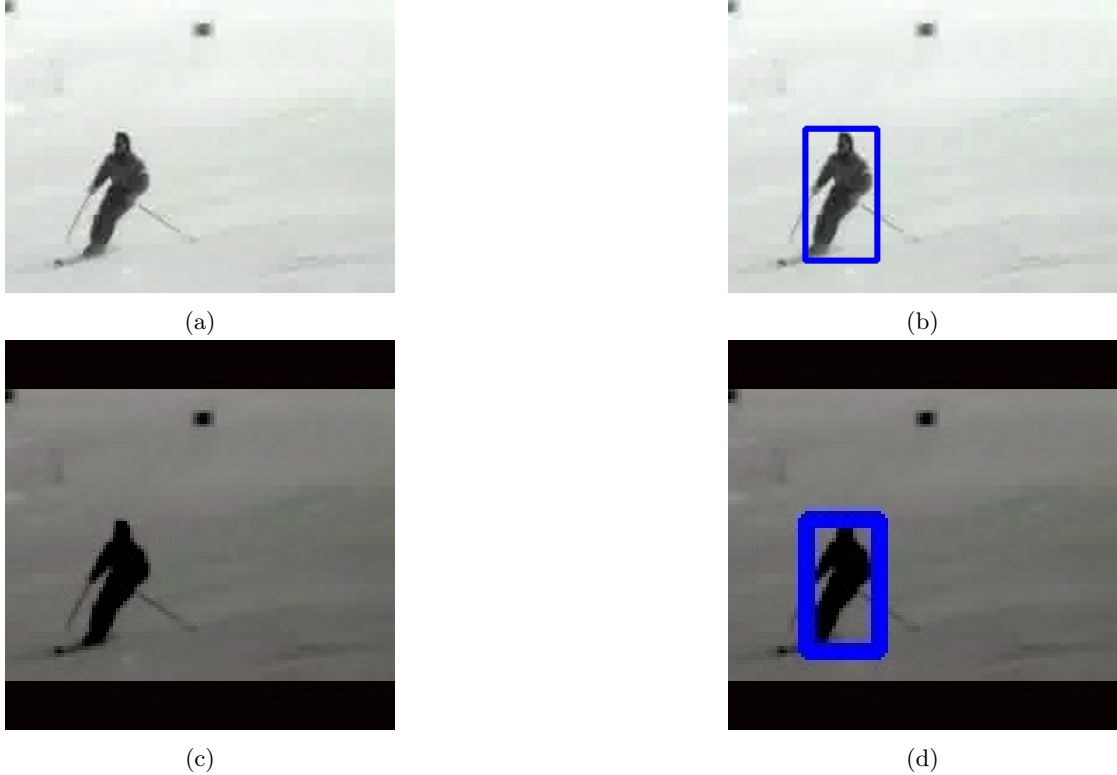


Figure 3.2: At (a), (b) frame is its original size and at (c), (d) same frame after preprocessing part

### 3.3.2 3D ResNet

Before using Tube Proposal Network, we extract spatio-temporal features from the video. In order to do so, we extract the 3 first Layers of a pretrained 3D ResNet34. This Network is pretrained in Kinetics dataset Kay et al. 2017 for sample duration equal with 16 frames and sample size equal with (112, 122).

This network normally is used for classifying the whole video, so some of its layers use temporal stride equal with 2. We set their temporal stride equal to 1 because we don't want to miss any temporal information during the process. So, the output of the third layer is a feature maps with dimesions (256,16,7,7). We feed this feature map to TPN, which is described in following sections.

## 3.4 3D anchors as 6-dim vector

### 3.4.1 First Description

We started desinging our TPN inspired by Hou, Chen, and Shah 2017. We consider each anchor as a 3D bounding box written as  $(x_1, y_1, t_1, x_2, y_2, t_2)$  where  $x_1, y_1, t_1$  are the upper front left coordinates of the cuboid and  $x_2, y_2, t_2$  are the lower back left as shown in figure 3.3.

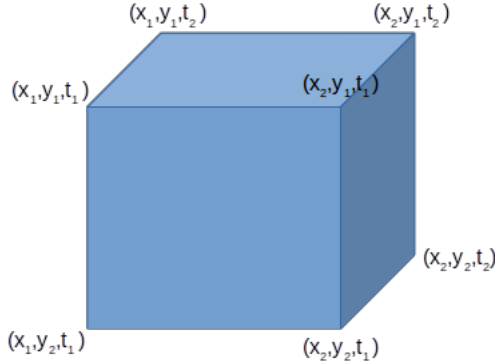


Figure 3.3: An example of the anchor  $(x_1, y_1, t_1, x_2, y_2, t_2)$

The main advantage of this approach is that except from x-y dims, dimension of time is mutable. As a result, the proposed TOIs have no fixed time duration. This will help us deal with untrimmed videos, because proposed TOIs would exclude background frames. For this approach, we use  $\mathbf{n = 4k = 60}$  anchors for each pixel in the feature map of TPN. We have  $k$  anchors for each anchor duration( 5 scales of 1, 2, 4, 8, 16, 3 aspect ratios of 1:1, 1:2, 2:1 and 4 durations of 16,12,8,4 frames). In Hou, Chen, and Shah 2017, network's anchors are defined according to the dataset most common anchors. This, however, creates the need to redesign the network for each dataset. In our approach, we use the same anchors for both datasets, because we want our network not to be dataset-specific but to be able to generalize for several datasets. As sample duration, we chose 16 frames per video segment because our pre-trained ResNet is trained for video clips with that duration. So the structure of TPN is:

- 1 3D Convolutional Layer with kernel size = 3, stride = 3 and padding = 1
- 1 classification layer outputs  $2n$  scores whether there is an action or not for  $n$  tubes.
- 1 regression layer outputs  $6n$  coordinates  $(x_1, y_1, t_1, x_2, y_2, t_2)$  for  $n$  tubes.

The structure of TPN is shown in figure 3.4. The output of TPN is the k-best scoring cuboids,which are most likely to contain an action.

### 3.4.2 Training

As mentioned before, TPN extracts TOIs as 6-dim vectors. For that reason, we modify out groundtruth ROIs to groundtruth Tubes. We take for granted that the actor cannot move a lot during 16 frames, so that's why we use this kind of tubes. As shown in figure 3.5, these tubes are 3D boxes which include all the groundtruth rois, which are different for each frame.

For training procedure, for each video, we randomly select a part of it which has duration 16 frames. We consider an anchor as foreground if its overlap score with a groundtruth action

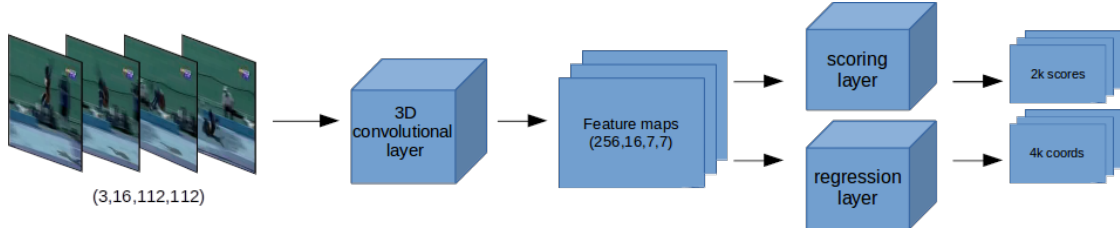


Figure 3.4: Structure of TPN

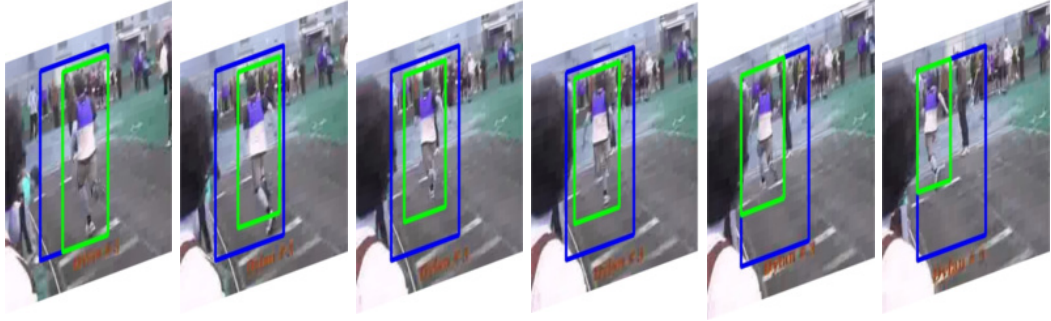


Figure 3.5: Groundtruth tube is coloured with blue and groundtruth rois with colour green

tube is bigger than 0.5. Otherwise, it is considered as background anchor. We use scoring layer in order to correctly classify those anchors and we use Cross Entropy Loss as loss function. We have a lot of anchors for proposing an action but a small number of per-video actions, so we choose 256 anchors in total for each batch. We set the maximum number of foreground anchors to be 25% of the 256 anchors and the rest are the background.

Classifying correctly an anchor isn't enough for proposing an action tube. It is also necessary, the anchors to overlap as much as possible with the groundtruth action tubes. That's the reason we use a regression layer. This layer "moves" the cuboid closer to the area that it is believed that is closer to the action. For regression loss we use smooth-L1 loss as proposed from Girshick et al. 2013. In order to calculate the regression targets, we use pytorch FasterRCNN implementation (Yang et al. 2017) for bounding box regression and we modified the code in order to extend it for 3 dimensions. So we have:

$$\begin{aligned}
 t_x &= (x - x_a)/w_a, & t_y &= (y - y_a)/h_a, & t_z &= (z - z_a)/d_a, \\
 t_w &= \log(w/w_a), & t_h &= \log(h/h_a), & t_d &= \log(d/d_a), \\
 t_x^* &= (x^* - x_a)/w_a, & t_y^* &= (y^* - y_a)/h_a, & t_z^* &= (z^* - z_a)/d_a, \\
 t_w^* &= \log(w^*/w_a), & t_h^* &= \log(h^*/h_a), & t_d^* &= \log(d^*/d_a),
 \end{aligned}$$

where  $x, y, z, w, h, d$  denote the 3D box's center coordinates and its width, height and duration. Variables  $x, x_a$ , and  $x^*$  are for the predicted box, anchor box, and groundtruth box respectively (likewise for  $y, z, w, h, d$ ). Of course, we calculate the regression loss only for the foreground anchors and not for the background, so at the most we will calculate 64 targets for each batch.

To sum up training procedure, we train 2 layers for our TPN, scoring and regression layers. The training loss includes the training losses obtained by these layers and its formula is:

$$L = \sum_i L_{cls}(p_i, p_i^*) + \sum_i p_i^* L_{reg}(t_i, t_i^*)$$

where:

- $L_{cls}$  is the Cross Entropy loss we use for classifying the anchors, with  $p_i$  is the predicted label,  $p_i^*$  is the groundtruth class and  $p_i, p_i^* \in \{0, 1\}$
- $L_{reg}$  is the smooth-L1 loss function, which is multiplied with  $p_i^*$  in order to be set active only when there is a positive anchor ( $p_i^* = 1$ ) and to be deactivated for background anchors ( $p_i^* = 0$ ).

### 3.4.3 Validation

Validation procedure is a bit similar to training procedure. We randomly select 16 frames from a validation video and we examine if there is at least 1 proposed TOI which overlaps  $\geq 0.5$  with each groundtruth action tube and we get recall score. In order to get good proposals, after getting classification scores and targets prediction from the corresponding layers, we use Non-Maximum Supresion (NMS) algorithm. We set NMS threshold equal with 0.7, and we keep the first 150 cuboids with the biggest score.

### 3.4.4 Modified Intersection over Union(mIoU)

During training, we get numerous anchors. We have to classify them as foreground anchors or background anchors. Foreground anchors are those which contain some action, and, respectively, background don't. As presented before, IoU for cuboids calculates the ratio between volume of overlap and volume of union. Intuitively, this criterion is good for evaluating 2 tubes if they overlap but it has one big drawback: it considers x-y dimesions to have same importance with time dimension, which we do not desire. That's because firstly we care to be accurate in time dimension, and then we can fix x-y domain. As a result, we change the way we calculate the Intesection Over Union. We calculate seperately the IoU in x-y domain (IoU-xy) and in t-domain (IoU-t). Finally, we multiply them in order to get the final IoU. So the formula for 2 tubes  $(x_1, y_1, t_1, x_2, y_2, t_2)$  and  $(x'_1, y'_1, t'_1, x'_2, y'_2, t'_2)$  is:

$$\begin{aligned} IoU_{xy} &= \frac{\text{Area of Overlap in x-y}}{\text{Area of Union in x-y}} \\ IoU_t &= \frac{\max(t_1, t'_1) - \min(t_2, t'_2)}{\min(t_1, t'_1) - \max(t_2, t'_2)} \\ IoU &= IoU_{xy} \cdot IoU_t \end{aligned}$$

The above criterion help us balance the impact of time domain in IoU. For example, let us consider 2 anchors:  $a = (22, 41, 1, 34, 70, 5)$  and  $b = (20, 45, 2, 32, 72, 5)$ . These 2 anchors in x-y domain have IoU score equal to 0.61. But they are not exactly overlaped in time dimension. Using the first approach we get 0.5057 IoU score and using the second approach we get 0.4889. So, the second criterion would reject this anchor, because there is a difference in time duration.

In order to verify our idea, we train TPN using both IoU and mIoU criterion for tube-overlapping. At Table 3.1 we can see the performance in each case for both datasets, JHMDB and UCF. Recall threshold for this case is 0.5 and during validation, we use regular IoU for defining if 2 tubes overlap.

Table 3.1 shows that modified-IoU give us slightly better recall performance only in UCF dataset. Thats reasonable, because JHMDB dataset uses trimmed videos so time duration doesn't affect a lot. So, from now own, during training we use mIoU as overlapping scoring policy.

Dataset	Criterion	Recall(0.5)
JHMDB	IoU	0.70525
	mIoU	0.7052
UCF	IoU	0.4665
	mIoU	0.4829

Table 3.1: Recall results for both datasets using IoU and mIoU metrics

### 3.4.5 Improving TPN score

After first test, we came with the idea that in a video lasting 16 frames, in time domain, all kind of actions can be separated in the following categories:

1. Action starts in the n-th frame and finishes after the 16th frame of the sampled video.
2. Action has already begun before the 1st frame of the video and ends in the n-th frame.
3. Action has already begun before the 1st frame of the video and finishes after the 16th video frame.
4. Action starts and ends in that 16 frames of the video.

On top of that, we noticed that most of actions, in our datasets, last more than 16 frame. So, we came with the idea to add 1 scoring layer and 1 regression layer which will proposed ToIs with fixed duration equal with sample duration (16 frames) and they will take into account the spatial information produced by activation maps. The new structure of TPN is shown in figure 3.6. After getting proposals from both scores, we concat them with ratio 1:1 between ToI extracted from those 2 subnetworks.

Our goal is to “compress” feature maps in temporal dimension in order to propose ToIs based only on the spatial information. So, we came with 2 techniques for doing such thing:

1. Use 3D Convolutional Layers with kernel size = (sample duration, 1,1), stride =1 and no padding for scoring and regression. This kernel “looks” only in the temporal dimension of the activation maps and doesn’t consider any spatial dependencies.
2. Get the average values from temporal dimension and then use a 2D Convolutional Layer for scoring and regression.

Training and Validation procedures remain the same. The only big difference is that now we have losses obtained from 2 different systems proposed ToIs. So, during validation, we, at first, concatenate proposed ToIs and, then, we follow the same procedure, which is calculating recall performance. For training loss, we have 2 different cross-entropy losses and 2 different smooth-L1 losses, each for every layer correspondingly. So training loss is, now, defined as :

$$L = \sum_i L_{cls}(p_i, p_i^*) + \sum_i L_{cls}(p_{fixed,i}, p_{fixed,i}^*) + \sum_i p_i^* L_{reg}(t_i, t_i^*) + \sum_i p_{fixed,i}^* L_{reg}(t_{fixed,i}, t_{fixed,i}^*) \quad (3.1)$$

where:

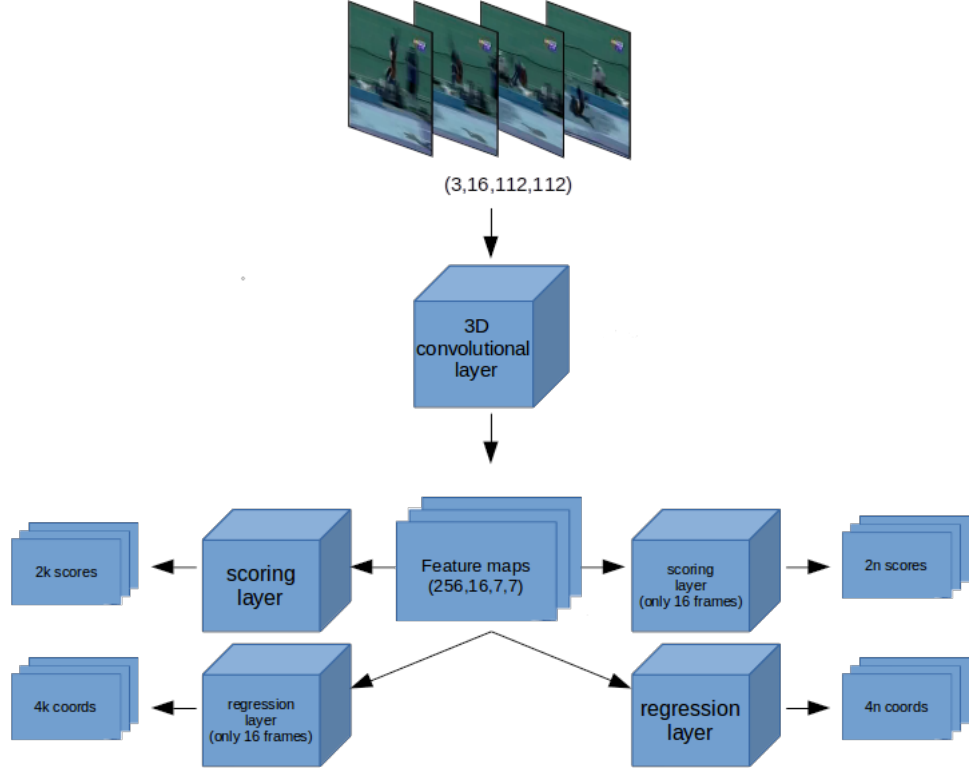


Figure 3.6: TPN structure after adding 2 new layers, where  $k = 5n$ .

- $L_{cls}$  is the Cross Entropy loss we use for classifying the anchors, with  $p_i$  is the predicted label,  $p_i^*$  is the groundtruth class and  $p_i, p_i^* \in \{0, 1\}$
- $L_{reg}$  is the smooth-L1 loss function, which multiply it with  $p_i^*$  in order to set active only when we have a positive anchor ( $p_i^* = 1$ ) and to be deactivated for background anchors ( $p_i^* = 0$ ).
- $p_i$  are the anchors from scoring and regression layers with mutable time duration and  $p_i^*$  are their corresponding groundtruth label.
- $p_{fixed,i}$  are the anchors from scoring and regression layers with fixed time duration = 16 and  $p_{fixed,i}^*$  are their corresponding groundtruth label.

We train our TPN Network using both techniques and their recall performance is show in Table 3.2.

As we can see from the previous results, the new layers increased recall performance significantly. On top of that, Table 3.2 shows that getting the average values from time dimension gives us the best results.

### 3.4.6 Adding regressor

The output of TPN is the  $\alpha$ -highest scoring anchors moved according to their regression prediction. After that, we have to turn the proposed anchors into ToIs. In order to do so, we

Dataset	Fix-time anchors	Type	Recall(0.5)
JHMDB	No	-	0.7052
	Yes	Kernel	0.6978
		Mean	0.7463
UCF	No	-	0.4829
		Kernel	0.4716
	Yes	Mean	0.4885

Table 3.2: Recall results after adding fixed time duration anchors

add a regressor system which gets as input cuboids' feature maps and returns a sequence of 2D boxes, one per every frame. The only problem is that the regressor needs as input a fixed size feature maps. This problem is already solved by R-CNNs which use roi pooling and roi align in order to get fixed size feature maps from ROIs with changing sizes. In our situation, we extend roi align operation, presented by Mask R-CNN(He et al. 2017b), and we call it **3D Roi Align**.

**3D Roi Align** 3D Roi align is a modification of roi align presented by Mask R-CNN . The main difference between those two is that Mask R-CNN's roi align uses bilinear interpolation for extracting ROI's features and ours 3D roi align uses trilinear interpolation for the same reason. Again, the 3rd dimension is time. So, we have as input a feature map extracted from ResNet34 with dimensions (64,16,28,28) and a tensor containing the proposed TOIs. For each TOI whose activation map has size equal with (64,16,7,7), we get as output a feature map with size (64, 16, 7, 7).

### Regression procedure

At first, for each proposed ToI, we get its corresponding activation maps using 3D Roi Align. These features are given as input to a regressor. This regressor returns  $16 \cdot 4$  predicted transforms  $(\delta_x, \delta_y, \delta_w, \delta_h)$ , 4 for each frame, where  $\delta_x, \delta_y$  specify the coordinates of proposal's center and  $\delta_w, \delta_h$  its width and height, as specified in Girshick et al. 2013. We keep only the predicted translations, for the frames that are  $\geq t_1$  and  $< t_2$  and for the other frames, we set a zero-ed 2D box. After that, we modify each anchor from a cuboid written like  $(x_1, y_1, t_1, x_2, y_2, t_2)$  to a sequence of 2D boxes, like:

$(0, 0, 0, 0, \dots, x_{T_1}, y_{T_1}, x'_{T_1}, y'_{T_1}, \dots, x_i, y_i, x'_i, \dots, x_{T_2}, y_{T_2}, x'_{T_2}, y'_{T_2}, 0, 0, 0, 0, \dots)$ ,  
where:

- $T_1 \leq i \leq T_2$ , for  $T_1 < t_1 + 1, T_2 < t_2$  and  $T_1, T_2 \in \mathbb{Z}$
- $x_i = x_1, y_i = y_1, x'_i = x_2, y'_i = y_2$ .

**Training** In order to train our Regressor, we follow about the same steps followed previously for previous TPN's training procedure. This means that we randomly pick 16 ToI from those proposed by TPN's scoring layer. From those 16 tubes, 4 are foreground tubes, which means 25% of the total number of the tubes as happened previously. We extract their corresponding features using 3D Roi Align and calculate their targets like we did for regression layer. We feed Regressor Network with these features and compare the predicted targets with the expected. Again, we use smooth-L1 loss for loss function, calculated only for foreground ToIs. So, we add

another parameter in training loss formula which is now defines as:

$$\begin{aligned}
 L = & \sum_i L_{cls}(p_i, p_i^*) + \sum_i L_{cls}(p_{fixed,i}, p_{fixed,i}^*) + \\
 & \sum_i p_i^* L_{reg}(t_i, t_i^*) + \sum_i p_{fixed,i}^* L_{reg}(t_{fixed,i}, t_{fixed,i}^*) + \\
 & \sum_i q_i^* L_{reg}(c_i, c_i^*)
 \end{aligned} \tag{3.2}$$

where except the previously defined parameters, we set  $c_i$  as the regression targets for picked tubes  $q_i$ . These tubes are the ones randomly selected from the proposed ToIs and  $q_i^*$  are their corresponding groundtruth action tubes, which are the closest to each  $q_i$  tube. Again we use  $q_i^*$  as a factor because we consider a tube as background when it doesn't overlaps with any groundtruth action tube more than 0.5 .

### First regression Network

The architecture of reggression network is show in Figure 3.7, and it is described below:

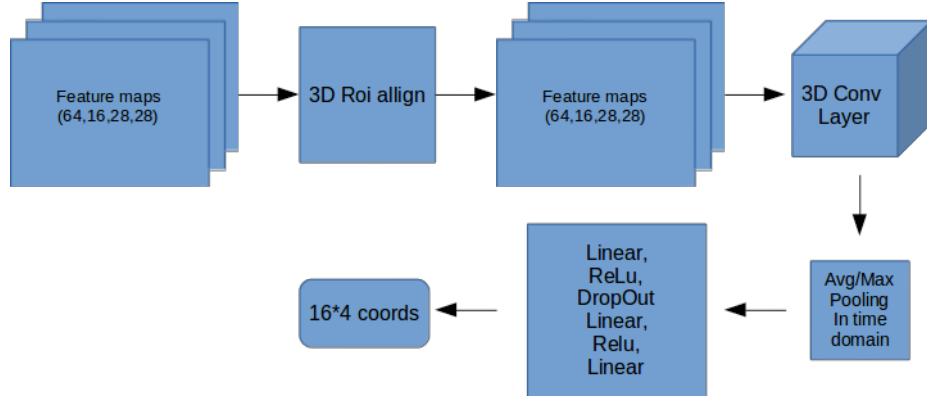


Figure 3.7: Structure of Regressor

1. Regressor is consisted, at first, with a 3D convolutional layer with kernel = 1, stride = 1 and no padding. This layer gets as input ToI's normalized activation map extracted by 3D Roi Align.
2. After that, we calculate the average value in time domain, so from a feature map with dimensions (64,16,7,7), we get as output a feature map (64,7,7).
3. These feature maps are given as input to a Linear layer followed by a Relu Layer, a Dropout Layer, another Linear Layer and Relu Layer and a final Linear.

We use Recall metric In order to assess the performance of regressor. We calculate 3 recall performances:

**Cuboid Recall**, which is the recall perfomance for proposed cuboids. We interested in this metric because, we want to know how good are our proposals before modifying them into sequences of boxes.

**Single frame Recall**, which is the recall performance for the proposed ToI against the groundtruth tubes.

**Follow-up Single Frame Recall**, which is the recall performance for only the cuboids that were over the overlap threshold between proposed cuboids and groundtruth cuboids. We use this metric in order to know how many of our proposed cuboids end up in being good proposals.

Dataset	Pooling	Cuboid	Singl. Fr.	Follow-up S.F.
JHMDB	avg	0.8545	0.7649	0.7183
	max	0.8396	0.7761	0.5783
UCF	avg	0.5319	0.4694	0.5754
	max	0.5190	0.5021	0.5972

Table 3.3: Recall results after converting cuboids into sequences of frames

As the above results show, we get lower recall performance in frame-level. On top of that, when we translate a cuboid into a sequence of boxes, we miss 20-40% of our proposals. This means that we don't modify good enough our cuboids, although we get only 10% decrease. Probably, we get such score from cuboids, that even though didn't overlap well (according to overlap threshold), achieve to become a good proposal in frame-level and in temporal level.

### 3.4.7 Changing Regressor - from 3D to 2d

After getting first recall results, we experiment using another architecture for the regressor network, in order to solve the modification problem, introduced in previous section. Instead of having a 3D Convolutional Layer, we will use a 2D Convolutional Layer in order to treat the whole time dimension as one during convolution operation. So, as shown in Figure 3.8, the 2<sup>nd</sup> Regression Network is about the same with first one, with 2 big differences:

1. We perform a pooling operation at the feature maps extracted by 3D Roi Align operation, after we are normalized.
2. Instead of a 3D Convolutional Layer, we have a 2D Convolutional Layer with kernel size = 1, stride = 1 and no padding.

On top of that, we tried to determine which feature map is the most suitable for getting best-scoring recall performance. This feature map will be given as input to Roi Align operation. At Table 3.4, we can see the recall performance for different feature maps and different pooling methods.

As we noticed from the above results, again, our system has difficulty in translating cuboids into 2D sequence of ROIs. So, that makes us rethink the way we designed our TPN.

## 3.5 3D anchors as 4k-dim vector

In this approach, we set 3D anchors as 4k coordinates ( $k = 16$  frames = sample duration). So a typical anchor is written as  $(x_1, y_1, x'_1, y'_1, x_2, y_2, \dots)$  where  $x_1, y_1, x'_1, y'_1$  are the coordinates for the 1st frame,  $x_2, y_2, x'_2, y'_2$  are the coordinates for the 2nd frame etc, as presented in Girdhar et al. 2017. In figure 3.9 we can see an example of this type of anchor.

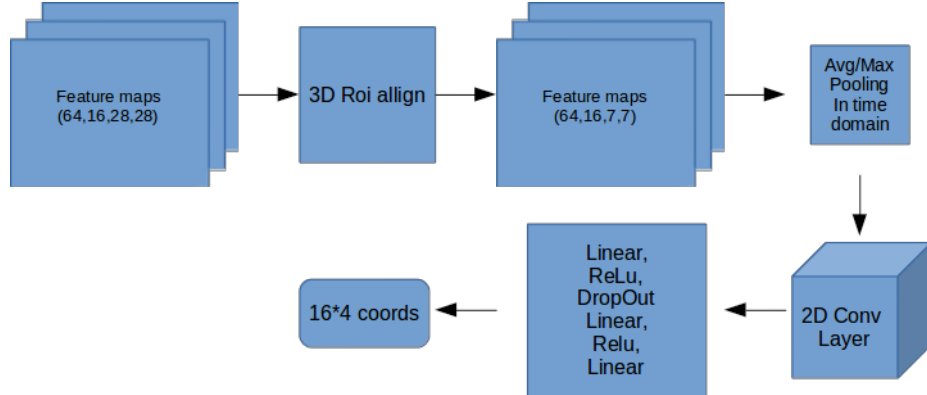


Figure 3.8: Structure of Regressor

Dataset	Pooling	F. Map	Recall	Recall SR	Recall SRF
JHMDB	mean	64	0.6828	0.5112	0.7610
		128	0.8694	0.7799	0.6756
		256	0.8396	0.7687	0.7029
	max	64	0.8582	0.7985	0.5914
		128	0.8358	0.7724	0.8118
		256	0.8657	0.8022	0.7996
UCF	mean	64	0.5055	0.4286	0.5889
		128	0.5335	0.4894	0.5893
		256	0.5304	0.4990	0.6012
	max	64	0.5186	0.4990	0.5708
		128	0.5260	0.4693	0.5513
		256	0.5176	0.4878	0.6399

Table 3.4: Recall performance using 3 different feature maps as Regressor's input and 2 pooling methods

The main advantage of this approach is that we don't need to translate the 3D anchors into 2D boxes, which caused many problems at the previous approach. However, it has a big drawback, which is the fact that this type of anchors has fixed time duration. In order to deal with this problem, we set anchors with different time durations, which are 16, 12, 8 and 4. Anchors with duration < sample duration (16 frames) can be written as 4k vector with zeroed coordinates in the frames bigger than the time duration. For example, an anchor with 2 frames duration, starting from the 2nd frame and ending at the 3rd can be written as (0, 0, 0, 0,  $x_1, y_1, x'_1, y'_1, x_2, y_2, x'_2, y'_2, 0, 0, 0, 0$ ) if sample duration is 4 frames.

This new approach led us to change the structure of TPN. The new one is presented in figure 3.10. As we can see, we added scoring and regression layers for each duration. So, TPN follows the upcoming steps in order to propose ToIs:

1. At first, we get the feature map, extracted by ResNet, as input to a 3D Convolutional Layer with kernel size = 1, stride = 1 and no padding.
2. From Convolutional Layer, we get as output an activation map with dimensions (256,16,7,7). For reducing time dimension, we use 4 pooling layer, one for each sample

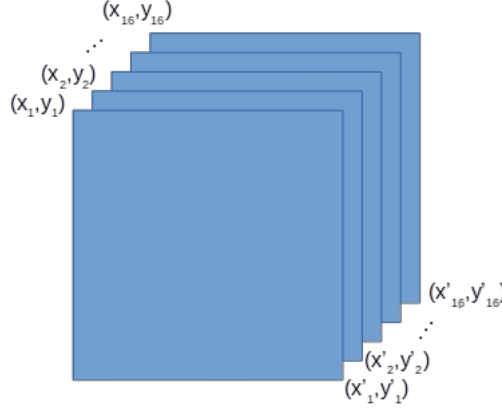


Figure 3.9: An example of the anchor  $(x_1, y_1, x'_1, y'_1, x_2, y_2, \dots)$

duration with kernel sizes  $(16,1,1)$ ,  $(12,1,1)$ ,  $(8,1,1)$  and  $(4,1,1)$  and stride = 1, for sample durations 16, 12, 8 and 4 respectively. So, we get activation maps with dimensions  $(256,1,7,7)$ ,  $(256,5,7,7)$ ,  $(256,9,7,7)$  and  $(256,13,7,7)$ , in which second dimension is the number of possible time variations. For example, in  $(256,5,7,7)$  feature map, which is related with anchors with duration 12 frames, we can have 5 possible cases, from frame 0 to frame 11, frame 1 to frame 12 etc.

3. Again, like in previous approach, for each pixel of the activate map we correspond  $\mathbf{n} = \mathbf{k} = 15$  anchors (5 scale of 1, 2, 4, 8, 16, 3 aspect ratios of 1:1, 1:2, 2:1). Of course, we have 4 different activate maps, with 1, 5, 9 and 13 different cases and a  $7 \times 7$  shape in each filter. So, in total we have  $28 \cdot 15 \cdot 49 = 20580$  different anchors. Respectively, we have 20580 different regression targets.

### 3.5.1 Training

Training procedure stays almost the same like previous approach's. So, again, we randomly choose a video segment and its corresponding groundtruth action tubes. But in this training procedure, we consider anchors as foreground when they overlap more than 0.7 with any groundtruth tube, alongside with background anchors whose overlap is bigger than 0.1 and smaller than 0.3. We are not concern about the rest of the anchors

Dataset	Pooling	Recall(0.5)	Recall(0.4)	Recall(0.3)
JHMDB	mean	0.6866	0.7687	0.8582
	max	0.8134	0.8694	0.9216
UCF	avg	0.5435	0.6326	0.7075
	max	0.6418	0.7255	0.7898

Table 3.5: Recall results using 2nd approach for anchors

As Table 3.5 shows, it is obvious that we get better recall performances compared to previous' approach. Additionally, we can see that 3D max pooling performs better than 3D avg pooling. The difference between max pooling and avg pooling is about 10%, which is big enough to make

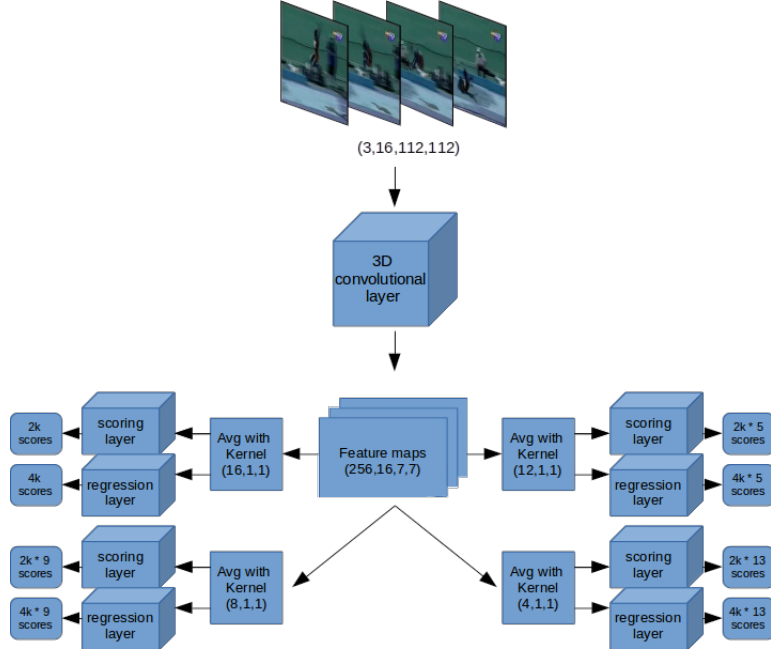


Figure 3.10: The structure of TPN according to new approach

us choose max pooling operation as pooling method before getting anchors' scores and regression targets.

### 3.5.2 Adding regressor

Even though, our TPN outputs frame-level boxes, we need to improve these predictions in order to overlap with the groundtruth boxes as well as possible. So, in full correspondance with the previous approach, we added an regressor for trying to get better recall results.

**3D Roi align** In this approach, we know already the 2D coordinates. So, we can use the method proposed from Girdhar et al. 2017. They extend RoiAlign operator by splitting the tube into  $T$  2D boxes. Then, they use classic RoiAlign to extract a region from each one of the temporal slices in the feature map. After that, they concatenate the region in time domain so they get a  $T \times R \times R$  feature map, where  $R$  is the output resolution of RoiAlign, which is 7 in our situation.

As a first approach, we use a 3D convolutional layer followed by 2 linear layer. Our regressors follows the following steps:

1. At first, use 3D RoiAlign in order to extract the feature maps of the proposed action tubes. We normalize them, and give them as input to the 3D convolutional layer.
2. The output of the 3D Convolutional Layer is fed into 2 Linear layers with ReLu activation between them and finally we get  $sampleduration \times 4$  regression targets. We keep only the proposed targets, that there is a corresponding 2D box.

We train our regressor using the same loss function as previous approach's formula which is:

$$\begin{aligned} L = & \sum_i L_{cls}(p_i, p_i^*) + \sum_i L_{cls}(p_{fixed,i}, p_{fixed,i}^*) + \\ & \sum_i p_i^* L_{reg}(t_i, t_i^*) + \sum_i p_{fixed,i}^* L_{reg}(t_{fixed,i}, t_{fixed,i}^*) + \\ & \sum_i q_i^* L_{reg}(c_i, c_i^*) + \end{aligned}$$

We want again to find the best matching feature maps, so we train our regressor for feature maps  $(64, 8, 7, 7)$  and  $(128, 8, 7, 7)$ . We didn't experiment using  $(256, 8, 7, 7)$  feature map because we got OutOfMemory error during training, despite several modifications we did in the implementation code.

Dataset	Feat. Map	Recall(0.5)	Recall(0.4)	Recall(0.3)
JHMDB	64	0.7985	0.903	0.9552
	128	0.7836	0.8881	0.944
UCF	64	0.5794	0.7206	0.8134
	128	0.5622	0.7204	0.799

Table 3.6: Recall performance when using a 3D Convolutional Layer in Regressor's architecture

According to Table 3.6, we got the best results when we use  $(64, 16, 7, 7)$  feature map. This is the expected result, because these feature maps are closer to the actual pixels of the actor, than  $(128, 16, 7, 7)$  feature maps, in which because of  $3 \times 3 \times 3$  kernels, which combine spatio-temporal information from neighbour pixels. However, as we can see, we got worst recall performance than when we didn't use any regressor if we compare results from Tables 3.5 and 3.6.

### 3.5.3 From 3D to 2D

Following the steps we used before, we design an architecture that uses instead of a 3D Convolutional Layer, a 2D. Unlike we did before, in this case, we don't use any pooling operation before feeding the first 2D Convolutional Layer. On the contrary, we manipulate our feature maps like not being spatio-temporal but, only spatial. So, our steps are:

1. At first, we use, again ,3D RoiAlign in order to extract the feature maps of the proposed action tubes and normalize them. Let us consider a feature map extracted from ResNet which has dimensions  $(64, sampleduration, 7, 7)$  and after applying RoiAlign and normalization, we get a  $(k, 64, sampleduration, 7, 7)$  feature map, where  $k$  is the number of proposed action tubes for this video segment.
2. We slice the proposed action tubes into T 2D boxes, so the dimensions of the Tensor, which contains the coordinates of action tubes, from  $(k, 4 \cdot sampleduration)$  become  $(k, sampleduration, 4)$ . We reshape the Tensor into  $(k \cdot sampleduration, 4)$ , in which, first  $k$  coordinates refer to the first frame, the second  $k$  coordinates refer to the second frame and so on.
3. Respectively, we reshape extracted feature maps from  $(k, 64, sampleduration, 7, 7)$  to  $(k \cdot sampleduration, 64, 7, 7)$ . So, now we deal with 2D feature maps, for which as we said before, we consider that contain only spatial information. So, we use 3 Linear Layers in order to get 4 regression targets. We keep only those we have a corresponding bounding box.

Again, we experiment using 64, 128 and 256 feature maps (in this case, there is no memory problem). The results of our experiments are shown at Table 3.7.

Dataset	Feat. Map	Recall(0.5)	Recall(0.4)	Recall(0.3)
JHMDB	64	0.8358	0.9216	0.9739
	128	0.8172	0.9142	0.9627
	256	0.7724	0.8731	0.9328
UCF	64	0.6368	0.7346	0.7737
	128	0.6363	0.7133	0.7822
	256	0.6363	0.7295	0.7822

Table 3.7: Recall performance when using a 2D Convolutional Layer instead of 3D in Regressor's model

As we can see, we get improve recall performance up 3% for JHMDB dataset and about the same perfomance for UCF dataset. Again, we get best performance if we choose (64, 16, 7, 7) feature maps.

### 3.5.4 Changing sample duration

After trying all the previous versions, we noticed that we get about the same recall performances with some small improvements. So, we thought that we could try to reduce the sample duration. This idea is based on the fact that reducing sample duration, means that anchor dimensions will reduce, so the number of candidate anchors. That's because, now we have smaller number of cases, so smaller number of parameters alongside with small number of dimensions for regression targets. We train our TPN for sample duration = 8 frames 4 frames. We use, of course, TPN's second architecture, because as shown before, we get better recall performance.

#### Without Regressor

At first, we train TPN, again without regressor. We do so, in order to compare recall performance for all sample durations, without using any regressor. The results are shown in Table 3.8. For all cases, we use max pooling before scoring and regression layers, and we didn't experiment at all with avg pooling. Of course, for sample duration = 16, we used the calculated one in Table 3.5.

Dataset	Sample dur	Recall(0.5)	Recall(0.4)	Recall(0.3)
JHMDB	16	0.8134	0.8694	0.9216
	8	0.9515	0.9888	1.0000
	4	0.8843	0.9627	0.9888
UCF	16	0.6418	0.7255	0.7898
	8	0.7942	0.8877	0.9324
	4	0.7879	0.8924	0.9462

Table 3.8: Recall results when reducing sample duration to 4 and 8 frames per video segment

According to Table 3.8, we notice that we get best performance for sample duration = 8 for both datasets. For dataset JHMDB sample duration equal with 8 is gets far better results from the others aprroaches, followed by approach with sample duration = 4. For UCF dataset,

although sample duration equal with 8 gives us best performances sample duration equal with 4 gives us about the same. The difference between those 2 duration is less than 1%.

### With Regressor

Following the idea of reducing sample duration for getting better recall performance, we trained TPN with a regressor. We trained for both approaches, which means both 3D and 2D Convolutional Layer approaches were trained. Recall performances are presented at Table 3.9.

Dataset	Sample dur	Type	Recall(0.5)	Recall(0.4)	Recall(0.3)
UCF	8	2D	0.8078	0.8870	0.9419
		3D	0.8193	0.8930	0.9487
	4	2D	0.7785	0.8914	0.9457
		3D	0.7449	0.8605	0.9362
JHMDB	8	2D	0.9366	0.9851	0.9925
		3D	0.8918	0.9776	0.9963
	4	2D	0.9552	0.9963	1.0000
		3D	0.9142	0.9701	0.9888

Table 3.9: Recall results when a regressor and sample duration equal with 4 or 8 frames per video segment

According to 3.9, it is clear that using a 2D Convolutional Layer as presented above results in better recall performance than using a 3D. Furthermore, we notice that the addition of a regressor causes both improvements and deteriorations in recall performances. For dataset UCF, approach with sample duration = 8 improves by about 1-2% recall performance but for sample duration = 4 it reduce it by 1-3%. On the other hand, for dataset JHMDB, now, sample duration = 4 gets better results by adding a regressor and sample duration = 8 gets worse. So, after considering both results from Tables 3.8 and 3.9, we think that the best approach is using sample duration equal with 8, with the addition of a regressor, which uses a 2D Convolutional Layer. We know that this approach gets worse performance at JHMDB but it gives us the best results in UCF. But, since JHMDB's results are high enough, we are most interested in improving UCF's results. That's the reason, we will use the aforementioned approach in the rest chapters.

## 3.6 General comments

In the previous section, we presented 2 different approaches for proposing sequences of bounding boxes which are likely to include an actor performing an action. After considering both approaches, we deduce that the second approach results in better proposals according to their recall performance. At Figure 3.11, 3 different generated ToIs are presented.

Our goal is bounding boxes to overlap with the actor precisely. According to Figure 3.11, all of three actions overlap with the actor to some degree. Of course, it is clear that ToI, presented at Figure 3.11b, doesn't overlap very well like those shown at Figures 3.11a and 3.11c. Intuitively, comparing proposals from 3.11a and 3.11c, we think that 3.11a overlaps better than 3.11c.

However, as shown at Figures 3.12a and 3.12b, the second ToI better overlaps with the groundtruth. It is clear that even though the first proposal overlaps very well with the upper body of the actor, it fails to capture the left leg, which may be a crucial factor for determining the class of the action. The ToI shown at Figure 3.12b manages to capture most of the actor's

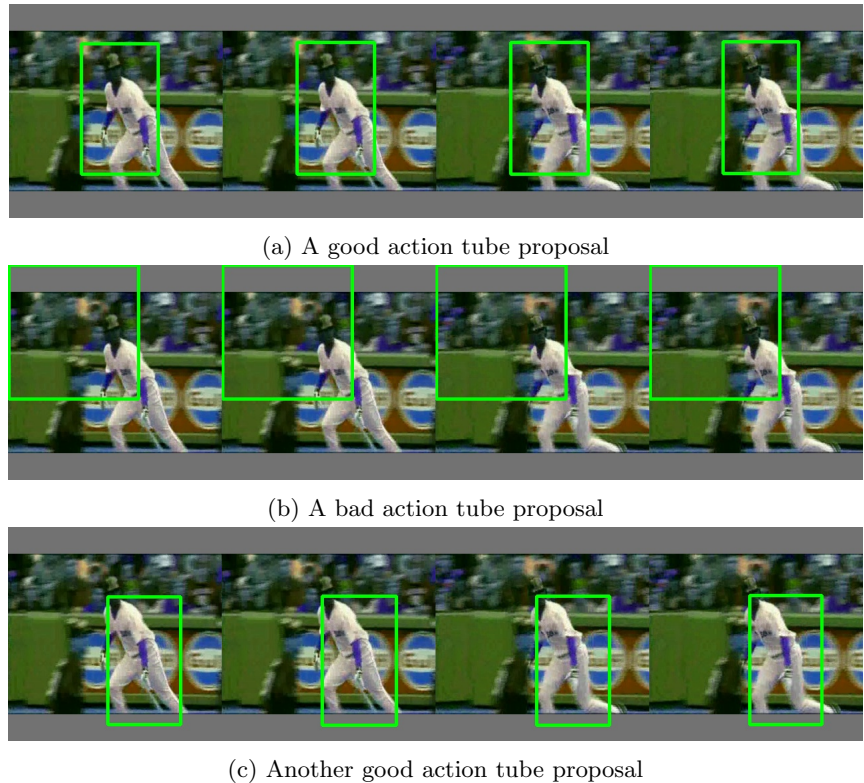


Figure 3.11: 3 Different candidate action tubes

body excluding only the head, which usually doesn't move a lot during an action. Althogh, judging intuitively, we would choose the first ToI, in reality, the second one is more preferable.

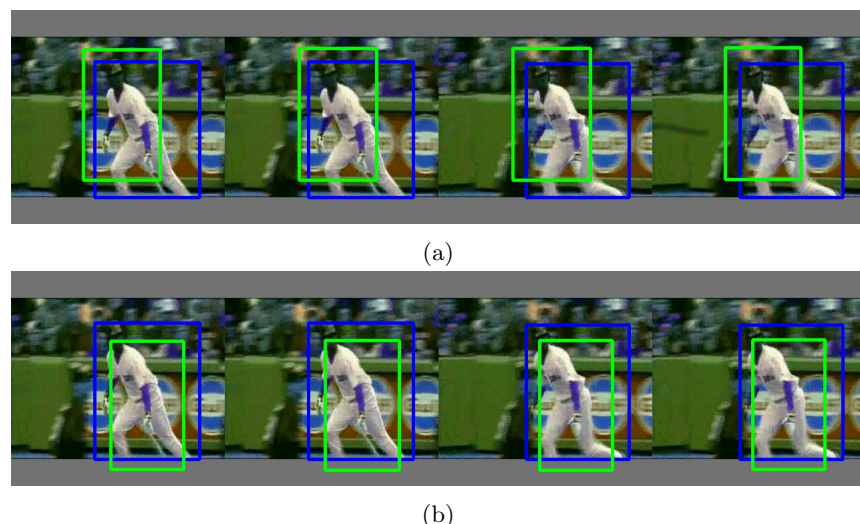


Figure 3.12: 3 Different candidate action tubes



# Chapter 4

## Connecting Tubes

### 4.1 Introduction

In previous chapter we described methods for generating candidate action tubes given a small video segment lasting 8 or 16 frames. However, actual videos and actual human actions, in the wild, last more than 16 frames most of the times. Current networks are unable to process a whole video at once, in order to generate action tubes due to memory and computing power issues. As mentioned in chapter 2, a lot action localization approaches deal with this situation by given a video either propose candidate areas in frame-level and then they connect these in order to generate action tube proposal either, separate it into video segments, proposing sequences of bounding boxes for each video segment and then link them in order to generate action proposal. Both aforementioned techniques makes the suitable choice of linking method an important factor for the performance of the network. That's because, even though frame-level or video segment-level proposals might be very good, if the proposed connection algorithm doesn't work well, final action tube proposals won't be efficient, so the final model will never be able to achieve high classification performance. In other words, if connecting algorithm doesn't generate action proposals with great recall and MABO performance, the model's classifier won't be able to perform suitable classification, because probably it would be given action tubes without any context. In this chapter, we present 3 different approaches used for linking proposed ToIs generated from TPN in the previous chapter.

### 4.2 First approach: combine overlap and actioness

Our algorithm is inspired by Hou, Chen, and Shah 2017, which calculates all possible sequences of ToIs. In order find the best candidate action tubes, it uses a score which tells us how likely a sequence of TOIs is to contain an action. This score is a combination of 2 metrics:

**Actioness**, which is the TOI's possibility to contain an action. This score is produced by TPN's scoring layers.

**TOIs' overlapping**, which is the IoU of the last bounding boxes of the first TOI and the first frames of the second TOI.

The above scoring policy can be described by the following formula:

$$S = \frac{1}{m} \sum_{i=1}^m Actioness_i + \frac{1}{m-1} \sum_{j=1}^{m-1} Overlap_{j,j+1}$$

For every possible combination of TOIs we calculate their score as show in figure 4.1.

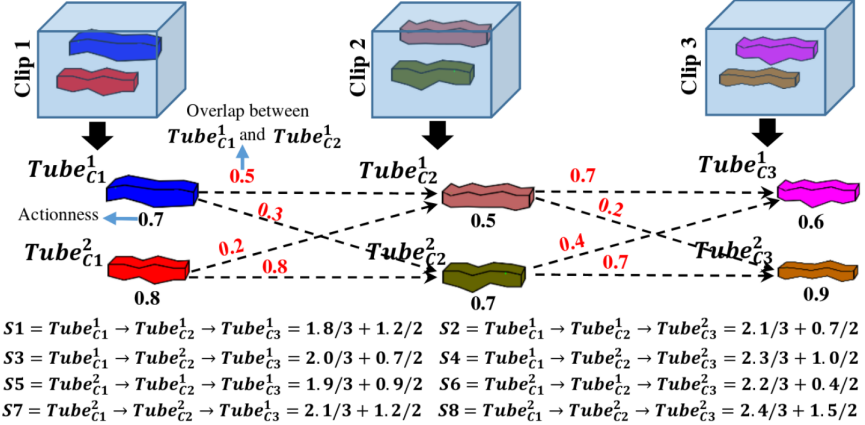


Figure 4.1: An example of calculating connection score for 3 random TOIs taken from Hou, Chen, and Shah 2017

The above approach, however, needs too much memory for all needed calculations, so a memory usage problem is appeared. The reason is, for every new video segments we propose  $k$  TOIs (16 during training and 150 during validation). As a result, for a small video seperated in **10 segments**, we need to calculate **150<sup>10</sup> scores** during validation stage. This causes our system to overload and it takes too much time to process just one video.

In order to deal with this problem, we create a greedy algorithm in order to find the candidates tubes. Intuitively, this algorithm after getting a new video segment, keeps tubes with score higher than a threshold, and deletes the rest. So, we don't need to calculate combinations with very low score. We wrote code for calculating tubes' scores in CUDA language, which has the ability to parallel process the same code using different data. Our algorithm is described below:

1. Firstly, initialize empty lists for the final tubes, final tubes' duration, their scores, active tubes, their correnspondig duration, active tubes' overlapping sum and actioness sum where:

- Final tubes list contains all tubes which are the most likely to contain an action, and their score list contains their corresponding scores. We refer to each tube by its index which is related a tensor, in which we saved all the ToIs proposed from TPN for each video segment.
- Active tubes list contains all tubes that will be match with the new TOIs. Their overlapping sum list and actioness sum list contain their sums in order to avoid calculating then for each loop.

Also, we initialize connection threshold equal to 0.5 .

2. For the first video segment, we add all the TOIs to both active tubes and final tubes. Their scores are only their actioness because there are no tubes for calculating their overlapping score. So, we set their overlapping sum equal to 0.
3. For each next video, after getting the proposed ToIs, firstly we calculate their overlapping score with each active tube. Then, we empty active tubes, active tubes' duration, overlapping sum and actioness score lists. For each new tube that has score higher than the connection threshold, we add both to final tubes and to active tubes and their corresponding lists, and we increase their duration.
4. If the number of active tubes is higher than a threshold, we set connection threshold equal with the score of the 100th higher score. On top of that, we update the final tubes list, removing all tubes that have score lower than the threshold.
5. After that, we add in active tubes, the current video segment's proposed TOIs, alongside with their actioness scores in actioness sum list and zero values in corrensponding positions in overlaps sum list (such as in the 1st step).
6. We repeat the previous 3 steps until there is no video segment left.
7. Finally, as we mentioned before, we have a list which contains the indexes of the saved tubes. So, we modify them in order to have the corresponding bounding boxes. However, 2 succeeding ToIs do not, always, have extactly the same bounding boxes in the frames that overlap. For example, ToIs from the 1<sup>st</sup> video segment start from frame 1 to frame 16. If we have video step equal with 8, these ToIs overlap temporally with the ToIs from the succeeding video segment in frames 8-16. In those frames, in final tube, we choose the area that contains both bounding boxes which is denoted as  $(\min(x_1, x'_1), \min(y_1, y'_1), \max(x_2, x'_2), \max(y_2, y'_2))$  for bounding boxes  $(x_1, y_1, x_2, y_2)$  and  $(x'_1, y'_1, x'_2, y'_2)$ .

### 4.2.1 JHMDB Dataset

In order to validate our algorithm, we firstly experiment in JHMDB dataset's videos in order to define the best overlapping policy and the video overlapping step. Again, we use recall as evaluation metric. A groundtruth action tube is considered to be found, as well as positive, if there is at least 1 video tube which overlaps with it over a predefined threshold, otherwise it . These thresholds are again 0.5, 0.4 and 0.3. We set TPN to return 30 ToIs per video segment. We chose to update threshold when active tubes are more than 500 and to keep the first 100 tubes as active. We did so, because, a big part of the code is performing in CPU. That's because, we use lists, which are very easy to handle for adding and removing elements. So, if we use bigger update limits, it takes much more time to process them.

**Sample duration equal with 16 frames** At first we use as sample duration = 16 and video step = 8. As overlapping frames we count frames (8...15) so we have #8 frames. Also, we use only #4 frames with combinations (8...11), (10...13) and (12...15) and #2 frames with combinations (8,9), (10,11), (12,13), and (14,15). The results are shown in Table 4.1 (in bold are the frames with which we calculate the overlap score).

combination	overlap thresh
	0.5
	0.4
	0.3

$0,1,\dots,\{8,\dots,15\}$	0.3172	0.4142	0.6418
$\{8,9,\dots,15\},16,\dots,23$			
$0,1,\dots,\{8,\dots,11,\}14,15$	0.3172	0.4142	0.6381
$\{8,\dots,11\},12,\dots,22,23$			
$0,1,\dots,\{10,\dots,13\}14,15,$	0.3209	0.4179	0.6418
$8,9,\{10,\dots,13\},14,\dots,22,23$			
$0,1,\dots,\{12,\dots,15\}$	0.3284	0.4216	0.6381
$8,9,\dots,\{12,\dots,15\},16,\dots,23,$			
$0,1,\dots,\{8,\dots,11,\}14,15,$	0.3172	0.4142	0.6381
$\{8,9,\dots,11\},12,\dots,22,23$			
$0,1,\dots,\{10,\dots,13\}14,15,$	0.3209	0.4179	0.6418
$\{10,\dots,13\},14,\dots,22,23$			
$0,1,\dots,\{12,\dots,15\}$	0.3284	0.4216	0.6381
$8,9,\dots,\{12,\dots,15\},16,\dots,$			
$0,1,\dots,\{8,9\},10,\dots,14,15,$	0.3134	0.4104	0.6381
$\{8,9\},10,11,\dots,22,23$			
$0,1,\dots,\{10,11\},12,\dots,14,15,$	0.3209	0.4216	0.6418
$8,9,\{10,11\},12,\dots,22,23$			
$0,1,\dots,\{12,13\},14,15,$	0.3246	0.4179	0.6418
$8,9,\dots,\{12,13\},14,\dots,22,23$			
$0,1,\dots,13,\{14,15\}$	0.3321	0.4216	0.6306
$8,9,\dots,\{14,15\},16,\dots,22,23$			

Table 4.1: Recall results for step = 8

As we can from the above table, generally we get very bad performance and we got the best performance when we calculate the overlap between only 2 frames (either 14,15 or 12,13). So, we thought that we should increase the video step because, probably, the connection algorithm is too strict into big movement variations during the video. As a results, we set video step = 12 which means that we have only 4 frames overlap. In this case, for #4 frames, we only have the combination (12...15), for #2 frames we have (12,13), (13,14) and (14,15) as shown in Table 4.2.

combination	overlap thresh		
	0.5	0.4	0.3
$0,1,\dots,11,\{12,\dots,15\}$			
$\{12,13,\dots,15\},16,\dots,26,27$	0.3769	0.4627	0.6828
$0,1,\dots,\{12,13\},14,15,$			
$\{12,13\},14,15,\dots,26,27$	0.3694	0.4627	0.6903
$0,1,\dots,12,\{13,14\},15,$			
$12,\{13,14\},15,\dots,26,27$	0.3843	0.4627	0.6828
$0,1,\dots,12,13,\{14,15\}$			
$12,13,\{14,15\},16,\dots,26,27$	0.3694	0.459	0.6828

Table 4.2: Recall results for step = 12

As we can see, recall performance is increase so that means that our assumption was correct. So again, we increase video step into 14, 15 and 16 frames and recall score is shown at Table 4.3

combination	overlap thresh		
	0.5	0.4	0.3
0,1,...,13{14,15} {14,15},16,...,28,29	0.3731	0.5336	0.6493
0,1,...,13,{14,}15, {14,}15,...,28,29	0.3694	0.5299	0.6455
0,1,...,14,{15} 14,{15,}16,...,28,29	0.3731	0.5187	0.6381
0,1,...,14,{15} {15},16,...,30	0.3918	0.5187	0.6381
0,1,...,14,{15} {16},17,...,31	0.4067	0.7313	0.8731

Table 4.3: Recall results for steps = 14, 15 and 16

The results show that we get the best recall performance when we have no overlapping steps and video step = 16 = sample duration. We try to improve more our results, using smaller duration because, as we saw from TPN recall performance, we get better results when we have sample duration = 8 or 4.

**Sample duration equal wit 8** We wanted to confirm that we get the best results, when we have no overlapping frames and step = sample duration. So Table 4.4 shows recall performance for sample duration = 8 and video step = 4 and Table 4.5 for video steps = 6, 7 and 8.

combination	overlap thresh		
	0.5	0.4	0.3
0,1,2,3,13{4,5,6,7} {4,5,6,7},8,9,10,11	0.2015	0.3582	0.5858
0,1,2,3,{4,5,}6,7 {4,5,}6,7,8,9,10,11	0.1978	0.3582	0.5933
0,1,2,3,4{5,6,}7 4,{5,6,}7,8,9,10,11	0.1978	0.3507	0.5821
0,1,2,3,4,5{6,7} 4,5,{6,7},8,9,10,11	0.194	0.3433	0.585

Table 4.4: Recall results for step = 4

combination	overlap thresh 0.5	overlap thresh 0.4	overlap thresh 0.3
0,1,2,3,4,5{6,7} {6,7},8,9,10,11,12,13	0.3134	0.7015	0.8619
0,1,2,3,4,5,{6,}7 {6,}7,8,9,10,11,12,13	0.3209	0.6679	0.847
0,1,2,3,4,5,6,{7} 6,{7}8,9,10,11,12,13	0.3172	0.6567	0.8507
0,1,2,3,4,5,6{7} {7,}8,9,10,11,12,13,14	0.5597	0.7687	0.903
0,1,2,3,4,5,6{7} {8}9,10,11,12,13,14,15	0.653	0.8396	0.9179

Table 4.5: Recall results for steps = 6, 7 and 8

According to Tables 4.4 and 4.5, it is clearly shown that, we achieve best results, for  $step = sampleduration$  and overlapping scores is calculated between the last box of the current tubes and the first box of next tubes.

#### 4.2.2 UCF dataset

In previous steps, we tried to find the best overlap policy for our algorithm in JHMDB dataset. After that, it's time to apply our algorithm in UCF dataset using the best scoring overlap policy. We did some modifications in the code, in order to use less memory and we moved most parts of the code to GPU. This happened by using tensors instead of lists for scores while most operations are, from now on, matrix operations. On top that, last step of the algorithm, which is the modification from indices to actual action tubes is written, now, in CUDA code so it takes place in GPU, too. So, we are now able to increase the number of ToIs returned by TPN, the max number of active tubes before updating threshold and the max number of final tubes.

The first experiments we performed were related with the number of the final tubes, our network proposes alongside with TPN's proposed tubes' number. We experiment for cases, in which TPN proposes 30, 100 and 150 ToIs, our final network proposes 500, 2000 and 4000 candidate action tubes for sample durations equal with 8 and 16 frames. For sample duration equal with 8 we return 100 ToIs because, when we tried to return 150 proposed ToIs, we got OutOfMemory error. Table 4.6 show the spatio-temporal recall and MABO performance of those approaches. Furthermore, Table 4.7 show their tempolar recall and MABO performance. We are interested in temporal performance, because UCF is consisted of untrimmed videos, unlike JHMDB which has only trimmed videos. So, we want to know how well our network is able to propose action tubes that overlap temporally with the groundtruth action tubes over a "big" threshold. For temporal localization, we don't use 0.5, 0.4 and 0.3 overlapping threshold, but instead, we use 0.9, 0.8 and 0.7, because it is very important our network to be able to propose tubes that contain an action, at least from the temporal perspective. In order to calculate the temporal overlap, we use IoU for 1 dimension as described before.

combination	TPN tubes	Final tubes	0.5	0.4	0.3	MABO
-------------	--------------	----------------	-----	-----	-----	------

0,1,...,6,{7, 8,}9,...,14,15	30	500	0.2829	0.4395	0.5817	0.3501
		2000	0.3567	0.4996	0.6289	0.3815
		4000	0.3749	0.5316	0.6487	0.3934
	100	500	0.2966	0.451	0.5947	0.356
		2000	0.3757	0.5163	0.6471	0.3902
		4000	0.3977	0.5506	0.6624	0.4029
	0,1,...,14,{15, 16,}17,18,...,23	500	0.362	0.5042	0.6243	0.3866
		2000	0.416	0.5468	0.6631	0.4108
		4000	0.4281	0.5589	0.6779	0.4182
		500	0.3589	0.4981	0.6198	0.3845
		2000	0.4129	0.5392	0.6563	0.4085
		4000	0.4266	0.5521	0.6722	0.4162

Table 4.6: Recall results for UCF dataset

combination	TPN tubes	Final tubes	overlap thresh			MABO
			0.9	0.8	0.7	
0,1,...,6,{7, 8,}9,...,15	30	500	0.4464	0.581	0.6844	0.7787
		2000	0.635	0.7665	0.8403	0.8693
		4000	0.7034	0.8228	0.8875	0.8973
	100	500	0.454	0.5924	0.692	0.783
		2000	0.651	0.7696	0.8441	0.8734
		4000	0.7209	0.8312	0.8913	0.9026
0,1,...,14,{15, 16,}17,18,...,23	30	500	0.6844	0.8327	0.9027	0.8992
		2000	0.7475	0.8684	0.9217	0.9175
		4000	0.7567	0.8745	0.9255	0.9211
	150	500	0.7498	0.8707	0.9171	0.9125
		2000	0.8243	0.911	0.9392	0.9342
		4000	0.8403	0.9179	0.9437	0.9389

Table 4.7: Temporal Recall results for UCF dataset

According to Table 4.6, we achieve better recall and MABO performance when we set sample duration equal with 16. In all cases, recall performance of simulations with sample duration equal with 16 outweigh the corresponding with 8, with the difference varying from 2% to 8%. In addition, we get best recall and MABO performance when our system proposes 4000 tubes. As we can see, the ratio of good proposals increases about 5%-7% when we change number of proposed tubes from 500 to 2000. This ratio increases more when we double returned action tubes, from 2000 to 4000. However, this increase is only about 1%-2%, which make us rethink if this increase is worth to be performed. That's because, this modification increases memory usage, because of 4000 proposed action tubes, instead of 2000. Finally, Table 4.6 shows that, for sample duration = 8, changing the number of ToIs produced by TPN, slightly helps our network to achieve better results. This contribution is measured about 1%-2%. On the contrary, when we set sample duration equal with 16, it slightly reduces network's performance. Taking all

the aforementioned results into account, we think that the most suitable choices for connection approaches are, for sample duration equal with 8, the one in which TPN returns 100 ToIs and our network proposes 4000 action tubes, and for sample duration equal with 16, the one in which, TPN returns 30 ToIs and the network 4000 action tubes.

Additionally, Table 4.7 shows some interesting facts, too. At first, it confirms that increasing the number of proposed action tubes, from 500 to 4000, increases recall and MABO performance. Also, we get better result when network has 16 frames as sample duration, too. However, unlike Table 4.6, Table 4.7 shows that when we increase TPN's number of proposed ToIs, it increases performances for both sample durations. For sample duration equal with 8, this increases results in Improving recall performances by 2% and MABO performance by 1% like spatio-temporal recall and MABO. For sample duration equal with 16, recall performance is increasing by about 8% and MABO by 1%-2%.

Taking both tables into cosideration, we think that the best approach is TPN returning 30 proposed ToIs, network returning 4000 proposed action tubes and sample duration equals with 16. We didn't choose TPN returning 150 proposed ToIs because, based on MABO performances, they different only by 1%, difference which is insignificant.

### Adding NMS algorithm

Previous section describe the performances of network's proposals for variations in the returnig number of TPN's ToIs, number of returned proposed aciton tubes and sample duration. For each situation, we choose the k-best scoring action tubes, without taking into account any relation between these aciton tubes, like their Spatio-temporal overlap. So, like TPN's approach, we thought that we should apply nms algorithm before choosing k-best scoring tubes, in order to further improve spatio-temporal and temporal, recall and MABO performance. We experiment using again two sample durations, 16 and 8 frames per video segment, number or TPN's returning tubes equal with 30 and number of final picked action tubes equal with 4000. NMS algorithm uses a threshold in order to choose if 2 action tubes overlap enough. We experiment setting this threshold equal with 0.7 and 0.8 and results are shown at Table 4.8 for Spatio-temporal perfomance and at Table 4.9 for temporal performace.

combination	NMS thresh	PreNMS tubes	overlap thresh			MABO
			0.9	0.8	0.7	
0,1,...,6,{7, 8,}9,...,15	0.7	20000	0.346	0.5202	0.657	0.3824685269
	0.8		0.3643	0.5392	0.6578	0.3904727407
	0.9		0.397	0.5574	0.6677	0.4031543642
0,1,...,14,{15, 16,}17,...,23	0.7	20000	0.3939	0.5559	0.6882	0.404689056
	0.8		0.4259	0.5764	0.6981	0.419487652
	0.9		0.4494	0.5856	0.7019	0.4302611039

Table 4.8: Spatio-temporal Recall results for UCF dataset

combination	NMS thresh	PreNMS tubes	overlap thresh			MABO
			0.9	0.8	0.7	
0,1,...,6,{7, 8,}9,...,15	0.7	20000	0.6281	0.8251	0.9027	0.8885141223
	0.8		0.7369	0.8616	0.9148	0.9106069806

	0.9		0.7787	0.8753	0.9209	0.9212593589
0,1,...,14,{15,} {16,}17,...,23	0.7	20000	0.7452	0.8920	0.9361	0.920331595
	0.8		0.8160	0.9278	0.9506	0.93612757
	0.9		0.854	0.9346	0.9529	0.9434986107

Table 4.9: Temporal Recall results for UCF dataset

Comparing Table 4.8 with Table 4.6, we notice that NMS algorithm impoves recall and MABO performance when NMS threshold is equal with 0.9. When we set it equal with 0.7 or 0.8, we get worse results. This happens, probably, because nms algorithm removes some good proposals. Comparing these results with results presented at Tables 4.6 and 4.7 it becomes clear that using NMS algorithm is very usefull. That's because, even though we get the same number of proposed action tubes, these tubes are not very close spatiotemporally, so this makes proposed action tubes more likely to contain actuall foreground action tubes.

### Stop updating threshold

In previous approaches, scoring threshold was updated each time our algorithm gathered a significant number of “active” tubes in order not to add action tubes with score below this score. However, after serious cosideration we came with the conclusion that some times, the updated threshold leads to not detecting action tubes that start after some frames. That's because, until then, linking threshold may be too big that won't let new action tubes to be created. So, we came with the modification of not updating linking threshold but just filtering proposed tubes, by keeping k-best scoring each time their number is bigger than the a specific number. The rest algorithm remains the same. Tables 4.10 and 4.11 show spatio-temporal and temporal, recall and MABO performace respectively. We experiment for cases in which either we don't use NMS algorithm at all, either we set overlap threshold equal with 0.7 and 0.9 as shown below.

combination	NMS thresh	PreNMS tubes	overlap thresh			MABO
			0.9	0.8	0.7	
0,1,...,6,{7,} {8,}9,...,15	-	20000	0.3779	0.5316	0.6471	0.393082961
	0.7		0.3483	0.5194	0.6471	0.3783524086
	0.9		0.416	0.5605	0.6722	0.4074053106
0,1,...,14,{15,} {16,}17,...,23	-	20000	0.438	0.5635	0.6829	0.4231788
	0.7		0.4525	0.5848	0.7034	0.429747438
	0.9		0.3802	0.5133	0.6068	0.3862278851848662

Table 4.10: Spatio-temporal Recall results for UCF dataset

combination	NMS thresh	PreNMS tubes	overlap thresh			MABO
			0.9	0.8	0.7	
0,1,...,6,{7,} {8,}9,...,15	-	20000	0.7087	0.8281	0.8913	0.899210587
	0.7		0.6586	0.854	0.9278	0.903373468
	0.9		0.8137	0.8973	0.9361	0.9333068498

0,1,...,14,{15,}	-	0.8327	0.9156	0.9399	0.940143272
	0.7	0.8646	0.9369	0.9567	0.946701832
	0.9	0.6183	0.7696	0.8388	0.8628507037919737

Table 4.11: Temporal Recall results for UCF dataset

Comparing recall and MABO performances shown at Table 4.10 with those included at Tables 4.8 and 4.6, we deduce that for sample duration equal with 8 stopping updating linking threshold results in worse performance when we set nms threshold equal with 0.7 but it achieves the best performances for nms threshold equal with 0.9 . Furthermore, for sample duration equal with 16, we get, now, best performance performance when we set nms threshold equal with 0.7 and worse performance for nms threshold equal with 0.9 .

### Soft-nms instead of nms

After widely experiment using NMS algorithm, we thought that we should try to use Soft-NMS algorithm, introduced by Bodla et al. 2017 and described in chapter 2. We implement our own soft-nms algorithm modifying it in order to calculate spatiotemporal overlapping scores, and not just spatial, like the one implemented by Bodla et al. 2017. As mentioned before, instead of removing action tubes, Soft-NMS algorithm just reduces their score for those which overlap over a predefined threshold, We experiment for sample duration equal with 8 and thresholds equal with 0.7 and 0.9, because, our implementation ran out of memory for sample duration equal with 16. Recall and MABO perfomance are presented at Tables 4.12 and 4.13

combination	NMS thresh	PreNMS tubes	overlap thresh			MABO
			0.9	0.8	0.7	
0,1,...,6,{7,}	0.7	20000	0.3916	0.5384	0.6464	0.3964639
	0.9		0.4023	0.5430	0.6502	0.398845313

Table 4.12: Spatio-temporal Recall results for UCF dataset using Soft-NMS

combination	NMS thresh	PreNMS tubes	overlap thresh			MABO
			0.9	0.8	0.7	
0,1,...,6,{7,}	0.7	20000	0.7521	0.8586	0.9110	0.915746097
	0.9		0.7741	0.8768	0.9255	0.922677864

Table 4.13: Temporal Recall results for UCF dataset using SoftNMS

Taking results at Tables 4.12 and 4.13 into consideration, alongside with those at Tables 4.10 and 4.11 for sample duration equal with 8, we notice that using softNMS results in slightly better results. This happens when we set overlapping threshold equal with 0.9, otherwise, for overlapping threshold 0.7, we get worst performace. Despite the fact that softnms results in

### 4.3. SECOND APPROACH: USE PROGRESSION AND PROGRESS RATE

better recall and MABO performance, our implementation is very slow, which means that for a 201-frame video, softNMS part lasts about 32 seconds on the contrary with standard NMS algorithm without updating linking threshold, in which this part last only 2 seconds. So, we choose to use standard NMS algorithm without updating linking threshold as an algorithm for removing overlapping action tubes.

### 4.3 Second approach: use progression and progress rate

As we saw before, our first connecting algorithm doesn't have very good recall results. So, we created another algorithm which is base on the one proposed by Hu et al. 2019. This algorithm introduces two new metrics according to Hu et al. 2019:

**Progression**, which describes the probability of a specific action being performed in the TOI.

We add this factor because we have noticed that actionness is tolerant to false positives. Progression is mainly a rescoring mechanism for each class (as mentioned in Hu et al. 2019)

**Progress rate**, which is defined as the progress proportion that each action class has been performed.

So, each action tube is described as a set of TOIs

$$T = \{\mathbf{t}_i^{(k)} | \mathbf{t}_i^{(k)} = (t_i^{(k)}, s_i^{(k)}, r_i^{(k)})\}_{i=1:n^{(k)}, k=1:K}$$

where  $t_i^{(k)}$  contains TOI's spatiotemporal information,  $s_i^{(k)}$  its confidence score and  $r_i^{(k)}$  its progress rate.

In this approach, each class is handled separately, so for the rest section, we discuss action tube generation for one class only. In order to link 2 TOIs, for a video with N video segments, the following steps are applied:

1. For the first video segment ( $k = 1$ ), initialize an array with the M best scoring TOIs, which will be considered as active action tubes ( AT ). Correspondingly, initialize an array with M progress rates and M confidence scores.
2. For  $k = 2:N$ , execute (a) to (c) steps:
  - (a) Calculate overlaps between  $AT^{(k)}$  and  $TOIs^{(k)}$ .
  - (b) Connect all tubes which satisfy the following criterions:
    - i.  $overlapscore(at_i^{(k)}, t_j^{(k)}) < \theta, at \in AT^{(k)}, t \in TOIs^{(k)}$
    - ii.  $r(at_i^{(k)}) < r(t_j^{(k)})$  or  $r(t_i^{(k)}) - r(at_i^{(k)}) < \lambda$
  - (c) For all new tubes update confidence score and progress rate as follows:

New confidence score is the average score of all connected TOIs:

$$s_z^{(k+1)} = \frac{1}{n} \sum_{n=0}^k s_i^{(n)}$$

New progress rate is the highest progress rate:

$$r(at_z^{(k+1)}) = \max(r(at_i^{(k)}), r(t_j^{(k)}))$$

- (d) Keep M best scoring action tubes as active tubes and keep K best scoring action tubes for classification.

This approach has the advantage that we don't need to perform classification again because we already know the class of each final tube. In order to validate our results, now, we calculate the recall only from the tubes which have the same class as the groundtruth tube. Again we considered a groundtruth tube as positive if there is at least one proposed tube that overlaps with it over the predefined threshold

combination		overlap thresh		
sample dur	step	0.5	0.4	0.3
8	6	0.3284	0.5	0.6082
8	7	0.209	0.459	0.6119
8	8	0.3060	0.5672	0.6866
16	8	0.194	0.4366	0.7164
16	12	0.3358	0.5336	0.7537
16	16	0.2649	0.4664	0.709

Table 4.14: Recall results for second approach with step = 8, 16 and their corresponding steps

According to Table 4.14, we get best performance when we set sample duration equal with 16 and overlap step equal with 12. Comparing this performance with first approach, for both sample durations equal with 8 and 16, we notice that second approach falls short comparing to the first one.

#### 4.4 Third approach : use naive algorithm - only for JHMDB

As mention in first approach, Hou, Chen, and Shah 2017 calculate all possible sequences of ToIs in order to the find the best candidates. We rethought about this approach and we concluded that it could be implement for JHMDB dataset if we reduce the number of proposed ToIs, produced by TPN, to 30 for each video clip. We exploited the fact that JHMDB dataset's videos are trimmed, so we do not need to look for action tubes starting in the second video clip which saves us a lot of memory. On top of that, we modified our code in order to be more memory efficient writing some parts in CUDA programming language, saving a lot of processing power, too.

So, after computing all possible combinations starting of the first video clip and ending in the last video clip, we keep only the **k-best scoring tubes (k = 500)**. We run experiments which have sample duration equal with 8 and 16 frames and we modify the video step each time. For sample duration = 8, we return only 15 ToIs and for sample duration = 16, we return 30 because, if we return more, we get "out of memory error". In the following table, we can see the recall results.

combination		overlap thresh		
sample dur	step	0.5	0.4	0.3

8	6	0.7873	0.8657	0.9366
8	7	0.7836	0.8731	0.9366
8	8	0.7910	0.8806	0.9515
16	8	0.7873	0.8843	0.9291
16	12	0.7948	0.8881	0.9403
16	16	0.7985	0.8918	0.9515

Table 4.15: Recall results for second approach with

From the above table, firstly, we confirmed that when video step is equal with sample duration gives us the best recall results. Also, we notice that when sample duration is equal with 16 frames recall gets slightly better than when sample duration is equal with 8. However, using 16 frames per video segment sample increases the memory usage even though it reduces the number of video segments, because of the need to process bigger videos, bigger feature maps etc. So for classification stage we will experiment using mostly sample duration equal with 8 frames.

## 4.5 General comments

Figure 4.2 shows the example presented in chapter 3, after linking first video segment's first ToI with a ToI proposed for the second video segment.



Figure 4.2: Example of connected tubes

# Chapter 5

## Classification stage

### 5.1 Introduction

In previous 2 chapters, we introduced the procedure we used to create candidate action tubes, which probably contain some action or may not. Most of the times, the proposed action tubes belong to the background, and for that reason, as mentioned and in the previous chapter, it is important to choose a good linking algorithm that generates good sequences of bounding boxes. However, it is quite important to choose the appropriate classifier who will be able very accurately predict whether a candidate action tube belongs to a known category of actions or it belongs to the background. This is because we may produce good proposals for candidate actions, but if our classifier is unable to distinguish them, our system will again fail to recognize the actions.

The right choice of a classifier is a big dilemma we are facing and we need to answer. However, this classifier will get as input some activation maps in order to be classified. Therefore, apart from the good selection of classifier, equally, good choice of features is important, too. Finally, the training process of the classifier plays a major role in order to be able to generalize and to avoid overfitting situations.

For our implementation, we implement approaches including a Linear Classifier, a Recursive Neural Network (RNN) Classifier, a Support Vector Machine (SVM) Classifier and a Multilayer perceptron (MLP). Additionally, we experiment using feature maps obtained from 3D RoiAlign using, also, avg or max pooling. Last but not least, we try to find the right ratio between foreground and background action tubes including their total number needed during training stage in order our classifier to perform efficiently.

The whole procedure of classification is consisted from the following steps:

1. Separate video into small video clips and feed TPN network those video clips and get as output k-proposed ToIs and their corresponding features for each video clip.
2. Connect the proposed ToIs in order to get video tubes which may contain an action.
3. For each candidate video tube, which is a sequence of ToIs, feed its feature maps into the classifier in order to perform classification.

The general structure of the whole network is depicted in figure 5.1, in which we can see the aforementioned steps if we follow the arrows.

In first steps of classification stage we refer only to JHMDB dataset because it has smaller number of video than UCF dataset which helped us save a lot of time and resources. That's

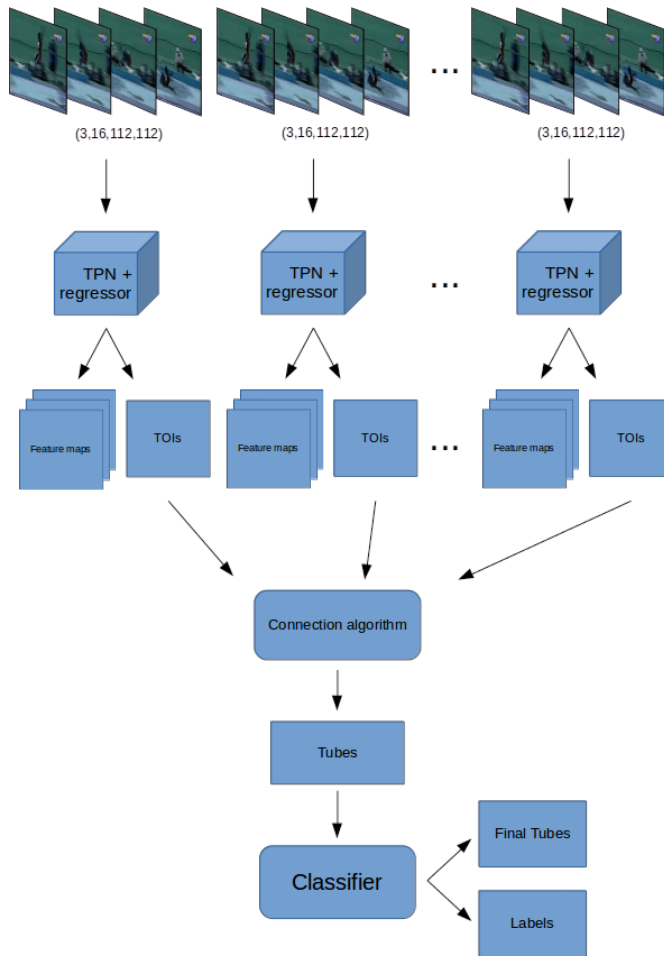


Figure 5.1: Structure of the whole network

because we performed most experiments only JHMDB and after we found the optimal approach, we implemented it for UCF dataset, too.

## 5.2 Preparing data and first classification results

For carrying out classification stage, we use, at first, a Linear classifier and a RNN classifier.

**Linear Classifier** Linear classifier is a type of classifier which is able to discriminate objects and predict their class based on the value of a *linear combination* of object's feature values, which usually are presented in a feature vector. If the input feature vector to the classifier is a real vector  $\vec{x}$ , then the output score is :

$$y = f(\vec{w} \cdot \vec{x}) = f \left( \sum_j w_j x_i \right)$$

**RNN** Recurrent neural networks, or RNNs for short, are a type of neural network that was designed to learn from sequence data, such as sequences of observations over time, or a sequence of words in a sentence. RNN takes many input vectors to process them and output other vectors. It can be roughly pictured like in the Figure 5.2 below, imagining each rectangle has a vectorial depth and other special hidden quirks in the image below. For our case, we choose **many to one** approach, because we want only one prediction, at the end of the action tube.

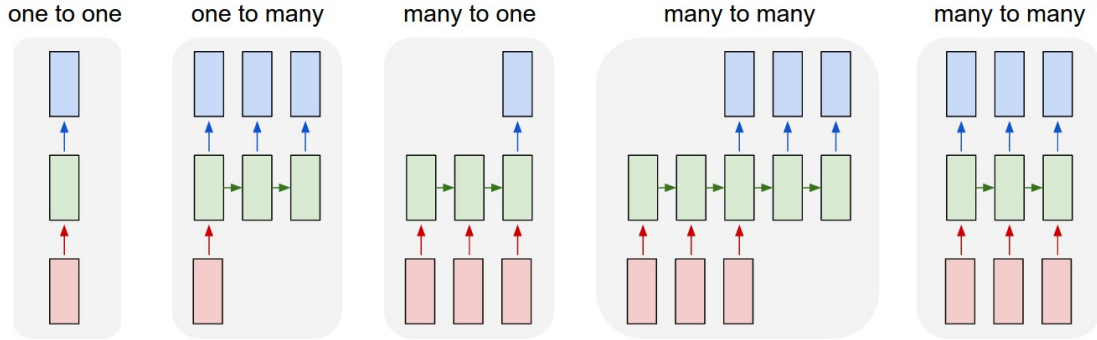


Figure 5.2: Types of RNN

**Training** In order to train our classifier, we have to execute the steps, presented in the first section, for each video. However, each video has different number of frames and reserves too much memory in the GPU. In order to deal with this situation and considering there are 4 GPUs available, we give as input one video per GPU. So we can handle 4 videos simultaneously. This means that a regular training session takes too much time for just 1 epoch.

The solution we came with, is to precompute the features for both foreground and background video tubes, and then to feed those features to our classifier for training it in order to discriminate classes. This solution includes the following steps:

1. At first, we extract only groundtruth action tubes' features. Also we extract feature maps from background action tubes, which are double the number of groundtruth action tubes. We chose this ratio between the number of positive and negative tubes inspired by Yang et al. 2017, in which it has 25% ratio between foreground and background rois and chooses 128 roi in total. Respectively, we chose a little bigger ratio because we have only 1 groundtruth video tube in each video. So, for each video we got 3 action tubes in total, 1 for positive and 2 for background. We considered background tubes those whose overlap scores with groundtruth tubes are  $\geq 0.1$  and  $\leq 0.3$ . Of course, in order to get those action tubes, we use a pre-trained TPN to generate ToIs for each video segment and then our proposed connection algorithm for linking proposed ToIs. Finally, we get each action tube's corresponding feature map using 3D RoiAlign
2. After extracting those features, we trained both Linear and RNN classifiers. The Linear classifier needs a fixed input size, so we used a pooling function in the dimension of the number of videos. So, at first we had a feature map of  $3,512,16$  dimensions and then we get as output a feature maps of  $512,16$  dimensions. We experimented using both max and avg pooling as shown at Table 5.1. For the RNN classifier, we do not use any pooling function before feeding it.

In order to train our classifiers, we use Cross-Entropy Loss as training loss function.

**Validation** Validation stage includes using both pre-trained TPN and classifier. So, for each video, we get classification scores for proposed action tubes. Most approaches usually consider a confidence score threshold for considering an action tube as foreground. However, we don't use any confidence score. On the contrary, because we know that JHMDB has trimmed videos with only 1 performed action, we just consider the best-scoring tube as our prediction.

Classifier	Pooling	mAP		
		0.5	0.4	0.3
Linear	mean	14.18	19.81	20.02
	max	13.67	16.46	17.02
RNN	-	11.3	14.14	14.84

Table 5.1: First classification results using Linear and RNN classifiers

Table 5.1 shows first classification results, which are not very good. The only useful deduction that we can come with, using above results is that, avg pooling method outclass max pooling. So, for all the rest classifications using Linear classifier, we use avg pooling before classification stage.

### 5.3 Support Vector Machine (SVM)

SVMs are classifiers defined by a separating hyper-plane between trained data in a N-dimensional space. The main advantage of using a SVM is that can get very good classification results when we have few data available.

The use of SVM is inspired from Girshick 2015 and it is trained using hard negative mining. This means that we have 1 classifier per class which has only 2 labels, positive and negative. We mark as positive the feature maps of the groundtruth action, and as negative groundtruth actions from other classes, and feature maps from background classes. As we know, SVM is driven by small number of examples near decision boundary. Our goal is to find a set of negatives that are the closest to the separating hyper-plane. So in each iteration, we update this set of negatives adding those which our SVM didn't perform very well. Each SVM is trained independently.

SVM code is take from Microsoft's Azure github page in which there is an implementation of Fast RCNN using a SVM classifier. We didn't modify its parameters which means that it has a linear kernel, uses L2-norm as penalty and L1-norm as loss during training. Training procedure starts with randomly picking 100 videos in order to calculate feature's scale. After that, each svm is provided by positive samples' feature maps and network looks for hard negatives for each class' svm. We consider as hard-negatives the tubes that got confidence score  $> -1.0$  during classification, and we add them to svm's sampels. When we gathen hard-negatives whose number is bigger than 500 or 1000 (depending on the approach) we retrain the class' SVM and remove samples with new score  $< -1.0$ .

This whole process makes the choice of the negatives a crucial factor. In order to find the best policy, we came with 5 different cases to consider as negatives:

1. Negatives are other classes's positives and all the background tubes
2. Negatives are only all the background videos
3. Negatives are only other classes's positives
4. Negatives are other classes's positives and background tubes taken only from videos that contain a positive tube

5. Negatives are only background tubes taken from videos that contain a positive tube

On top of that, we use 2 pooling functions in order to have a fixed input size.

In the next tables, we show our architecture's mAP performance when we follow each one of the above policies. Also, we experimented for 2 feature maps,  $(64,8,7,7)$  and  $(256,8,7,7)$  where 8 equals with the sample duration. Both feature maps were extracted by using 3D RoiAlign procedure from feature maps with dimensions  $(64,8,28,28)$  and  $(256,8,7,7)$  respectively (in the second case, we just add zeros in the feature map outsize from the bounding boxes for each frame). Table 5.2 contains the first classification results. At first column we have the dimensions of feature maps before pooling function, where  $k = 1,2,\dots,5$ . At second column we have feature maps' dimensions after pooling, and at the next 2 columns, the type of pooling function and the policy we followed. Finally in the last 3 columns we have the mAP performance when we have threshold equal with 0.3, 0.4 and 0.5 respectively. During validation, we keep only the best scoring tube because we know that we have only 1 action per video.

Dimensions		Pooling	Type	mAP precision		
before	after			0.5	0.4	0.3
(k,64,8,7,7)	(1,64,8,7,7)	mean	1	3.16	4.2	4.4
			2	2.29	2.68	2.86
			3	1.63	3.16	4
			4	2.42	4.83	5.46
			5	0.89	1.12	1.21
(k,64,8,7,7)	(1,64,8,7,7)	max	1	1.11	2.35	2.71
			2	2.31	2.62	2.64
			3	1.11	2.35	2.71
			4	1.41	2.76	3.84
			5	0.33	0.51	0.58
(k,256,8,7,7)	(1,256,8,7,7)	mean	1	11.41	11.73	11.73
			2	10.35	10.92	11.89
			3	8.93	9.64	9.94
			4	12.1	13.04	13.04
			5	5.92	6.92	7.79
(k,256,8,7,7)	(1,256,8,7,7)	max	1	<b>22.07</b>	<b>24.4</b>	<b>25.77</b>
			2	14.07	16.56	17.74
			3	14.22	18.94	21.6
			4	21.05	24.63	25.93
			5	11.6	13.92	15.81

Table 5.2: Our architecture's performance using 5 different policies and 2 different feature maps while pooling in tubes' dimension. With bold is the best scoring case

From the above results we notice that features map with dimension  $(256,8,7,7)$  outperform in all cases, both for mean and max pooling and for all the policies. Also, we can see that max pooling outperforms mean pooling in all cases, too. Last but not least, we notice that policies 2, 3 and 5 give us the worst results which means that svm needs both data from other classes positives and from background tubes.

### 5.3.1 Modifying 3D Roi Align

As we mentioned before, we extract from each tube its activation maps using 3D Roi Align procedure and we set equal to zero the pixels outside of bounding boxes for each frame. We came with the idea that the environment surrounding the actor sometimes help us determine the class of the action which is performed. This is base in the idea that 3D Convolutional Networks use the whole scene in order to classify the action that is performed. We thought to extend a little each bounding box both in width and height. So, during Roi Align procedure, after resizing the bounding box into the desired spatial scale (in our case 1/16 because original sample size = 112 and resized sample size = 7) we increase by 1 both width and height. According to that if we have a resized bounding box  $(x_1, y_1, x_2, y_2)$  our new bounding box becomes  $(\max(0, x_1 - 0.5), \max(0, y_1 - 0.5), \min(7, x_2 + 0.5), \min(7, y_2 + 0.5))$  (we use *min* and *max* functions in order to avoid exceeding feature maps' limits). We just experiment in policies 1 and 4 for both (256,8,7,7) and (64,8,7,7) feature maps as show in Table 5.3

Dimensions before	Dimensions after	Pooling	Type	mAP precision		
				0.3	0.4	0.5
(k,64,8,7,7)	(1,64,8,7,7)	mean	1	9.75	11.92	13.34
			4	5.74	6.62	7.59
(k,64,8,7,7)	(1,64,8,7,7)	max	1	6.46	10.26	10.83
			4	4.19	6.27	7.52

Table 5.3: Our architecture's performance using 2 different policies and 2 different pooling methods using modified Roi Align.

According to Table 5.3, modified Roi Align doesn't improve mAP performance. On the contrary, it reduces it. However, the gap between those 2 approaches is small, so we don't abandon this idea, because, for different approaches, modified Roi Align may outclass regular Roi Align.

### 5.3.2 Temporal pooling

After getting first results, we implement a temporal pooling function inspired from Hou, Chen, and Shah 2017. We need a fixed input size for the SVM. However, our tubes' temporal stride varies from 2 to 5, because a video lasting 15 frames is consisted of 2 ToIs and a video of 40 frames is consisted of 5. So we use as fixed temporal pooling equal with 2. As pooling function we use 3D max pooling, one for each filter of the feature map. So for example, for an action tube with 4 consecutive ToIs, we have (4, 256, 8, 7, 7) as feature size. We separate the feature map into 2 groups using *linspace* function and we reshape the feature map into (256, k, 8, 7, 7) where k is the size of each group. After using 3D max pooling, we get a feature map with dimensions (256, 8, 7, 7), so we concat them and finally get feature maps with size of (2, 256, 8, 7, 7). In this case we didn't experiment with feature maps with size (64, 8, 7, 7) because they wouldn't performed better than feature maps with size (256, 8, 7, 7) as noticed from the previous section.

We experiment using a SVM classifier for training policies 1 and 4 and using both regular and modifier Roi Align. The performance results are presented at Table 5.4.

Dimensions before	after	Pooling	Type	mAP precision		
				0.5	0.4	0.3
k,256,8,7,7	2,256,8,7,7	RoiAlign	1	24.97	26.91	29.11
			4	23.27	25.96	28.25
		mod RoiAlign	1	7.01	9.69	10.52
			4	5.5	7.25	8.99

Table 5.4: mAP results using temporal pooling for both RoiAlign approaches

Comparing Tables 5.3 and 5.4, we clearly notice that we get better results when using temporal pooling. Also, the difference between regular Roi Align and modified Roi Align become much bigger than previously, so this makes us abandon the idea of modified Roi Align. So, the rest section, we only experiment using regular Roi Align.

## 5.4 Increasing sample duration to 16 frames

Next, we thought that a good idea would be to increase the sample duration from 8 frames to 16 frames. We experiment both using and not using temporal pooling, again for policies 1 and 4. Results are included at table 5.5.

Dimensions before	after	Temporal Pooling	Type	mAP precision		
				0.5	0.4	0.3
k,256,16,7,7	1,256,16,7,7	No	1	23.4	27.57	28.65
			4	22.7	26.95	28.05
k,256,16,7,7	2,256,16,7,7	Yes	1	21.12	24.07	24.36
			4	18.36	23.09	23.75

Table 5.5: mAP results for policies 1,4 for sample duration = 16

As shown at Table 5.5, we get better performance when we don't use temporal pooling, fact that is unexpected. However, the difference between those performances is about 2%. Probably, this is caused by the fact that, in the temporal pooling approach, SVM classifier has to train too many parameters when it uses temporal pooling, on the contrary with the approach not using temporal pooling, in which SVM has to train half the number of parameters. Furthermore, comparing above results with results shown at Table 5.3, we can see that we get about the same results for both approaches. So, we choose to keep using approach with sample duration equal with 8. That's because, we don't have to use too much memory during training and validation.

## 5.5 Adding more groundtruth tubes

The previous results came from when we train classifiers using only 1 groundtruth action tube and 2 background. We thought that we should experiment with the number of foreground action tubes and the ratio between foreground and background tubes because in previous approaches

these numbers were a little arbitraly. So, we choose to train our previous classifiers using 2, 4 and 8 foreground tubes and a ratio of 2:3, 1:2, 1:3, and 1:4 between the number of foreground tubes and the total number of both foreground and background tubes.

Firstly, we train the RNN classifier using feature maps with dimensions  $(256, 8, 7, 7)$  and mAP performance is presented at Table 5.6 for overlap threshold equal with 0.5, 0.4 and 0.3 .

<b>F. map</b>	<b>FG tubes</b>	<b>Total tubes</b>	<b>mAP</b>		
			0.5	0.4	0.3
(k,256,8,7,7)	2	1	3	11.3	14.14
		3	1.96	5.07	7.27
		4	3	5.03	5.77
		6	1.34	3.89	4.49
		8	0.77	1.51	2.72
	4	6	13.23	21.74	25.4
		8	20.73	28.25	29.50
		12	16.55	24.35	25.22
		16	20.11	25.50	27.62
	8	12	13.82	19.93	22.80
		16	15.47	23.08	24.19
		24	15.88	23.44	24.48
		32	12.66	23.50	25.61

Table 5.6: RNN results

According to Table 5.6, firstly we can see that increasing the number of foreground tubes from 1 to 2 leads to reduce rapidly mAP performance. But, when we set foreground tubes equal to 4 we get better results. On top of that, we get best performance when the ratio is equal with 1:2 and 1:4. Finally, when we set the number of foreground tubes equal with 8, performance gets slightly better comparing with the initial number and ratio but, this situation doesn't get us the best results.

Next, it's time to experiment using the Linear classifier. We use again the same cases like we did for RNN classification. As mentioned before, we need a pooling method before classification step. According to Table 5.1, avg pooling method results in better mAP performance than max pooling, so we use avg pooling for all following cases. Results are included at Table 5.7.

<b>F. map</b>	<b>FG tubes</b>	<b>Total tubes</b>	<b>mAP</b>		
			0.5	0.4	0.3
(k,256,8,7,7)	2	1	3	14.18	19.81
		3	12.68	13.38	15.14
		4	11.5	14.95	16.22
		6	10.74	13.36	15.18
		8	8.00	9.83	11.17
	4	6	15	17.55	19.39
		8	17.04	20.12	22.07
		12	17.57	19.9	21.88
		16	14.24	17.24	17.95

		12	17.91	22.51	24.62
		16	16.76	20.34	22.72
		24	17.61	19.12	24.48
		32	14.45	18.07	19.14

Table 5.7: Linear results

First of all, after considering results presented at both Tables 5.6 and 5.7, it becomes clear that when we set the number of foreground tubes equal with 2, for both case, we get worse results than the initial. This probably is due to the fact that we increase also the number of background tubes for cases when ratio is 1:2, 1:3 and 1:4 resulting in considering more proposed tubes as background tubes. On the other hand when we set ratio equal with 2:3, instead of considering most proposed action tubes as background, classifiers classify them as a specific action class, which means there is an overfitting situation. So, although we think that we shouldn't investigate any more for cases with 2 foreground action tubes, we will train our SVM classifier using 2 foreground tubes and all the aforementioned ratio because we want to be sure about our assumption. On the other hand we notice that using 4 or 8 foreground tubes both get us better results than the initial results. The best results come when ratio between foreground and total tubes is 1:3 for both cases. Then we get good results for ratios 2:3 and 1:2, and we get the worst while using ratio 1:4. This is caused probably from the big number of background tubes in total Comparing with the foreground.

As mentioned before, we train SVM classifier using aforementioned cases only for policy 1 because it gives us the best results for all previous cases. Classification performance using mAP metric is shown at Table 5.8.

F. map	FG tubes	Total tubes	mAP		
			0.5	0.4	0.3
(2,256,8,7,7)	2	1	3	24.97	26.91
		3	13.87	18.74	21.29
		4	14.21	19.67	21.75
		6	12.88	18.62	21.59
		8	12.66	18.7	21.97
	4	6	25.04	26.91	27.82
		8	24.34	25.67	26.34
		12	23.47	25.31	25.9
		16	21.94	23.55	24.23
	8	12	24.83	27.13	27.46
		16	23.97	26.38	26.94
		24	24.17	26.24	26.76
		32	24.17	26.24	26.76

Table 5.8: SVM results

Results shows us some interesting facts. Firstly, it confirms our assumption about not training cases with only 2 foreground tubes, so from now on, we will investigate training situations using 4

or 8 foreground action tube during training. Also, a strange facts occurs, which is that we get almost the same results with the results obtained for using policy 1, only one foreground tube, 3 in total and temporal pooling. This is probably because during training we don't get such good sample set of video like we did during aforementioned situation. But we think that it is better to keep testing using 4 or 8 foreground action tubes. Last but not least, it is clear that we get the best result when we have ration 2:3 between number of foreground and total action tubes. Also, it is more preferable to have 4 foreground action tubes instead of 8. This means that given too many action tubes confuse SVM classifier, so it fails to perform well.

### 5.5.1 Increasing again sample duration (only for RNN and Linear)

Table 5.5 showed that SVM classifier gets about the same performance for both sample durations 8 and 16 frames. Triggered by this fact, we trained RNN and Linear classifiers for sample duration equal with 16 frames. Table 5.9 shows RNN's mAP performance and Table 5.10 Linear's mAP performance. We started experimenting with RNN classifier because it performed better than Linear classifier previously. As mentioned before, we experiment using 4 or 8 foreground tubes and ratios 2:3, 1:2, 1:3 and 1:4 between the number of foreground and total action tubes provided.

FG tubes	Total tubes	mAP		
		0.5	0.4	0.3
4	6	7.94	13.51	14.95
	8	10.88	14.02	14.74
	12	14.05	19.23	20.99
	16	11.69	15.77	16.87
8	12	10.47	15.06	19.93
	16	12.29	19.51	23.11
	24	12.85	18.35	20.00
	32	9.38	14.33	16

Table 5.9: RNN results for sample duration equal with 16

Comparing results from Table 5.9 and previous table 5.6 one by one, it is clear that RNN outperforms when sample duration equals with 8 frames. This results was expected, because, the increase of sample duration reduce the number of video segments needed for each video. So, this means that RNN has to classify sequences with 3 video segments at the most, which is more difficult than classifying bigger sequence like previously.

Next, we experiment using Linear classifier for the same cases like RNN's.

FG tubes	Total tubes	mAP		
		0.5	0.4	0.3
4	6	13.79	19.75	23.63
	8	15.11	19.78	21.14
	12	11.39	15.74	18.15
	16	13.62	16.11	18.15

8	12	10.63	19.37	21.65
	16	12.98	17.52	19.10
	24	12.92	17.64	19.95
	32	11.51	13.98	14.82

Table 5.10: Linear results for sample duration equal with 16

In this case, results from table 5.10 are worse than those presented at Table 5.7, with the difference being about 2%. So, after considering both cases, it becomes clear that it is preferable to experiment using sample duration equal with 8 and not to increase it to 16 frames.

## 5.6 MultiLayer Perceptron (MLP)

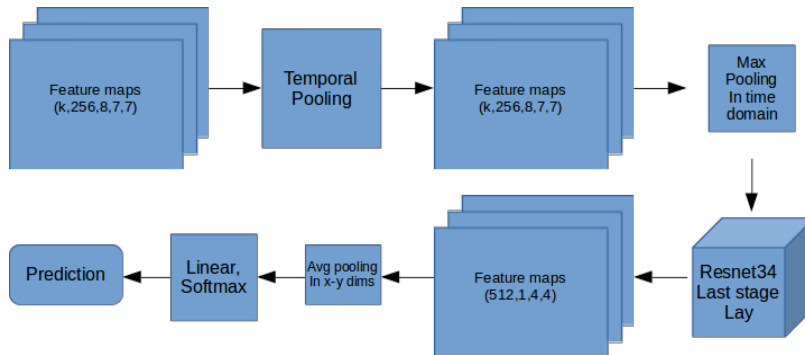


Figure 5.3: Structure of the MLP classifier

In previous sections we used classic classifiers like Linear, RNN and SVM. Last but not least approach, another widely category of classifiers is Multilayer Perceptron (MLP) classifiers. MLP is a class of feedforward Neural Network, so its function is described in chapter 2. So, we design a MLP which is shown in Figure 5.3 for sample duration equal with 8, and is described below:

- At first, after 3D Roi align and for sample duration = 8, we get an activation map of  $(k, 256, 8, 7, 7)$  where  $k$  is the number of linked ToIs. Inspired by previous sections, we perform temporal pooling followed by a max pooling operation in sample duration's dimension. So, we now have an activation maps with dimensions equal with  $(2, 256, 7, 7)$ , which we reshape it into  $(256, 2, 7, 7)$ . We extracted layers from the last stage of ResNet34. This stages includes 3 Residual Layers with stride equal with 2 in all 3 dimensions and output number of filters equal with 512.
- After Residual Layers, we perform temporal pooling for x-y dimensions. So we get as output activation maps with dimension size equal with  $(512,)$ . Finally, we feed these feature maps to a linear layer in order to get class confidence score, after applying soft-max function.

### 5.6.1 Regular training

According to figure 5.1, the trainable parts of our network is TPN and the classifier. As mentioned before, training code requires running only one video per GPU, because, videos have different duration. For previous approaches we came with the idea of pre-calculating video features and then training only the classifier. However, for this step, we normally trained our in order to get classification results. Of course, we used a pre-trained TPN, whose layers were freezed in order not to be trained. We tried to explore different ratios between the number of foreground tubes and the total number of tubes per video. First 3 simulations included fixed number of total tubes and variable ratio between the number of foreground and background tubes. We started using only foreground tubes, which means 32 out 32 tubes are foreground, then half of the proposed tubes aka 16 out of 32 and finally less than half, namely 14 out of 32. After that, we experiment using a fixed number of foreground tubes and variable number of total tubes, which are 16, 24 and 32. The performance results are presented at Table 5.11.

<b>FG tubes</b>	<b>Total tubes</b>	<b>mAP</b>		
		0.5	0.4	0.3
32	32	1.28	1.73	1.87
16		3.98	4.38	4.38
14		0.40	0.40	0.40
8	16	9.41	12.59	14.61
	24	12.32	15.53	18.57
	32	7.16	10.92	13.00

Table 5.11: MLP'smAP performance for regular training procedure

The results show that when first 3 approaches give us very bad results. Comparing them with the rest 3, we came with the conclusion that we need at the most 8 foreground tubes, even though the ration between the number of foreground and background is in favor the second one. Probably, too many foreground action tubes make our architecture overfitted so unable to generalize.

### 5.6.2 Extract features

As previously performed, we trained MLP classifier using pre-computed feature maps. These feature maps include both foreground and background action tubes. Base on the conclusion made in previous sections, we will train our classifier only for number of foreground tubes equal with 4 and 8. Furthermore, we will train it for 3 different ratios between the number of foreground and background action tubes, which are 1:1, 1:2 and 1:3. Table 5.12 shows these cases and their respective mAP performance during validation step.

<b>FG tubes</b>	<b>Total tubes</b>	<b>mAP</b>		
		0.5	0.4	0.3
4	6	4,37	8,54	10,12
	8	5.89	9.54	13.61
	12	9.51	12.8	14.6
	16	6.80	13.17	14.67

8	12	8.62	12.32	14.74
	16	8.49	13.94	15.09
	24	6.72	12.17	15.30
	32	13.27	17.64	18.97

Table 5.12: mAP results for MLP trained using extracted features

Comparing results from Tables 5.12 and 5.11, it is clear we need 8 foreground tubes in order to perform well. However, it isn't very clear which of these two proposed training approaches is better, but if we have to decide one method, we would choose using pre-extracted features training. This approach manages to achieve the best results, and especially when we have 8 foreground action tubes and 32 in total. Also, comparing methods using 4 or 8 positive action tubes, it is clear that we would prefer using 8 generally. However, it's not clear which ratio is better because, we get best results when we have 8 foreground action tubes and ratio 1:4 while we get best results when ratio is 1:3 having 4 positive action tubes.

## 5.7 Adding nms algorithm

After getting previous classification results, we came with the idea that a lot of proposed action tubes overlap spatiotemporally like presented in chapter 4, for the first linking algorithm. On top of that, even though, at last, we will keep only the best scoring action tube, maybe, our Network sometimes doesn't score the best overlapping action tube but a neighbour, which should have been removed. So, similar with chapter 4, we added NMS algorithm before classification stage in order to remove unnecessary overlapping action tubes. The structure of this approach is presented at Figure 5.4. So, we run again validation stage for our classifiers and results are presented at Tables 5.13, 5.14, 5.15 and 5.16 for SVM, RNN, Linear and MLP classifiers respectively.

We start experimenting using SVM classifier, whose mAP performance is presented at Table 5.13 when we use NMS algorithm.

FG tubes	Total tubes	mAP		
		0.5	0.4	0.3
4	6	21.42	24.3	25.11
	8	21.3	24.06	24.85
	12	21.73	24.19	25.04
	16	21.11	23.98	24.84
8	12	20.47	22.55	23.41
	16	21.21	23.89	24.97
	24	21.71	23.8	24.82
	32	21.43	23.5	24.52

Table 5.13: mAP results for SVM classifier after adding NMS algorithm

According to Table 5.13 and taking Table's 5.8 results into consideration, it is clear that mAP

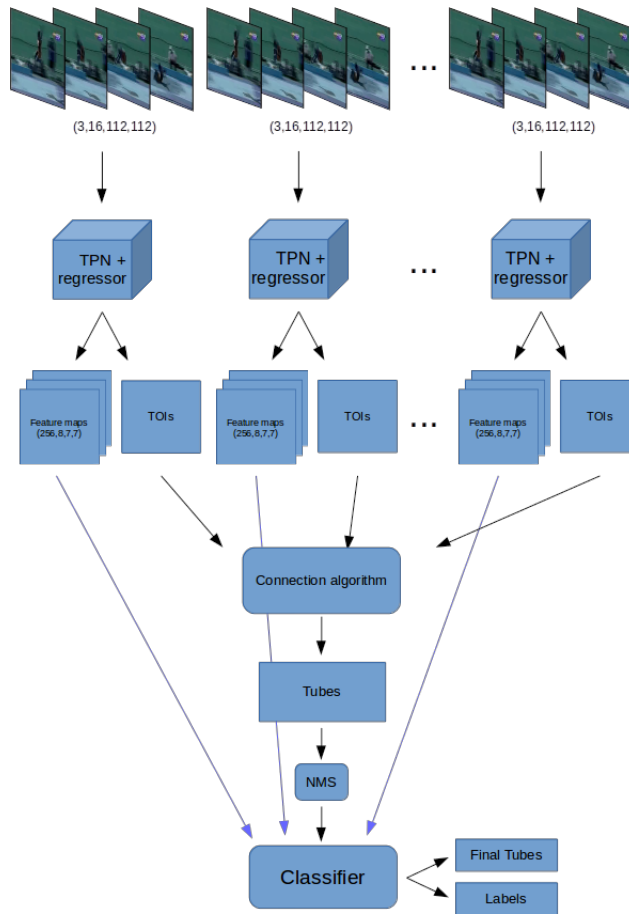


Figure 5.4: Structure of the network with NMS

performance decreases while using NMS algorithm. We run only for case with foreground tubes equal with 4 or 8 and we didn't experiment using initial ratio, because we think that we are going to get the same attitude. This is probably because NMS algorithm removes some overlapping action tubes, so SVM classifier doesn't get the right action tubes for classifying them.

Next, we experiment using RNN classifier for sample duration equal with 8 frames per video segment. Results are included at Table 5.14

<b>FG tubes</b>	<b>Total tubes</b>	<b>mAP</b>		
		0.5	0.4	0.3
4	6	13.27	26.12	30.69
	8	16.06	25.81	27.63
	12	13.93	22.48	23.99
	16	17.24	26.44	28.36
8	12	2	5.11	7.75
	16	11.11	20.98	23.97
	24	13.84	22.77	24.31
	32	12.74	21.49	25.39

Table 5.14: mAP results for RNN classifier after adding NMS algorithm

Alongside with SVM's mAP performances, RNN doesn't achieve any improvement in its mAP performance when adding NMS algorithm. On the contrary, it reduce about 5% in some cases, so it is more preferable to use ActionNet's architecture without NMS algorithm included while using RNN as classifier.

Following RNN, we investigate the same situations with Linear classify instead of RNN. Its performance is presented at Table 5.15.

<b>FG tubes</b>	<b>Total tubes</b>	<b>mAP</b>		
		0.5	0.4	0.3
4	6	12.59	14.91	17.79
	8	15.89	21.92	23.28
	12	13.23	19.72	23.17
	16	15.07	17.38	18.27
8	12	18.88	24.37	26.72
	16	15.42	22.31	24.70
	24	15.60	19.71	21.08
	32	16.1	19.99	21.47

Table 5.15: mAP results for Linear classifier after adding NMS algorithm

On the contrary with SVM and RNN's performances, Linear's mAP performance is getting better when adding NMS algorithm, comparing results presented at Tables 5.15 and 5.7. This is probably because Linear classifier gets now less proposed action tubes comparing with previous approach. So, now it is less likely to misclassify an action tube, probably considering it as foreground when actually is a background action tube. Even though its performance increased, it doesn't achieve our best results, fact which may corroborate our previous claim. Last but not least, we need to experiment using MLP classifier in order to determine if NMS algorithm is needed during classification. The results are presented at Table 5.16.

<b>FG tubes</b>	<b>Total tubes</b>	<b>mAP</b>		
		0.5	0.4	0.3
4	6	3.66	7.23	9.43
	8	3.43	8.17	12.77
	12	6.32	11.26	16.15
	16	4.82	11.38	15.85
8	12	5.92	12.42	15.81
	16	6	12.55	14.66
	24	4.73	11.33	15.25
	32	9.67	14.82	16.74

Table 5.16: mAP results for MLP classifier after adding NMS algorithm

Finally, comparing results from Tables 5.16 and ??, again adding NMS algorithm approach decreases mAP performance. Consequently, after considering all situations it is clear that NMS algorithm doesn't contribute at the improvement of Network's mAP performance, but, on the contrary, it reduces it. So, as a final comment, it is more preferable not to use it, except when we use Linear classifier for classification.

### 5.7.1 General comments

To sum up, in this section we tried to find the most suitable classifier for achieve good classification results based on mAP metric. It is clear that when using a SVM classifier, which uses temporal pooling in order to have a fix-size input, we get the best results. The most suitable method for training is using about 4 foreground action tubes and only 2 background which using both background action tubes and action tubes from other classes as hard-negatives.

## 5.8 Classifying dataset UCF

### 5.8.1 Introduction

During previous section we explore different classification methods using several classifiers. On top of that, it became clear how important is generating good proposal considering the situation where we added NMS algorithm. NMS algorithm reduce the number of proposed action tubes, so most of classifiers failed to improve their performance. Considering recall and MABO performances presented in chapter 5, it is clear that our network would fail recognizing most of spatiotemporal action tubes and to correctly classify them. However, in most cases, MABO performance got score about 92-94%. So, we came with the idea of rather than performing spatiotemporal localization and classification, for dataset UCF, we perform only temporal localization. This means that we tried to detect video segments in which an action is performed, and also we try to determine the class of the performed action.

### 5.8.2 Only temporal classification

As presented in chapter 5, our connection algorithm is able to get good temporal recall and MABO performance. In order to temporally localize action in videos, we use only the temporal information containing in the proposed action tubes, which means the first and the last frame of the action tube. After that, we will classify the proposed action tubes without performing spatiotemporal localization, but only temporal. Although we don't use the extracted bounding boxes for classification, we take advantage of the spatial information in order to perform better temporal localization. Intuitively, that's because, in order to extract the action tubes, we consider the spatial overlap between the connected ToIs. This aforementioned approach includes the following steps:

1. First, we use TPN in order to propose spatiotemporal ToIs, just like we did in previous approaches. Then, we link those ToIs based on the proposed algorithm in the chapter 5, using spatiotemporal NMS algorithm with threshold equal with 0.9, for removing overlapping action tubes.
2. Previous steps is exactly the same as previous classification approaches. However, in this approach, we don't use any kind of Roi Align in order to extract action tubes' feature

maps. On the contrary, for all the proposed action tubes, we find their duration, aka their first and their last frame. After that, we perform temporal nms in order to remove overlapping action tubes. The only difference between spatiotemporal and temporal nms is the overlapping criterion, which is used. For spatiotemporal nms, we use spatiotemporal IoU and respectively, for temporal we use temporal IoU as presented in chapter 2.

3. Of course, the proposed action tubes last more than 16 frames, which we set as sample duration. So, we separate action tubes into video clips lasting 16 frames (like our sample duration). These video segments are fed, again at a 3D resNet34 (Hara, Kataoka, and Satoh 2018), but this time, we don't use it only for feature extraction but, also for classification for each video segment.
4. So, for each video clip, for each class we get a confidence score after performing softmax operation. Finally, we get average confidence score for each class, and we consider the best-scoring class as the class label of each action tube. Of course, some action tubes may not contain any action, so we set a confidence score for separate foreground action tubes with background.

**Training** The only trainable part of this architecture is the ResNet34. We use a pre-trained TPN as presented in chapter 4. ResNet34 training procedure is based on the code given by Hara, Kataoka, and Satoh 2018. We modified it in order to be able to be trained for dataset UCF-101, only for the 24 classes, for which there are spatiotemporal notations and our TPN is trained.

**Validation** Based on the aforementioned steps, it is clear that the parameters that can be modified are temporal NMS' threshold and confidence threshold for deciding if an action is contained or not. All the different combinations used during validation are presented at Table 5.17.

NMS thresh	Conf thresh	mAP		
		0.5	0.4	0.3
0.9	0.6	0.3	0.54	0.64
	0.75	0.25	0.45	0.55
	0.85	0.2	0.38	0.49
0.7	0.6	0.63	1.02	1.27
	0.75	0.5	0.84	1.05
	0.85	0.4	0.68	0.89
0.5	0.6	0.96	1.21	1.75
	0.75	0.63	0.93	1.38
	0.85	0.57	0.72	1.03
0.4	0.6	1.07	1.52	2.03
	0.75	0.79	1.18	1.63
	0.85	0.71	0.98	1.33
0.3	0.6	1.1	1.66	2.53
	0.75	0.93	1.39	2.08
	0.85	0.81	1.12	1.6
0.2	0.6	0.84	1.38	2.17
	0.75	0.73	1.13	1.78
	0.85	0.65	0.81	1.31

Table 5.17: UCF's temporal localization mAP performance

NMS thresh	Recall			MABO
	0.9	0.8	0.7	
0.9	0.7361	0.8935	0.9422	0.9138130172
0.7	0.3194	0.6875	0.9293	0.8412186326
0.5	0.1757	0.3331	0.6281	0.7471525429
0.4	0.1483	0.2829	0.4707	0.6986400756
0.3	0.111	0.2038	0.3848	0.6429232202

Table 5.18: UCF's temporal localization recall and MABO performances

According to Table 5.17, mAP performance for temporal localization and classification is very bad. The best performance is about 2%, score which is very low. Comparing these results with results shown at Table 5.18, we deduce that our method is not at all efficient. Even though mAP results increase slightly, recall and MABO performance decrease rapidly. Of course, this result is anticipated because, by decreasing NMS threshold, the number of rejected action tubes is increased.

We tried another approach, which applies NMS algorithm after classification stage, and not before it like we did previously. Also, we noticed in previous results that in most cases, we get these low performances because of the number of false positives, which don't get removed during NMS procedure. To be more specific, Table 5.19 shows all the detected true and false positives when we set NMS threshold equal with 0.2, mAP overlap threshold equal with 0.3 and confidence threshold equal with 0.6 for both aforementioned approaches.

Class	Appr 1		Appr 2		Class	Appr 1		Appr 2	
	TP	FP	TP	FP		TP	FP	TP	FP
Basketball	5	279	6	403	BasketballDunk	7	7	12	13
Biking	0	3	0	5	CliffDiving	11	55	1	1
CricketBowling	0	0	10	75	Diving	20	189	23	272
Fencing	11	222	25	336	FloorGymnastics	2	86	6	131
GolfSwing	4	51	6	78	HorseRiding	0	33	4	58
IceDancing	8	29	6	38	LongJump	1	24	6	43
PoleVault	0	202	9	296	RopeClimbing	1	24	4	43
SalsaSpin	3	158	5	237	SkateBoarding	0	10	0	13
Skiing	0	0	0	0	Skijet	1	27	6	43
SoccerJuggling	3	94	1	153	Surfing	11	102	23	159
TennisSwing	0	125	0	166	TrampolineJumping	4	18	4	32
VolleyballSpiking	20	704	20	1044	WalkingWithDog	0	5	0	9

Table 5.19: Comparing TP and FP for both approaches

Considering those two facts we came with the following solution. In previous approach, we sorted candidate action tubes using connection scores obtained from linking algorithm and then

we removed the overlapping action tubes. In our new approach, we firstly remove action tubes with same temporal limits, in order to get unique temporal action tubes. Then, we classify all the proposed action tubes exactly like we did in step 3 previously. After that, we perform temporal NMS using the confidence scores extracted by the last layer of the 3D ResNet34 and finally we keep those which their confidence score is over a predefined threshold.

<b>NMS thresh</b>	<b>Conf thresh</b>	<b>mAP</b>		
		0.5	0.4	0.3
0.9	0.6	0.31	0.54	0.65
	0.75	0.26	0.46	0.55
	0.85	0.2	0.39	0.49
0.7	0.6	0.66	0.95	1.22
	0.75	0.55	0.80	1.01
	0.85	0.41	0.67	0.87
0.5	0.6	0.98	1.43	1.63
	0.75	0.75	1.14	1.29
	0.85	0.64	0.92	1.04
0.4	0.6	1.19	1.73	2.15
	0.75	0.9	1.35	1.63
	0.85	0.79	1.16	1.38
0.3	0.6	1.12	1.85	2.23
	0.75	0.96	1.54	1.7
	0.85	0.83	1.28	1.43
0.2	0.6	2.05	2.68	3.7
	0.75	1.61	2.17	3
	0.85	1.51	1.88	2.54

Table 5.20: UCF's temporal localization mAP performance

Comparing Tables 5.20 and 5.18, we get about the same results for overlap thresholds 0.9, 0.7, 0.5, 0.4 and 0.3 . But for overlap threshold 0.2 we notice that mAP performance is improved about 1%. So, we thought that we should use even smaller overlap thresholds, which are 0.15, 0.1, and 0.05 which are presented at Table 5.21.

<b>NMS thresh</b>	<b>Conf thresh</b>	<b>mAP</b>		
		0.5	0.4	0.3
0.15	0.6	2.01	2.66	3.62
	0.75	1.62	2.21	2.97
	0.85	1.51	1.91	2.56
0.10	0.6	1.87	2.74	3.77
	0.75	1.62	2.28	3.08
	0.85	1.5	2	2.7
0.05	0.6	1.85	2.71	3.73
	0.75	1.61	2.28	3.1
	0.85	1.5	2	2.7

Table 5.21: UCF's temporal localization mAP performance for even smaller NMS threshold

Using very small NMS threshold results in a tiny improvement in mAP performance. However, these scores are far away from state-of-the-art results. So, we think that we should rethink the way we trained our classifier and the way it classifies given action tubes, in order to be able to classify efficiently. This research is left for future work, and won't be investigated in this thesis.

# Chapter 6

## Conclusion - Future work

### 6.1 Conclusion

In this thesis we explore the problem of action recognition and localization. We design a network base on Hou, Chen, and Shah 2017 combined with some elements from Girdhar et al. 2017, Ren et al. 2015, Girshick 2015, Hu et al. 2019 and Hara, Kataoka, and Satoh 2018.

We write a pytorch implementation expanding code only from Yang et al. 2017. Futhermore, we wrote our own code using some CUDA functions designed by us (like calculating connection scores, modifying tubes etc.).

We tried to design a design a Tube Proposal Network for proposing action tubes in given video segments, inspired by Faster R-CNN's RPN. We designed it using general anchors and not dataset specific anchors in order to try to generalize our approach for several datasets, on the contrary with the approach proposed by Girdhar et al. 2017, in which it uses the most frequently appearing anchors as the general anchors.

On top of that, we designed a naive connection algorithm for connecting our proposed action tubes based on the one proposed by Girdhar et al. 2017. In our approach, we use the same scoring policy, which is a combination between actioness and overlaping scores. The main difference is that we avoid to calculate all the possible combinations using an updating threshold. We, also, tried another connection algorithm inspired by Hu et al. 2019. However, our implementation wasn't very good so, we didn't explore all of its pontentials.

Finally, we explored several classifiers for the classification stage of our network, which are a RNN, a SVM and a MLP. We used an implementation taken from Fast RCNN for the SVM classifier, which included hard negatives mining trainig procedure. Futhermore, we explore some training techniques for best classification performance and 2 training approaches, the classic one and using pre-extracted features.

### 6.2 Future work

There is a lot of room for improvement for our network, in order to achieve state-of-the-art results. The most important are described in next paragraphs.

**Improving TPN proposals** We implemented 2 networks for proposing action tubes in a video segment. We managed to achieve about 63% recall score for sample duration = 16 and about 80% recall for sample duration = 8. Theses scores show that there is plenty room for

improvement especially for sample duration = 16. Even though a lot of networks' architectures have been explored for regression, a good idea would be to try other networks, not necessarily inspired by object detection networks like we did. On top of that, adding a  $\lambda$  factor in training loss would be a good idea and exploring which is the best approach. So training loss could be defined as:

$$L = \sum_i L_{cls}(p_i, p_i^*) + \lambda_1 \sum_i p_i^* L_{reg}(t_i, t_i^*) + \lambda_2 \sum_i q_i^* L_{reg}(c_i, c_i^*) \quad (6.1)$$

Furthermore, it would be a good idea to use SSD's (Liu et al. 2015) proposal network instead of RPN, in order to compare result. Finally, we could experiment using Feature Pyramid Networks, which could be extracted in 3 dimensions as another feature extractor or some other type of 3D ResNet.

**Changing Connection algorithm** In this thesis, another challenge we came was connecting proposed ToIs for proposing action tubes. We implemented a very naive algorithm, which wasn't able to give us very good proposals despite the changes we tried to do. We implemented another connection algorithm which was base in a estimation on temporal progress of an action and their overlap. Although it also didn't give us very good proposals, we believe that we should explore this algorithm's potentials. That's because it takes advantage of the progress of the action, which the previous algorithm didn't.

**Explore other classification techniques** For classification stage, we experiment mainly on a SVM classifier for JHMDB dataset and we didn't get involved a lot with UCF dataset. We found the best feature maps from JHMDB and we used the same for UCF. We think that we should explore UCF's feature maps even though we believe that there will be the same. It is essential to confirm our assumption. In addition, we could try other classification techniques like random forest or experiment more with RNN classifier for the UCF dataset. Finally, another classification procedure would be a good idea, like extracting first all the possible action tubes and then using other network's features for classification stage.

# Bibliography

- [1] O. Chomat and J. L. Crowley. “Probabilistic recognition of activity using local appearance”. In: *Proceedings. 1999 IEEE Computer Society Conference on Computer Vision and Pattern Recognition (Cat. No PR00149)*. Vol. 2. 1999, 104–109 Vol. 2. doi: 10.1109/CVPR.1999.784616.
- [2] Aaron Bobick and J.W. Davis. “The recognition of human movement using temporal templates”. In: *Pattern Analysis and Machine Intelligence, IEEE Transactions on* 23 (Apr. 2001), pp. 257 –267. doi: 10.1109/34.910878.
- [3] L. Zelnik-Manor and M. Irani. “Event-based analysis of video”. In: *Proceedings of the 2001 IEEE Computer Society Conference on Computer Vision and Pattern Recognition. CVPR 2001*. Vol. 2. 2001, pp. II–II. doi: 10.1109/CVPR.2001.990935.
- [4] Laptev and Lindeberg. “Space-time interest points”. In: *Proceedings Ninth IEEE International Conference on Computer Vision*. 2003, 432–439 vol.1. doi: 10.1109/ICCV.2003.1238378.
- [5] Alper Yilmaz and Mubarak Shah. “Actions sketch: a novel action representation”. In: *2005 IEEE Computer Society Conference on Computer Vision and Pattern Recognition (CVPR’05)*. Vol. 1. 2005, 984–989 vol. 1. doi: 10.1109/CVPR.2005.58.
- [6] M. Blank et al. “Actions as space-time shapes”. In: *Tenth IEEE International Conference on Computer Vision (ICCV’05) Volume 1*. Vol. 2. 2005, 1395–1402 Vol. 2. doi: 10.1109/ICCV.2005.28.
- [7] P. Dollar et al. “Behavior recognition via sparse spatio-temporal features”. In: *2005 IEEE International Workshop on Visual Surveillance and Performance Evaluation of Tracking and Surveillance*. 2005, pp. 65–72. doi: 10.1109/VSPETS.2005.1570899.
- [8] E. Shechtman and M. Irani. “Space-time behavior based correlation”. In: *2005 IEEE Computer Society Conference on Computer Vision and Pattern Recognition (CVPR’05)*. Vol. 1. 2005, 405–412 vol. 1. doi: 10.1109/CVPR.2005.328.
- [9] Y. Sheikh, M. Sheikh, and M. Shah. “Exploring the space of a human action”. In: *Tenth IEEE International Conference on Computer Vision (ICCV’05) Volume 1*. Vol. 1. 2005, 144–149 Vol. 1. doi: 10.1109/ICCV.2005.90.
- [10] A. Yilmaz and M. Shah. “Recognizing human actions in videos acquired by uncalibrated moving cameras”. In: *Tenth IEEE International Conference on Computer Vision (ICCV’05) Volume 1*. Vol. 1. 2005, 150–157 Vol. 1. doi: 10.1109/ICCV.2005.201.
- [11] Juan Carlos Niebles, Hongcheng Wang, and Fei Fei Li. “Unsupervised Learning of Human Action Categories Using Spatial-Temporal Words.” In: vol. 79. Sept. 2006, pp. 1249–1258.
- [12] M.S. Ryoo and J.K. Aggarwal. “Semantic Understanding of Continued and Recursive Human Activities”. In: Jan. 2006, pp. 379 –378. doi: 10.1109/ICPR.2006.1043.

- [13] Y. Ke, R. Sukthankar, and M. Hebert. “Spatio-temporal Shape and Flow Correlation for Action Recognition”. In: *2007 IEEE Conference on Computer Vision and Pattern Recognition*. 2007, pp. 1–8. DOI: 10.1109/CVPR.2007.383512.
- [14] M. D. Rodriguez, J. Ahmed, and M. Shah. “Action MACH a spatio-temporal Maximum Average Correlation Height filter for action recognition”. In: *2008 IEEE Conference on Computer Vision and Pattern Recognition*. 2008, pp. 1–8. DOI: 10.1109/CVPR.2008.4587727.
- [15] Mark Everingham et al. “The Pascal Visual Object Classes (VOC) Challenge”. In: *Int. J. Comput. Vision* 88.2 (June 2010), pp. 303–338. ISSN: 0920-5691. DOI: 10.1007/s11263-009-0275-4. URL: <http://dx.doi.org/10.1007/s11263-009-0275-4>.
- [16] P. F. Felzenszwalb et al. “Object Detection with Discriminatively Trained Part-Based Models”. In: *IEEE Transactions on Pattern Analysis and Machine Intelligence* 32.9 (2010), pp. 1627–1645. DOI: 10.1109/TPAMI.2009.167.
- [17] J.K. Aggarwal and M.S. Ryoo. “Human Activity Analysis: A Review”. In: *ACM Comput. Surv.* 43.3 (Apr. 2011), 16:1–16:43. ISSN: 0360-0300. DOI: 10.1145/1922649.1922653. URL: <http://doi.acm.org/10.1145/1922649.1922653>.
- [18] H. Kuehne et al. “HMDB: a large video database for human motion recognition”. In: *Proceedings of the International Conference on Computer Vision (ICCV)*. 2011.
- [19] Khurram Soomro, Amir Roshan Zamir, and Mubarak Shah. “UCF101: A dataset of 101 human actions classes from videos in the wild”. In: *arXiv preprint arXiv:1212.0402* (2012).
- [20] Ross B. Girshick et al. “Rich feature hierarchies for accurate object detection and semantic segmentation”. In: *CoRR* abs/1311.2524 (2013). arXiv: 1311.2524. URL: <http://arxiv.org/abs/1311.2524>.
- [21] H. Jhuang et al. “Towards understanding action recognition”. In: *International Conf. on Computer Vision (ICCV)*. Dec. 2013, pp. 3192–3199.
- [22] Shuiwang Ji, Ming Yang, and Kai Yu. “3D convolutional neural networks for human action recognition.” In: *IEEE transactions on pattern analysis and machine intelligence* 35.1 (2013), pp. 221–31.
- [23] Santiago Manen, Matthieu Guillaumin, and Luc Van Gool. “Prime Object Proposals with Randomized Prim’s Algorithm”. In: *Proceedings of the 2013 IEEE International Conference on Computer Vision. ICCV ’13*. Washington, DC, USA: IEEE Computer Society, 2013, pp. 2536–2543. ISBN: 978-1-4799-2840-8. DOI: 10.1109/ICCV.2013.315. URL: <http://dx.doi.org/10.1109/ICCV.2013.315>.
- [24] Y. Tian, R. Sukthankar, and M. Shah. “Spatiotemporal Deformable Part Models for Action Detection”. In: *2013 IEEE Conference on Computer Vision and Pattern Recognition*. 2013, pp. 2642–2649. DOI: 10.1109/CVPR.2013.341.
- [25] J.R.R. Uijlings et al. “Selective Search for Object Recognition”. In: *International Journal of Computer Vision* (2013). DOI: 10.1007/s11263-013-0620-5. URL: <http://www.huppelen.nl/publications/selectiveSearchDraft.pdf>.
- [26] Jeff Donahue et al. “Long-term Recurrent Convolutional Networks for Visual Recognition and Description”. In: *CoRR* abs/1411.4389 (2014). arXiv: 1411.4389. URL: <http://arxiv.org/abs/1411.4389>.
- [27] Georgia Gkioxari and Jitendra Malik. “Finding Action Tubes”. In: *CoRR* abs/1411.6031 (2014). arXiv: 1411.6031. URL: <http://arxiv.org/abs/1411.6031>.

- [28] M. Jain et al. “Action Localization with Tubelets from Motion”. In: *2014 IEEE Conference on Computer Vision and Pattern Recognition*. 2014, pp. 740–747. DOI: 10.1109/CVPR.2014.100.
- [29] A. Karpathy et al. “Large-Scale Video Classification with Convolutional Neural Networks”. In: *2014 IEEE Conference on Computer Vision and Pattern Recognition*. 2014, pp. 1725–1732. DOI: 10.1109/CVPR.2014.223.
- [30] Dan Oneata et al. “Spatio-Temporal Object Detection Proposals”. In: Sept. 2014. DOI: 10.1007/978-3-319-10578-9\_48.
- [31] Karen Simonyan and Andrew Zisserman. “Two-stream convolutional networks for action recognition in videos”. In: *Advances in Neural Information Processing Systems*. 2014, pp. 568–576.
- [32] Du Tran et al. “Learning Spatiotemporal Features with 3D Convolutional Networks”. In: *2015 IEEE International Conference on Computer Vision (ICCV)* (2014), pp. 4489–4497.
- [33] W. Chen and J. J. Corso. “Action Detection by Implicit Intentional Motion Clustering”. In: *2015 IEEE International Conference on Computer Vision (ICCV)*. 2015, pp. 3298–3306. DOI: 10.1109/ICCV.2015.377.
- [34] Jan C. van Gemert et al. “APT: Action localization proposals from dense trajectories”. In: *Proceedings of the British Machine Vision Conference (BMVC)*. BMVA Press, 2015, pp. 177.1–177.12. ISBN: 1-901725-53-7. DOI: 10.5244/C.29.177. URL: <https://dx.doi.org/10.5244/C.29.177>.
- [35] Ross Girshick. “Fast R-CNN”. In: *Proceedings of the 2015 IEEE International Conference on Computer Vision (ICCV)*. ICCV ’15. Washington, DC, USA: IEEE Computer Society, 2015, pp. 1440–1448. ISBN: 978-1-4673-8391-2. DOI: 10.1109/ICCV.2015.169. URL: <http://dx.doi.org/10.1109/ICCV.2015.169>.
- [36] Kaiming He et al. “Deep Residual Learning for Image Recognition”. In: *CoRR* abs/1512.03385 (2015). arXiv: 1512.03385. URL: <http://arxiv.org/abs/1512.03385>.
- [37] Wei Liu et al. “SSD: Single Shot MultiBox Detector”. In: *CoRR* abs/1512.02325 (2015). arXiv: 1512.02325. URL: <http://arxiv.org/abs/1512.02325>.
- [38] Joe Yue-Hei Ng et al. “Beyond Short Snippets: Deep Networks for Video Classification”. In: *CoRR* abs/1503.08909 (2015). arXiv: 1503.08909. URL: <http://arxiv.org/abs/1503.08909>.
- [39] Joseph Redmon et al. “You Only Look Once: Unified, Real-Time Object Detection”. In: *CoRR* abs/1506.02640 (2015). arXiv: 1506.02640. URL: <http://arxiv.org/abs/1506.02640>.
- [40] Shaoqing Ren et al. “Faster R-CNN: Towards Real-time Object Detection with Region Proposal Networks”. In: *Proceedings of the 28th International Conference on Neural Information Processing Systems - Volume 1*. NIPS’15. Montreal, Canada: MIT Press, 2015, pp. 91–99. URL: <http://dl.acm.org/citation.cfm?id=2969239.2969250>.
- [41] K. Soomro, H. Idrees, and M. Shah. “Action Localization in Videos through Context Walk”. In: *2015 IEEE International Conference on Computer Vision (ICCV)*. 2015, pp. 3280–3288. DOI: 10.1109/ICCV.2015.375.
- [42] Philippe Weinzaepfel, Zaïd Harchaoui, and Cordelia Schmid. “Learning to track for spatio-temporal action localization”. In: *CoRR* abs/1506.01929 (2015). arXiv: 1506.01929. URL: <http://arxiv.org/abs/1506.01929>.

- [43] G. Yu and J. Yuan. “Fast action proposals for human action detection and search”. In: *2015 IEEE Conference on Computer Vision and Pattern Recognition (CVPR)*. 2015, pp. 1302–1311. DOI: 10.1109/CVPR.2015.7298735.
- [44] R. G. Cinbis, J. Verbeek, and C. Schmid. “Weakly Supervised Object Localization with Multi-Fold Multiple Instance Learning”. In: *IEEE Transactions on Pattern Analysis and Machine Intelligence* 39.1 (2016), pp. 189–203. DOI: 10.1109/TPAMI.2016.2535231.
- [45] Christoph Feichtenhofer, Axel Pinz, and Andrew Zisserman. “Convolutional Two-Stream Network Fusion for Video Action Recognition”. In: *CoRR* abs/1604.06573 (2016). arXiv: 1604.06573. URL: <http://arxiv.org/abs/1604.06573>.
- [46] Gao Huang, Zhuang Liu, and Kilian Q. Weinberger. “Densely Connected Convolutional Networks”. In: *CoRR* abs/1608.06993 (2016). arXiv: 1608.06993. URL: <http://arxiv.org/abs/1608.06993>.
- [47] Pascal Mettes, Jan C. van Gemert, and Cees G. M. Snoek. “Spot On: Action Localization from Pointly-Supervised Proposals”. In: *CoRR* abs/1604.07602 (2016). arXiv: 1604.07602. URL: <http://arxiv.org/abs/1604.07602>.
- [48] Xiaojiang Peng and Cordelia Schmid. “Multi-region two-stream R-CNN for action detection”. In: *ECCV - European Conference on Computer Vision*. Vol. 9908. Lecture Notes in Computer Science. Amsterdam, Netherlands: Springer, Oct. 2016, pp. 744–759. DOI: 10.1007/978-3-319-46493-0\_45. URL: <https://hal.inria.fr/hal-01349107>.
- [49] Suman Saha et al. “Deep Learning for Detecting Multiple Space-Time Action Tubes in Videos”. In: *CoRR* abs/1608.01529 (2016). arXiv: 1608.01529. URL: <http://arxiv.org/abs/1608.01529>.
- [50] Limin Wang et al. “Temporal Segment Networks: Towards Good Practices for Deep Action Recognition”. In: *CoRR* abs/1608.00859 (2016). arXiv: 1608.00859. URL: <http://arxiv.org/abs/1608.00859>.
- [51] Philippe Weinzaepfel, Xavier Martin, and Cordelia Schmid. “Towards Weakly-Supervised Action Localization”. In: *CoRR* abs/1605.05197 (2016). arXiv: 1605.05197. URL: <http://arxiv.org/abs/1605.05197>.
- [52] Anton Winschel, Rainer Lienhart, and Christian Eggert. “Diversity in Object Proposals”. In: *CoRR* abs/1603.04308 (2016). arXiv: 1603.04308. URL: <http://arxiv.org/abs/1603.04308>.
- [53] Bowen Zhang et al. “Real-time Action Recognition with Enhanced Motion Vector CNNs”. In: *CoRR* abs/1604.07669 (2016). arXiv: 1604.07669. URL: <http://arxiv.org/abs/1604.07669>.
- [54] Harkirat S. Behl et al. “Incremental Tube Construction for Human Action Detection”. In: *CoRR* abs/1704.01358 (2017). arXiv: 1704.01358. URL: <http://arxiv.org/abs/1704.01358>.
- [55] Navaneeth Bodla et al. “Improving Object Detection With One Line of Code”. In: *CoRR* abs/1704.04503 (2017). arXiv: 1704.04503. URL: <http://arxiv.org/abs/1704.04503>.
- [56] João Carreira and Andrew Zisserman. “Quo Vadis, Action Recognition? A New Model and the Kinetics Dataset”. In: *CoRR* abs/1705.07750 (2017). arXiv: 1705.07750. URL: <http://arxiv.org/abs/1705.07750>.
- [57] Ali Diba et al. “Temporal 3D ConvNets: New Architecture and Transfer Learning for Video Classification”. In: *CoRR* abs/1711.08200 (2017). arXiv: 1711.08200. URL: <http://arxiv.org/abs/1711.08200>.

- [58] Rohit Girdhar and Deva Ramanan. “Attentional Pooling for Action Recognition”. In: *CoRR* abs/1711.01467 (2017). arXiv: 1711.01467. URL: <http://arxiv.org/abs/1711.01467>.
- [59] Rohit Girdhar et al. “Detect-and-Track: Efficient Pose Estimation in Videos”. In: *CoRR* abs/1712.09184 (2017). arXiv: 1712.09184. URL: <http://arxiv.org/abs/1712.09184>.
- [60] Chunhui Gu et al. “AVA: A Video Dataset of Spatio-temporally Localized Atomic Visual Actions”. In: *CoRR* abs/1705.08421 (2017). arXiv: 1705.08421. URL: <http://arxiv.org/abs/1705.08421>.
- [61] Kensho Hara, Hirokatsu Kataoka, and Yutaka Satoh. “Learning Spatio-Temporal Features with 3D Residual Networks for Action Recognition”. In: *CoRR* abs/1708.07632 (2017). arXiv: 1708.07632. URL: <http://arxiv.org/abs/1708.07632>.
- [62] Jiawei He et al. “Generic Tubelet Proposals for Action Localization”. In: *CoRR* abs/1705.10861 (2017). arXiv: 1705.10861. URL: <http://arxiv.org/abs/1705.10861>.
- [63] Kaiming He et al. “Mask R-CNN”. In: *CoRR* abs/1703.06870 (2017). arXiv: 1703.06870. URL: <http://arxiv.org/abs/1703.06870>.
- [64] Rui Hou, Chen Chen, and Mubarak Shah. “Tube Convolutional Neural Network (T-CNN) for Action Detection in Videos”. In: *CoRR* abs/1703.10664 (2017). arXiv: 1703.10664. URL: <http://arxiv.org/abs/1703.10664>.
- [65] Vicky Kalogeiton et al. “Action Tubelet Detector for Spatio-Temporal Action Localization”. In: *ICCV 2017 - IEEE International Conference on Computer Vision*. Venice, Italy, Oct. 2017.
- [66] Will Kay et al. “The Kinetics Human Action Video Dataset”. In: *CoRR* abs/1705.06950 (2017). arXiv: 1705.06950. URL: <http://arxiv.org/abs/1705.06950>.
- [67] Chih-Yao Ma et al. “TS-LSTM and Temporal-Inception: Exploiting Spatiotemporal Dynamics for Activity Recognition”. In: *CoRR* abs/1703.10667 (2017). arXiv: 1703.10667. URL: <http://arxiv.org/abs/1703.10667>.
- [68] Pascal Mettes and Cees G. M. Snoek. “Spatial-Aware Object Embeddings for Zero-Shot Localization and Classification of Actions”. In: *CoRR* abs/1707.09145 (2017). arXiv: 1707.09145. URL: <http://arxiv.org/abs/1707.09145>.
- [69] Suman Saha, Gurkirt Singh, and Fabio Cuzzolin. “AMTnet: Action-Micro-Tube regression by end-to-end trainable deep architecture”. In: *CoRR* abs/1704.04952 (2017). arXiv: 1704.04952. URL: <http://arxiv.org/abs/1704.04952>.
- [70] Gurkirt Singh et al. “Online Real time Multiple Spatiotemporal Action Localisation and Prediction”. In: 2017.
- [71] K. Soomro and M. Shah. “Unsupervised Action Discovery and Localization in Videos”. In: *2017 IEEE International Conference on Computer Vision (ICCV)*. 2017, pp. 696–705. DOI: 10.1109/ICCV.2017.82.
- [72] Du Tran et al. “A Closer Look at Spatiotemporal Convolutions for Action Recognition”. In: *CoRR* abs/1711.11248 (2017). arXiv: 1711.11248. URL: <http://arxiv.org/abs/1711.11248>.
- [73] Jianwei Yang et al. “A Faster Pytorch Implementation of Faster R-CNN”. In: <https://github.com/jwyang/faster-rcnn.pytorch> (2017).
- [74] H. Zhu, R. Vial, and S. Lu. “TORNADO: A Spatio-Temporal Convolutional Regression Network for Video Action Proposal”. In: *2017 IEEE International Conference on Computer Vision (ICCV)*. 2017, pp. 5814–5822. DOI: 10.1109/ICCV.2017.619.

- [75] Yi Zhu et al. “Hidden Two-Stream Convolutional Networks for Action Recognition”. In: *CoRR* abs/1704.00389 (2017). arXiv: 1704.00389. URL: <http://arxiv.org/abs/1704.00389>.
- [76] Mohammadreza Zolfaghari et al. “Chained Multi-stream Networks Exploiting Pose, Motion, and Appearance for Action Classification and Detection”. In: *CoRR* abs/1704.00616 (2017). arXiv: 1704.00616. URL: <http://arxiv.org/abs/1704.00616>.
- [77] Ali Diba et al. “Temporal 3D ConvNets Using Temporal Transition Layer”. In: *2018 IEEE Conference on Computer Vision and Pattern Recognition Workshops, CVPR Workshops 2018, Salt Lake City, UT, USA, June 18-22, 2018*. 2018, pp. 1117–1121. URL: [http://openaccess.thecvf.com/content\\_cvpr\\_2018\\_workshops/w19/html/Diba\\_Temporal\\_3D\\_ConvNets\\_CVPR\\_2018\\_paper.html](http://openaccess.thecvf.com/content_cvpr_2018_workshops/w19/html/Diba_Temporal_3D_ConvNets_CVPR_2018_paper.html).
- [78] Alaaeldin El-Nouby and Graham W. Taylor. “Real-Time End-to-End Action Detection with Two-Stream Networks”. In: *CoRR* abs/1802.08362 (2018). arXiv: 1802.08362. URL: <http://arxiv.org/abs/1802.08362>.
- [79] Rohit Girdhar et al. “A Better Baseline for AVA”. In: *CoRR* abs/1807.10066 (2018). arXiv: 1807.10066. URL: <http://arxiv.org/abs/1807.10066>.
- [80] Michelle Guo et al. “Neural Graph Matching Networks for Fewshot 3D Action Recognition”. In: *The European Conference on Computer Vision (ECCV)*. 2018.
- [81] Kensho Hara, Hirokatsu Kataoka, and Yutaka Satoh. “Can Spatiotemporal 3D CNNs Retrace the History of 2D CNNs and ImageNet?” In: *Proceedings of the IEEE Conference on Computer Vision and Pattern Recognition (CVPR)*. 2018, pp. 6546–6555.
- [82] Yu Kong and Yun Fu. “Human Action Recognition and Prediction: A Survey”. In: *CoRR* abs/1806.11230 (2018). arXiv: 1806.11230. URL: <http://arxiv.org/abs/1806.11230>.
- [83] Diogo C. Luvizon, David Picard, and Hedi Tabia. “2D/3D Pose Estimation and Action Recognition using Multitask Deep Learning”. In: *CoRR* abs/1802.09232 (2018). arXiv: 1802.09232. URL: <http://arxiv.org/abs/1802.09232>.
- [84] Bo Hu et al. “Progress Regression RNN for Online Spatial-Temporal Action Localization in Unconstrained Videos”. In: *CoRR* abs/1903.00304 (2019). arXiv: 1903.00304. URL: <http://arxiv.org/abs/1903.00304>.